UNIVERSITY OF CALIFORNIA, SAN DIEGO

Identification and Characterization of the Autophagy Initiating Kinase ULK1 as a Substrate of AMP-Activated Protein Kinase (AMPK)

A dissertation submitted in partial satisfaction of the requirements for the degree Doctor of Philosophy

in

Biology

by

Daniel Francis Egan

Committee in charge:

Professor Reuben J. Shaw, Chair
Professor Andrew Dillin
Professor Steven F. Dowdy
Professor William McGinnis
Professor Alexandra C. Newton

2014

The Dissertation of Daniel F. Egan is approved, and it is acceptable in quality and form for publication on microfilm and electronically:

_____

_____

Chair

_____

_____

_____

University of California, San Diego

2014

DEDICATION

I dedicate this thesis to my amazing girlfriend Margherita Paschini, whose support, both intellectual and emotional, throughout the years have been invaluable for its completion. Her keen intellect and compassion is inspiring, and I look up to her everyday.

TABLE OF CONTENTS

LIST OF FIGURES

LIST OF TABLES

ACKNOWLEDGMENTS

I would first like to thank my advisor, Reuben Shaw, for the opportunity to complete this work in his lab. His guidance throughout my graduate career has been invaluable to my scientific development.

Many thanks to my committee members, Andy Dillin, Bill McGinnis, Alexandra Newton, and Steve Dowdy for their scientific guidance, rigorous mentorship and feedback.

I am grateful to the members of the Shaw lab, past and present, especially Dana Gwinn, Maria Mihaylova, Dave Shackelford, Nate Young, Jon Goodwin and Matthew Chun, for their support, advice, and companionship throughout my graduate studies.

Chapter One contains excerpts from material as it appears in Egan, D.F., Kim, J., Shaw, R. J., & Guan, K.-L. (2011). The autophagy initiating kinase ULK1 is regulated via opposing phosphorylation by AMPK and mTOR. Autophagy, *7*(6), 643–644. On this publication, I was the primary author. Reuben Shaw directed and supervised the writing that provides the basis of this chapter.

Chapter Two contains excerpts from material as it appears in Egan, D. F., Shackelford, D.B., Mihaylova, M.M., Gelino, S., Kohnz, R.A., Mair, W., Vasquez, D.S., Joshi, A., Gwinn, D.M., Taylor, R., Asara, J.M., Fitzpatrick, J., Dillin, A., Viollet, B., Kundu, M., Hansen, M., Shaw, R.J. (2011). Phosphorylation of ULK1

(hATG1) by AMP-activated protein kinase connect energy sensing to mitophagy. Science 331(6016), 456-461.

VITA

EDUCATION

2014	University of California, San Diego, La Jolla, CA Doctor of Philosophy in Biology
2005	Colby College, Waterville, ME Bachelor of Science in Biology

PUBLICATIONS

Gwinn, D.M., Shackelford, D.S., **Egan, D.F**., Mihaylova, M.M., Mery, A., Vasquez, D.S., Turk, B.E., and Shaw, R.J. (2008) AMPK phosphorylation of raptor mediates a metabolic checkpoint. Molecular Cell 30(2), 214-26.

Lamia, K. A., Sachdeva, U. M., Ditacchio, L., Williams, E. C., Alvarez, J. G., **Egan, D. F**., Vasquez, D. S., Juguilon, H., Panda, S., Shaw, R. J., Thompson, C. B., Evans, R. M. (2009). AMPK Regulates the Circadian Clock by Cryptochrome Phosphorylation and Degradation. Science 326 (5951), 437–440.

Egan, D. F., Shackelford, D.B., Mihaylova, M.M., Gelino, S., Kohnz, R.A., Mair, W., Vasquez, D.S., Joshi, A., Gwinn, D.M., Taylor, R., Asara, J.M., Fitzpatrick, J., Dillin, A., Viollet, B., Kundu, M., Hansen, M., Shaw, R.J. (2011). Phosphorylation of ULK1 (hATG1) by AMP-activated protein kinase connect energy sensing to mitophagy. Science 331(6016), 456-461.

Egan, D. F., Kim, J., Shaw, R. J., & Guan, K. L. (2011). The autophagy initiating kinase ULK1 is regulated via opposing phosphorylation by AMPK and mTOR. *Autophagy*, *7*(6), 643–644.

ABSTRACT OF THE DISSERTATION

Identification and Characterization of the Autophagy Initiating Kinase ULK1 as a Substrate of AMP-Activated Protein Kinase (AMPK)

by

Daniel Francis Egan

Doctor of Philosophy in Biology

University of California, San Diego 2014

Professor Reuben Shaw, Chair

All eukaryotic cells must not only be able to interpret their energy, or ATP, status but also enact downstream effectors to regain homeostasis upon energy crisis. One of the ways that eukaryotic cells achieve this regulation is through the highly conserved serine/threonine kinase AMP-Activated Protein Kinase (AMPK). When cellular energy levels decrease, AMPK becomes activated and can turn off many anabolic processes while at the same time turning on catabolic ones through acute phosphorylation of its downstream substrates. The net result is that a cell undergoing energy stress stops what it is doing until homeostasis is restored. AMPK has been implicated in regulating many disparate processes in efforts to regain homeostasis,

however few known bone fide in vivo substrates of AMPK could explain this diverse and wide-ranging regulation. In order to better understand AMPK and processes downstream, our lab conducted a screen for novel substrates of this energy sensing kinase. Using a bioinformatics and proteomic approach, we have identified about 50 potential substrates of AMPK, which are also conserved across evolution and contain a consensus site for AMPK. One substrate in particular that I chose to focus on was a poorly studied autophagy initiating kinase, ULK1. AMPK directly phosphorylates ULK1 in vivo and in vitro, and cells that are unable to engage in this regulation are defective in engaging the cytoprotective mechanism of autophagy. Additionally, we show that this regulation is an important node for mitochondrial homeostasis because these mutant cells accumulated damaged mitochondria which should be otherwise degraded by autophagy. Finally, in order to better understand ULK1 function and to manipulate it pharmacologically in vivo, we have developed small molecule ATP-competitive inhibitors of ULK1/2. These molecules will be useful tools to not only dissect ULK1/2 function, but to also to inhibit ULK1/2 in various oncogenic settings where autophagy could be enabling tumor survival.

Taken together, these findings contribute to our understanding of how cellular energy crisis can trigger the cytoprotective process, autophagy. This AMPK-dependent regulation of the ULK1 complex represents one of the first signals triggered by energy crisis to activate the cytoprotective autophagy cascade.

CHAPTER ONE:

Introduction to AMPK and autophagy signaling: key pathways that regulate cellular and organismal growth and homeostasis

Introduction

The ability of a cell to both understand its nutrient and energy status and enact processes to regain homeostasis is critical for a cells survival. The decisions to grow, divide, turn on anabolism or catabolism may be the most basic and highly conserved checkpoints in the eukaryotic cell. The highly conserved AMP activated protein kinase (AMPK) serves as a cellular energy sensor by binding directly to 5' adenosine monophosphate (AMP), thus gauging the ratio of AMP:ATP and enacting downstream effectors (Hardie, 2011). By negatively regulating anabolic pathways, while positively regulating catabolic ones, AMPK serves as a cellular rheostat to regain energy homeostasis during times of stress. This pathway, once engaged, turns off costly biosynthetic processes, while turning on processes that can generate ATP, the net result is that the cell stops what it is doing until energy is restored.

Two well conserved and characterized substrates of AMPK provide a mechanism for AMPK to negatively regulate the pro-growth Target Of Rapamycin pathway (TOR) pathway which is a crucial mediator of protein synthesis. Under conditions of energy stress AMPK can directly phosphorylate mTOR's obligate subunit Raptor (Gwinn et al., 2008)and an upstream tumor suppressor Tuberin (TSC2) (Inoki et al., 2003)in a cellular effort to turn off protein synthesis when cellular ATP levels fall. Given that a large portion of the cellular ATP budget is allocated to protein synthesis it is logical that an energy sensor wired to conserve ATP would have multiple inputs to dampen this costly process. A major theme of inactivation or mutation of the AMPK pathway is upregulation of the pro-growth mTOR pathway.

In addition to negatively regulating protein synthesis, AMPK can positively regulate a pathway to systematically degrade its organelles and proteins to regain cellular ATP – autophagy. Autophagy is a catabolic process where the cell cannibalizes its proteins and damaged organelles, such as mitochondria, in an effort to regain cellular ATP. To date, no known biochemical steps that directly initiate autophagy have been reported. However, I have identified a key highly conserved autophagy specific kinase, hATG1/ULK1, as a substrate of AMPK, thus providing the first positive link between cellular energy status and autophagy initiation (Egan et al., 2011b)which will be the subject of Chapter 2. For my graduate work, I have worked at better understanding the biochemical link between ULK1 and AMPK in order to elucidate the mechanisms and effectors that this pathway uses to maintain energy homeostasis.

In order to better understand ULK1 function and the mechanism whereby it controls autophagy, I have begun mapping the phosphorylation sites in novel ULK1 substrates which we have identified. We collaborated with Cell Signaling Technology (Danvers, MA) to develop phospho-specific antibodies against these phosphorylation sites which now represent some of the first biomarkers of ULK1 kinase activity that can be used in vivo to monitor the first steps of the autophagy cascade.

Leveraging this biological insight we have learned about ULK1, and AMPK, we have screened for ATP-competitive inhibitors of ULK1/2 which will not only allow for careful dissection of the kinase in vivo, but will also allow us to pharmacologically manipulate ULK1/2 and autophagy in vivo and test many

hypothesis about the requirement for autophagy in various pathological contexts, such as cancer. These data will be the subject of Chapter 3.

AMPK

The story of the serine/threonine kinase AMP-activated Kinase (AMPK) begins with the purification of an unknown kinase from rat liver that inactivated two crucial enzymes of fatty acid and sterol biosynthesis: 3-hydroxy-3-methylglutaryl-CoA reductase (HMGR) (Ingebritsen et al., 1978)and acetyl-CoA carboxylase (ACC) (Yeh et al., 1980). The kinase that was responsible for phosphorylating these enzymes was activated by 5'-adenosine monophosphate (AMP), however it was thought that these were two separate enzymes that were responsible for these phosphorylation events. It wasn't until 1987 when the Hardie group showed that the "HMGR Kinase" and the "ACC Kinase" purified from rat liver were in fact one single enzyme, which they named AMPK after its allosteric regulator, and demonstrated it to be the kinase responsible for these phosphorylation events (Carling et al., 1987). Since these seminal studies AMPK has been shown to regulate a diverse array of cellular processes, not just lipid biosynthesis (Shackelford and Shaw, 2009).

AMPK is highly conserved across all eukaryotes, and is widely accepted to be a master energy sensor for the eukaryotic cell (Hardie et al., 2012). It is an obligate heterotrimer composed of a catalytic alpha subunit, and two regulatory subunits (beta, and gamma). When the cellular ATP:AMP drops, AMP binds directly to the gamma subunits, which results in a 10-fold increase in AMPK kinase activity. However, a

more dramatic increase of about 100-fold is achieved when a conserved threonine residue in the activation loop of AMPK is phosphorylated by its upstream kinase (Suter et al., 2006). In mammals this site can be phosphorylated by the Ca^{2+}/calmodulin-activated protein kinase kinases, most notably CaMKK β, but the dominant upstream kinase in most tissues appears to be the tumor suppressor LKB1. Phosphorylation of AMPK in its activation loop at Thr172 by either of these upstream kinases is required for its activity and represents not only a direct gauge of cellular energy but also a connection between tumor suppression and metabolism. AMPK alpha responds by acutely turning off energy consuming pathways, and turning on energy promoting pathways. This regulation is achieved by direct phosphorylation of specific substrates representing an array of growth and metabolic pathways (Mihaylova and Shaw, 2011). The direct connection between the LKB1 tumor suppressor and the metabolic enzyme AMPK underscored the importance of, and rekindled, the field of cancer metabolism which had been largely been pushed aside by the explosion of studies on proto oncogenes (Hardie and Alessi, 2013).

Specificity

The ability of kinases to recognize their substrates with specificity is determined by layers of criteria. Sub cellular compartmentalization, co-localization with anchoring proteins and scaffolds, cell type specific co-expression partners, docking motifs, and the structural characteristics of the kinase active site all play a role in the ability of the kinase to find its appropriate substrate in cellular contexts with

tens of thousands of possible peptides (Ubersax and Ferrell, 2007). The amino acids surrounding the phospho-acceptor site provide an additional layer of selection by the protein kinase, and indeed many optimal substrate motifs of the kinome have been determined (Mok et al., 2010). An important breakthrough in better understanding the substrates downstream of AMPK, was the delineation of its optimal consensus motif. Using three main approaches by different groups: amino acid substitutions of recombinant substrates (Scott et al., 2002), synthetic peptides (Weekes et al., 1993), and, most recently, a peptide library approach to unbiasedly interrogate which residues are preferred relative to the phospho acceptor site (Gwinn et al., 2008). Surprisingly, compared to nearly all other kinases to date, many of which only require a few residues (or merely a priming phosphorylation site as does GSK-3), AMPK appears highly specific with regards to the amino acids flanking the phospho-acceptor site. In addition to preferring serine, AMPK optimally phosphorylates peptides with a hydrophobic sidechain at the -5 and +4 positions, basic sidechains at the -3 or -4, and about half of the known substrates contain proline in the +2 and have been shown to bind the 14-3-3 scaffold protein. This specificity allows for directed biochemical and bioinformatic screening approaches to uncover novel substrates of AMPK which will be discussed in later chapters. Given that the AMPK consensus overlaps with other less-specific motifs such as PKA, and AKT, genetic manipulation of AMPK is crucial when interpreting potential candidates.

Regulation of Growth and Proliferation

Despite the fact that very few inactivating mutations have been found in AMPK itself, loss of function mutations in its upstream kinase LKB1 are commonly mutated in non-small cell lung cancer(NSCLC) (Sanchez-Cespedes et al., 2002), and these inactivating mutations have been shown to be cause of the familial cancer syndrome Peutz-Jeghers Syndrome (PJS) (Hemminki et al., 1998). The germline mutations that humans with PJS posses in the catalytic region of LKB1 result in gastrointestinal hamartomas and an increased predisposition to other malignancies such as ovarian, endometrial and pancreatic tumors, thus underscoring the kinase function of LKB1 as a tumor suppressor. Other familial cancer syndromes with similar presentations as PJS such as Neurofibromatosis Type I, Cowden's Disease, Tuberous sclerosis contain mutations that, like LBK1, converge upstream of the mTOR pathway (NF-1, PTEN, and TSC respectively) underscoring the significance of tumor cells exploiting this pro-growth pathway. Moreover, LKB1 is one of the most commonly mutated genes in sporadic human lung cancer, and over 20% of cervical carcinomas (Wingo et al., 2009).

Inactivation of the LKB1 tumor suppressor leads to subsequent hyperactivation of the pro-growth Mechanistic Target Of Rapamycin (mTOR) pathway and is a common theme throughout many cancers. The nutrient sensor TOR is a highly conserved atypical serine/threonine kinase that lies downstream of many mitogenic signals and is positioned at the crux of many nutrient regulated signaling pathways in the eukaryotic cell (Laplante and Sabatini, 2012). Because so many pathways feed

downstream to mTOR it can not only respond to upstream energy sensors such as AMPK, but can also respond to levels of amino acids through the RAG family of GTPases and insulin signaling through PI3K and Akt which activate mTOR (Sancak et al., 2008). The mTOR kinase is inactivated by AMPK by a two-fold mechanism – the first is AMPK dependent inhibitory phosphorylation of one of TOR's binding partners, raptor, and the second is AMPK dependent phosphorylation of the TSC2 tumor suppressor which inhibits a positive regulator of mTOR, thus providing a mechanism for increased mTOR signaling which are seen with loss of LKB1 - AMPK activation.

Given these findings our lab has tested the hypothesis of inhibiting mTOR in our mouse model of LKB1 inactivation, and demonstrated that treatment with rapamycin (an allosteric inhibitor of the mTOR kinase) can reduce tumor burden (Shackelford et al., 2009), thus providing proof-of-concept for using rapamycin and rapalogs (synthetic derivatives of rapamycin) to treat PJS patients.

Pharmacological and Metabolic activation

AMPK's role as a intracellular energy sensor make it an important node for recognizing energy crisis from any perturbation that disrupts the cellular ATP:AMP balance either on a single cell level or a whole organismal level. Indeed any type of inhibition of ATP generating processes such glycolysis, oxidative phosphorylation, or induction of ATP consuming processes such as muscle contraction, the cell cycle, or biosynthesis of lipids, proteins or ribosomal RNA can engage this pathway. Genetic

ablation of AMPK or its upstream activator, LKB1 in metabolic cell tissues such as muscle or liver have shown increased AMP:ATP ratio when compared to wt controls upon metabolic stress, highlighting the importance of AMPK acting as a cellular rheostat to conserve energy in the face of metabolic stress (Foretz et al., 2010). Additionally, genetic or pharmacolgical inhibition of AMPK or its orthologs across all eukaryotes usually results in an overgrowth phenotype or an inability to curtail metabolism in the face of changing nutrient conditions, preventing metabolic adaptation, and growth arrest (Hardie, 2007).

Importantly, activation of the LKB1/AMPK pathway has been of therapeutic interest, either prophylactically or as a treatment, for our lab and other investigators in various pathological settings to curb metabolism (in the case of diabetes) or growth (in the case of cancer). Indeed, epidemiological studies have also shown that diabetics taking metformin (an AMPK agonist also sold as Glucophage®) showed a statistical reduction in tumor burden when compared to patients taking other drugs (Evans et al., 2005). Importantly, our lab has shown the hypersensitivity of LKB1-defective cells to metabolic stress and tested the therapeutic use of a biguanide called phenformin, which is a more potent analog of metformin that also exhibits increased tissue bioavailability in mouse models of NSCLC. Phenformin prolonged survival and reduced tumor burden in Kras;Lkb1 compound mutant mice but not Kras;p53 mice. These findings suggest phenformin, or related drugs, may be efficacious in the treatment of RAS driven tumors bearing LKB1 loss-of-function mutations (Shackelford et al., 2013).

Regulation of whole-body lipid and glucose metabolism

In addition to cell autonomous regulation of ATP expenditure, AMPK also plays important roles in regulating the metabolism of the whole organism. The ability of AMPK to negatively regulate fatty acid and sterol biosynthesis in the liver date to its initial discovery in the mid-1980s, and the data demonstrating that AMPK could directly phosphorylate two rate-limiting enzymes in these processes - ACC1 and HMGR - established some of the first physiological evidence of AMPK activation. Further work has shown that by regulating ACC1 and ACC2, AMPK can control the fate of lipids at both ends of the life cycle - their biosynthesis and their oxidation. By directly phosphorylating ACC1, AMPK negatively regulates fatty acid synthesis (Davies et al., 1992) and AMPK-dependent phosphorylation of ACC2 results in decreased ACC2 activity, and concomitant decrease in malonyl-CoA (a negative regulator of fatty acid transport of into the mitochondria) the end result being increased Beta Oxidation (Merrill et al., 1997). Thus, this dual pronged regulation of these two ACC isoforms allows for both the inhibition of fatty acid synthesis and increased breakdown during times of energy crisis to restore cellular ATP. Furthermore, these in vitro data have been corroborated by an elegant knock-in strategy whereby both of the AMPK dependent phosphorylation sites in both ACC1 and ACC2 have been substituted for alanine (Fullerton et al., 2013). Compared to their wild type littermates, these ACC double knock in (AccDKI) animals had both lower fatty acid oxidation and higher levels of fatty acid synthesis, and became insulin

resistant and glucose intolerant. These data strongly support the role of AMPK in regulating lipid metabolism at the whole organismal level. In addition to these acute metabolic changes through ACC1/2, recent evidence suggests that AMPK can directly phosphorylate a lipogenic transcription factor, SREBP1, on a conserved serine near its requisite cleavage site, in an effort to negatively regulate a gene expression program which includes FASN, and ACC1 (Li et al., 2011) two important genes for lipogenesis. This AMPK-dependent regulation of both enzymes and transcription factors is an emerging theme of the short- and long-term adaptations that AMPK administers.

In addition to regulating lipid metabolism, AMPK and its related kinases play a major role in glucose metabolism both by its production in the liver and uptake in peripheral tissues such as fat and muscle. Indeed, pharmacological activation of AMPK by the first line drug for Type II diabetes, Metformin, which is also a well-characterized AMPK agonist, is widely appreciated for its ability to dampen gluconeogenesis in the liver, and this largely dependent on the upstream kinase, LKB1 (Shaw et al., 2005). The AMPK-dependent regulation of glucose production in the liver is thought to work through at least two sets of transcription factors - CREB and FOXO. By negatively regulating CRTC2, and the Class II HDACs, AMPK and its related family members can repress the transcriptional output of CREB and FOXO respectively to downregulate two rate-limiting enzymes in gluconeogensis, phosphoenolpyruvate carboxykinase (PEPCK) and glucose-6-phosphatase (G6Pase). Additionally, other AMPK agonists such as the AMP mimetic, AICAR, and the small

molecule A769662 which directly binds to and activates AMPK, can both lower blood glucose levels (Cool et al., 2006; Halseth et al., 2002) highlighting the importance of this node as therapeutic target for lowering blood glucose to treat Type II Diabetes. Conversely, the activation of AMPK in peripheral metabolic tissues, such as fat and muscle during times of metabolic stress or lowered ATP (such as muscle contraction) result in direct phosphorylation of the RABGAP TBC1D1, the conversion of RABs to its active GTP bound form, and subsequent translocation of the glucose transporter GLUT4 to the plasma membrane and glucose uptake from the blood (Kurth-Kraczek et al., 1999). These data highlight the importance of AMPK dependent metabolic changes by both short- and long-term regulation of enzymes and transcription factors.

Autophagy

Macroautophagy (autophagy hereafter) is a highly conserved pathway across all eukaryotes for the degradation of long-lived or damaged proteins and dysfunctional organelles either to maintain a healthy proteome, or in response to metabolic stress to generate ATP. The resulting autophagic breakdown products generated at the final step of the pathway are recycled back into cellular metabolism as building blocks for more necessary biosynthetic processes, or for energy generation in the form of ATP (Mizushima, 2011). Autophagy, like the AMPK pathway, represents a highly conserved cascade that allows cells from yeast to human to adapt to their changing environment.

By degrading large protein aggregates, macromolecules such as lipids carbohydrates, nucleic acids, and glycogen, and dysfunctional organelles, autophagy is thought to achieve two major functions. The first of which is an housekeeping one; by complementing the Ubiquitin Proteasome System (UPS), autophagy provides a vital alternative degradative pathway to maintain a healthy proteome. Unlike the sterically hindered proteasome, the modular autophagosome is a custom recycle bin which can fit massive areas of entire cytoplasm, allowing for whole organelles and large macromolecular aggregates to be disposed of (Kraft et al., 2010). Indeed, there is much cross talk between these two catabolic pathways and genetic or pharmacological inhibition of one has been shown to result in the upregulation of the other. Secondly, the metabolites that are liberated by autophagy provide an important energy source during periods of energy stress allowing for an adaptable metabolic response, and thus cell survival under nutrient poor conditions in all organisms tested from yeast (Tsukada and Ohsumi, 1993) to mammalian cells (Egan et al., 2011b).

Discovery

Piggy backing on the discovery of the lysosome by Christian de Duve in 1955, the story of autophagy begins with the observation of double membrane bound structures which contained portions of cytoplasm that were in various stages of disintegration by Dr. Thomas Ashford at Rockefeller who was performing electron microscopy on rat liver which had been perfused with the hormone glucagon to mimic starvation (Ashford and Porter, 1962). Ashford and his colleagues observed that

cytoplasmic particles which they termed "microbodies" were up to 3-fold enriched after perfusion with glucagon, suggesting that this rapid rearrangement of organelles was an acute response to starvation.

Later groups went on to show that these organelles indeed contained lysosomal hydrolases (Deter et al., 1967) and posited that the cell was purposefully and systematically digesting portions of the cytoplasm, and mitochondria to some unknown end. Christian de Duve later coined the term "autophagy" at the Ciba Foundation Symposium on Lysosomes in 1963 to describe this self-eating process.

Since these initial observations, the field of autophagy languished until the molecular era when the first genetic screen in the budding yeast saccharomyces cerevisiae was performed in Yoshinori Ohsumi's lab to better understand the genetics of how autophagy is orchestrated (Tsukada and Ohsumi, 1993). This seminal study identified many of the core genes regulating autophagy, most of which have a direct homolog in higher eukaryotes.

Molecular Mechanisms

Much of our genetic understanding of how autophagy is regulated comes from work in budding yeast which has identified at least 30 AuTophagy Genes (ATGs), and while many of these ATG have homologs in higher eukaryotes, they have poorly defined molecular functions. The exact biochemical mechanisms of this process are still not fully understood to date, and much is to be determined but what is clear is that these isolated autophagy mutants were unable to survive periods of nitrogen

starvation, despite normal growth in nutrient-replete media, thus underscoring autophagy's role as a cytoprotective mechanism to ensure survival in nutrient poor conditions.

In yeast, the highest ATG in the hierarchical signaling cascade (Itakura and Mizushima, 2010) is the only protein kinase in the pathway - Atg1 (the human homolog of which is ULK1). Together with Atg13 and Atg17, the ULK1 kinase complex controls the early steps in autophagosome formation through poorly understood mechanisms. Under nutrient-replete conditions ULK1 is negatively regulated by the upstream kinase, mTOR. mTOR directly hyperphosphorylates ULK1 inhibiting its kinase activity and thus autophagy when it is not needed (Kamada et al., 2000). Indeed, mitogenic stimuli that activate mTOR such as amino acids and insulin have long been appreciated as antagonists of the pathway. Conversely, under conditions of low ATP, AMPK is activated and phosphorylates ULK1 on 4 residues to positively regulate ULK1 to activate autophagy in times of energy crisis. Thus, autophagy activation is achieved by the opposing phosphorylation by these two important energy sensors (Figure 1.1) and the ULK1 complex is an important node of signal integration to provide a graded response (Egan et al., 2011a).

Downstream of the ULK1 complex, the autophagy pathway continues with the formation of a double membrane structure called the isolation membrane. ULK1 directly phosphorylates Beclin-1 to regulate VPS34 activity (Russell et al., 2013). This nascent autophagosome is enriched with Phosphatidylinositol 3-phosphate (PtdIns3P) by the Class III PI3-kinase vacuolar protein sorting 34 (VPS34) which is

the catalytic subunit of the Beclin-1 (mammalian homolog of Atg6) complex. This PtdIns3P rich membrane structure provides a docking site for FYVE domain containing phospholipid binding proteins such WIPI and DFCP1. Once bound, WIPI and DFCP1 recruit additional autophagy proteins to continue the elongation of the membrane (Matsunaga et al., 2010).

Although autophagy was once thought to be a bulk, non-selective process, it is becoming appreciated that there is indeed a highly orchestrated way for the cell to target macromolecules and organelles for preferential degradation. Recent studies suggest a model whereby the cargo adaptor proteins, Sequestosome-1 (p62) and Neighbor of BRCA1 gene 1 (NBR1) bind to ubiquitinated proteins, then subsequently homo-oligermerize. This larger oligomer is recognized by receptors on the inner membrane of the autophagosome, thus allowing insertion of the cargo into the nascent autophagosome (Itakura and Mizushima, 2011). Indeed, genetic loss of autophagy leads to increases in ubiquitin aggregates and p62 levels (Komatsu et al. 2005) underscoring not only their importance in the process but also their use as biomarkers of autophagic flux (Mizushima et al., 2010).

Once the cargo destined for degradation is loaded, the autophagosomes are mobilized through the cytoplasm on microtubules with the aid of the molecular motors dynein and kinesin until the reach the lysosome where they fuse with the aid of the recently described autophagy-specific SNARE, syntaxin 17 (Stx17) (Itakura and Mizushima, 2013). The pathway ends with the lysosomal transporters and permeases

facilitating the movement of the degraded components back into the cytoplasm for biosynthesis of new molecules or ATP generation.

The diversity of macromolecules and organelles that can be broken down and recycled back into cellular metabolism by autophagic degradation highlights the flexible utility of the pathway. Indeed there are many types of specialized autophagy for lipids (lipophagy), ribosomes, (ribophagy), mitochondria (mitophagy), endoplasmic reticulum (reticulophagy), and peroxisomes (pexophagy) all of which seem to engage much of the same core machinery. Whether or not one single autophagosome contains a mixture of these components or a homogeneous set, and the exact details of the selection process remains to be elucidated, but it is clear that this adaptive modularity allows for much customization.

Depending on the context, breakdown products can either be used for de novo biosynthesis of new macromolecules, or for energy production in a cell-autonomous manner (Rabinowitz and White, 2010). In times of energy crisis, amino acids liberated from autophagic breakdown of proteins can be used to generate ATP through multiple metabolic inputs of central carbon metabolism including oxidative phosphorylation. In addition to serving as building blocks for de novo lipogeneis, fatty acids released from the breakdown of lipids or membranes can be used to make acetyl-CoA in order to fuel ATP and citrate production via the tricarboxylic acid cycle (TCA) cycle. Nucleosides from the breakdown of nucleic acids and sugars from the breakdown of larger carbohydrates or glycogen can either be used for new nucleic acid synthesis or for metabolism in the Pentose Phosphate Pathway (PPP) to yield

glycolytic substrates for ATP generation. Moreover, specialized metabolic tissues such as the liver can allocate breakdown products such as lipids, nucleosides, and amino acids into ketogenesis and gluconeogenesis which can then be used to dispense ketone bodies and glucose throughout the entire organismal via its blood supply as a cell-nonautonomous mechanism to maintain energy homeostasis.

Though there was once confusion about whether autophagy was a mechanism for cell survival, or cell death, the most recent studies suggest the former. Autophagy is a requirement for cell and organismal survival in nutrient poor conditions in all model organisms tested. Yeast undergo rapid cell death upon nitrogen deprivations (Matsuura et al., 1997), flies cannot survive past the larval stage (Arsham and Neufeld, 2009) worms cannot undergo dauer formation (Meléndez et al., 2003), and mice cannot survive the neonatal starvation period just after birth (Kuma et al., 2004). Taken together these data underscore the importance that these metabolites generated as a product of autophagy play in conditions of metabolic or environmental stress and that the primary role of autophagy is a cytoprotective one.

AMPK and mTOR regulation of ULK1

The Shaw and Guan labs, independently studying ULK1 regulation and performing a screen for new AMPK substrates, both identified ULK1 as a direct substrate of AMPK (Egan et al., 2011b; Kim et al., 2011). Collectively, we found six different AMPK sites (S317, S467, S555, T575, S637, and S777) in ULK1 in vivo using mass spectrometry and antibodies directed against four of these sites. We

observed that the phosphorylation of these residues is dependent on AMPK and mirrors the kinetics of the known AMPK substrates ACC and raptor. Two of the AMPK phosphorylation sites in ULK1 (S555 and T575) also appear to be 14-3-3 binding sites, which parallels the two AMPK phosphorylation sites in raptor that serve as 14-3-3 binding sites. Notably, ULK1 kinase activity increases in an AMPK-dependent manner following glucose deprivation. Moreover, ULK1 can be directly activated in vitro by AMPK, demonstrating a direct role of AMPK in ULK1 regulation. Interestingly, two of the sites, S317 and S777, do not match the AMPK consensus motif, but they contribute to AMPK-dependent ULK1 kinase activation. Furthermore, a few additional sites bearing elements of the well-defined AMPK consensus motif also exist in ULK1, so future studies will be needed to fully quantitatively annotate all the phosphorylation sites in ULK1.

Both studies found that mutation of AMPK phosphorylation sites in ULK1 resulted in loss of ULK1 function, reflecting the fact that both AMPK and ULK1 act to stimulate autophagy in many different contexts. Reconstitution of *ULK1*-knockout cells with the AMPK non-phosphorylatable ULK1 mutants resulted in defective autophagy, altered mitochondrial homeostasis, and reduced cell survival upon starvation, which phenocopied *ULK1* deletion or RNAi for *ATG5*, a core component of the downstream autophagy machinery. These observations demonstrate the functional importance of ULK1 phosphorylation by AMPK in autophagy induction.

Interestingly, our studies, along with additional recent reports (Shang et al., 2011), have found that the AMPK kinase complex is tightly bound to the ULK1

kinase complex in cells. Notably, rapamycin treatment increases co-immunoprecipitation of AMPK and ULK1, suggesting that mTORC1 activity may regulate their association. Indeed, we determined that mTORC1 phosphorylates ULK1 on S757 and this phosphorylation disrupts the interaction between ULK1 and AMPK. Consistently, phosphorylation of the AMPK sites and mTORC1 site in ULK1 are inversely regulated under various conditions. Phosphorylation of the two AMPK sites, S317 and S777, is suppressed in *TSC1*$^{-/-}$ MEFs, or by *RHEB* co-transfection, conditions that have elevated mTORC1 activity. Taken together, these data suggest that under nutrient-rich condition, active mTORC1 phosphorylates ULK1 to disrupt ULK1-AMPK interaction, thus keeping ULK1 inactive. Once cellular energy is depleted, such as during glucose deprivation, AMPK is activated and then inhibits mTORC1 via phosphorylation of both TSC2 and raptor, therefore, reducing S757 phosphorylation on ULK1. The S757 unphosphorylated ULK1 is able to associate with, and be activated by, AMPK (Figure 1.1). This coordinated phosphorylation of ULK1 by mTORC1 and AMPK may provide a mechanism by which cells can properly respond to a wide range of stimuli. Therefore, a balance of the activity of these three kinase complexes serves to modulate many of the cellular decisions about autophagy induction, growth, and survival.

Given the concerted actions of the AMPK, ULK1, and mTORC1 complexes, each of which contain multiple regulatory subunits, it is likely that additional layers of biochemical complexity are embedded in the crosstalk of these kinase complexes and their control of growth, autophagy, and cell survival. Given the derangement of

autophagy in a number of human pathologies, it will be of interest to determine whether ULK1 regulation is abnormally altered in these conditions. Cells have adapted diverse uses for autophagy to custom tailor intracellular bioenergetics and homeostasis, which are just now beginning to be decoded. With a deeper understanding of the critical connections governing autophagy, future therapeutic options utilizing this pathway will no doubt arise.

Transcriptional regulation of autophagy

Though many core autophagy proteins are thought to be constitutively expressed, and regulated mainly by post-translational modifications to ensure timely activation in response to acute environmental changes, there is evidence in support of regulation at the transcriptional level. The data now points to at least four master transcription factors regulating autophagy: FOXO3, TFEB, p53, and ZKSCAN3.

Marco Sandri's group first reported that the transcription factor FOXO3 is necessary and sufficient for the induction of autophagy in skeletal muscle in vivo, most notably by regulating LC3 expression and that this autophagy induction by FOXO3 was blocked by Akt activation (Mammucari et al., 2007). More recently, it has been shown that the basic-helix-loop-helix (bHLH)-leucine zipper transcription factor, transcription factor EB (TFEB), is a major regulator of not only autophagy but also lysosomal biogenesis at the transcriptional level, and that this is negatively regulated by mTOR, thus indicating that mTOR is regulating autophagy at multiple

levels, transcriptionally and post-translationally (Sardiello et al., 2009; Settembre et al., 2011).

The zinc finger transcription factor ZKSCAN3, having Kruppel-associated box (KRAB) and SCAN domains, is thought to act as a transcriptional repressor of autophagy (Chauhan et al., 2013). ZKSCAN3 was shown to transcriptionally modulate the expression of more than 60 genes encoding proteins involved in the various steps of lysosome biogenesis and autophagy. In support of their gene expression analysis, silencing of ZKSCAN3 promoted the induction of a selected portion of the identified gene array set as read out by quantitative real-time PCR with a selected set of genes (27 genes), and they were able to ChIP ZKSCAN3 to the promotor region of some of the targets, suggesting that they are indeed direct targets of ZKSCAN3. This regulation could be downstream of mTOR signaling, as inhibition of mTOR via starvation or a small molecule ATP competitive inhibitor of mTOR, TORIN1, caused cytoplasmic sequestration of ZKSCAN3 and depression of target genes.

In an effort to better understand the global response to p53 activation in an unbiased manner, the Attardi lab uncovered a surprising role for p53 in autophagy regulation. Using ChIP sequencing (ChIP-seq) and RNA sequencing (RNA-seq) they show that the p53 transcriptional response included an induction of an autophagy program in primary fibroblasts, and that many core ATGs such as ULK1 and ULK2 are direct transcriptional targets of p53 (Kenzelmann Broz et al., 2013). This early

p53 response may represent an early cellular response to upregulate autophagy in order to minimize genotoxic stress that could spur oncogenic mutations.

Taken together these data suggest a highly regulated network involved, of which we are just beginning to understand, in both the induction and suppression of autophagy at the transcriptional level that poises cells with the proper machinery which can then be fine-tuned at the post-translational level for an acute response.

Role of Autophagy in Disease

This fundamental autophagic pathway that yeast evolved to survive periods of starvation plays an invaluable role in the overall homeostasis of multicellular organisms serving a critical roles not only in the quality of individual proteins but more importantly that of organelles, whole tissues and that of the entire organism. The roles of autophagy in neurodegeneration, aging, the immune response, and cancer are all open areas of investigation.

Dating back to the first cell based studies from David Rubinsztein's lab which showed that aggregate-prone proteins with polyglutamine and polyalanine expansions are degraded by autophagy (Ravikumar et al., 2002), autophagy has been implicated in a variety of neurodegenerative states such as Parkinson’s Disease (Irrcher and Park, 2009), Alzheimer’s Disease (Wolfe et al., 2013) and Huntington's Disease. Indeed, induction of autophagy by mTOR inhibition has been shown to lessen the accumulation of aggregate-prone proteins in fly and mouse models of Huntington's disease thus ameliorating the neurodegeneration and providing a proof-of-concept for

the further investigation into activating autophagy for therapeutic purposes (Ravikumar et al., 2004). More importantly, the first genetic evidence of the importance of autophagy in preventing neurodegeneration showed that core autophagy genes Atg7 (Komatsu et al., 2006) and Atg5 (Hara et al., 2006) were required in the central nervous system to prevent the accumulation of inclusion bodies, and polyubiquitinated proteins which contributed to the neurodegenerative state. An active area of research is investigation into activating autophagy in these pathological contexts in an effort to therapeutically target human afflictions such as Parkinson's Disease, Alzheimer's Disease, and Huntington's Disease.

The ability of cells to maintain a pristine proteome and defend against toxic aggregates, and damaged organelles has long been appreciated to decline with age (Wolff et al., 2014) and lysosomal function has been shown to be reduced in almost all tissues in aging organisms (Cuervo, 2008). The consequences of these aggregates which usually results in increased reactive oxygen species (ROS) from this reduced function is particularly detrimental for terminally differentiated cells such as neurons and cardiomyocytes, which cannot dilute out the toxic aggregates by cell division. Importantly, autophagic flux (which depends on lysosome function) and the expression, both at the mRNA level and the protein level, of core ATGs has been shown to decline with age (Cuervo and Dice, 2000). Conversely, one of the most well-characterized antagonists of aging across all eukaryotes, dietary restriction (DR), is not only a also a potent inducer of autophagy but can also prevent age-related decline of autophagy (Donati et al., 2001). Additionally, genetic data in

Caenorhabditis elegans suggests that Beclin-1 is needed for the lifespan extension of worms lacking insulin like growth factor 1 (daf-2) highlighting the requirement of autophagy in antagonizing the aging process (Hansen et al., 2008).

Role of Autophagy in Cancer

The role of autophagy in cancer has been controversial, and depending on the context, it has either been implicated as playing a role in its progression, or suppression. The data to date suggest that, in general, autophagy suppresses tumorigenesis by maintaining a healthy proteome thus reducing ROS and genomic stability, but also acts in a cytoprotective manner to ensure tumor cell survival in the harsh tumor microenvironment (White, 2012). The core ATG, Beclin-1, maps to a region on chromosome 17q21, located 150 kb centromeric to BRCA1 and is commonly lost in human prostate, breast and ovarian cancers. Beclin-1 has been shown to be mono-allelically deleted in 40 – 75% of sporadic human ovarian and breast cancers (Aita et al., 1999), but the first direct evidence that loss of autophagic flux contributed to tumor progression was from Beth Levine's group (Qu et al., 2003). Heterozygous deletion of Beclin-1 increased the incidence of spontaneous tumors in the lung, liver, spleen, and B Cell compartment in mice less than 2 years old. Importantly the expression of the other copy of Beclin-1 is maintained in these tumors, thus establishing its role as a haploinsufficient tumor suppressor. Though the mechanism of this tumor progression is poorly understood, it is thought to arise from the genomic instability and ROS accumulated after the cells being unable to “clean its

house" and may also involve the failure to clear the cargo adaptor proteins (such as p62) themselves.

Taken together these genetic data from mice suggest an important role for autophagy in maintaining a healthy proteome by degrading long-lived proteins, macromolecular aggregates and damaged, dysfunctional organelles with the goal of minimizing genotoxic stress and serving a tumor suppressor function that maintains healthy cells, tissues and organs.

Despite autophagy's role in maintaining the integrity of the proteome which ensures the proper function of cells, tissues, and organs, there is mounting evidence to support that this cytoprotection may serve as an adaptive response for tumor cells to maintain their high metabolic needs and to survive their harsh, nutrient poor microenvironment especially before it gets vascularized. Indeed, the role autophagy plays as a survival mechanism in cell culture has prompted many researchers to explore its role promoting tumorigenesis. Some of the first observations demonstrated that activation of the oncogene V-Ki-ras2 Kirsten rat sarcoma viral oncogene homolog (KRAS) is a potent inducer of autophagy and that these Ras expressing cells need proper autophagic flux to generate metabolites and maintain a functional pool of mitochondria to support their high metabolic demand (Guo et al., 2011). Expression of H-ras^{V12} or K-ras^{V12} in nontumorigenic baby mouse kidney epithelial (iBMK) cells upregulated the autophagy pathway at a very high basal level in cultured cells through a still poorly defined mechanism. iBMK cells lacking Atg5 or Atg7 which cannot undergo autophagic flux, rapidly undergo cell death when cultured with low nutrients

(serum starvation or glutamine deprivation) and are also unable to form tumors when injected in the flank of nude mice, strongly supporting the hypothesis that autophagy is required for the progression of some tumors. Indeed the altered metabolism of tumors and the addiction of various k-ras driven tumor-derived cell lines to metabolites such as glutamine to fuel the TCA cycle and other anabolic processes has been long been appreciated (Son et al., 2013), and provide supporting evidence for importance of autophagy in providing these metabolites.

Springboarding off their own and other xenograft studies, the White lab provided the first direct genetic evidence that autophagy promotes tumorigenesis in a spontaneously arising model of non-small cell lung cancer (NSCLC). Using conditional deletion of Atg5 or Atg7 and concomitant activation of Ras (LSL-$KRAS^{G12D}$; $Atg5^{flox/flox}$ and LSL-$KRAS^{G12D}$; $Atg7^{flox/flox}$), they show that autophagy is required for KRAS driven lung tumors to reach the more aggressive adenoma and adenocarcinoma stage, and that defective autophagy leads to benign oncocytomas characterized by the accumulation of respiration-defective mitochondria (Guo et al., 2013a). These data, and similar work in a KRAS driven model of PDAC (Rosenfeldt et al., 2013) provide strong supporting evidence for the role autophagy may play in promoting tumor growth.

Taken together these data suggest that targeting autophagy in different oncogenic contexts could provide a therapeutic window to treat certain types of cancers. While KRAS and BRAF have been shown to be important driver mutations that require autophagy for their high metabolic needs and progression to the more

aggressive adenocarcinoma stage, more investigation is needed to find additional contexts in which autophagy should be targeted. Moreover, additional work to identify other driver mutations that affect this "autophagy addiction" is needed to better understand contexts that would (or would not) warrant autophagy inhibition for therapeutic purposes. Given the role that p53 status may play in dictating the response to autophagy inhibition in pancreatic cancer, more investigation is clearly needed to delineate these genetic considerations.

Therapeutic potential of targeting autophagy

Discovered by scientists at Bayer in 1934, the lysosomotropic agent chloroquine is a commonly used first line anti-malarial drug since its introduction as a prophylactic in 1947. Chloroquine is thought to exert its therapeutic effects by de-acidifying the lysosome of the parasite *Plasmodium falciparum* which require the degradative organelle in order to digest their food source - haemoglobin. Indeed, a point mutation in the *P. falciparum* chloroquine-resistance transporter gene (*PfCRT*) is associated with chloroquine-resistant falciparum malaria highlighting its role inhibiting the lysosome (Djimdé et al., 2001).

Given its role a lysosomotropic agent, chloroquine is commonly used in the laboratory to inhibit autophagic flux (Mizushima et al., 2010), and is one of the most well-characterized, widely used pharmacological inhibitors of autophagy. More importantly, chloroquine is FDA approved in humans and there are a number of clinical trials using chloroquine and its derivative, hydroxychloroquine, to target

autophagy in the context of cancer. Currently there are active and recruiting clinical trials evaluating the role of hydroxychloroquine in patients with advanced pancreatic cancer, Small Cell Lung Cancer, Multiple Myeloma, Glioblastoma Multiforme and breast cancer (ClinicalTrials.gov) Moreover, derivatives of chloroquine are being tested in combination with classic chemotherapeutics and targeted therapies such as sirolimus (also known as Rapamycin) in drug refractory advanced sarcomas.

Since chloroquine and its derivatives are general lysosomotropic molecules that are not autophagy specific, and can cause kidney damage when combined with chemotherapies (Kimura et al., 2013), more potent and specific autophagy inhibitors are needed for the treatment of various cancers.

Importantly, of the more than 30 ATGs identified to date, the only protein kinase in the cascade is ULK1/2. This kinase complex represents the most viable druggable option for a kinase inhibitor that would, in theory, inhibit the autophagy pathway at the most upstream component of the hierarchy.

Conclusions and future directions

The LKB1/AMPK signaling pathway lies at a crucial node of growth and metabolism. By sensing energy stress and enacting downstream growth and metabolic effectors, AMPK can rewire the cellular circuitry both through short-term acute regulation of enzymes, and long-term adaptation through transcription factors and gene expression. The discovery of the autophagy initiating kinase, ULK1, as a substrate of AMPK provides a direct mechanism for the loss of cellular ATP to trigger

the cytoprotective autophagy cascade as a means to restore energy balance by the liberation of metabolites both for the generation of more ATP and additional building blocks for macromolecules. We show that cell lines that express a mutant ULK1 which cannot be phosphorylated by AMPK display decreased autophagic flux and an inability to degrade damaged mitochondria as part of their normal life cycle, thus highlighting the importance of the phosphorylation in this signaling cascade.

Using the biological insight we have gleaned regarding the ULK1 pathway, we sought to characterize small molecule ATP-competitive inhibitors of ULK1 in order to not only better understand ULK1 function, but also to inhibit autophagy in vivo in different oncogenic contexts. We have established a pipeline to test these small molecules using phospho-specific antibodies against novel substrates of ULK1 that we have decoded in order to ascertain the efficacy of the molecules in live cells. These molecules will be the first-ever ATP-competitive kinase inhibitors of the autophagy cascade and will be instrumental in testing the requirement for autophagy in various oncogenic settings such as oncogene activation (such as KRAS and BRAF) and in combination therapy with clinically approved drugs that target the PI3K/mTOR pathway, glycolysis, or the proteasome.

Taken together these findings provide novel biological insight into the mechanistic regulation of the autophagy cascade. We provide the first direct evidence for the initiation of the ULK1 complex under energy stress by the energy sensor AMPK and show that it is required for proper autophagic flux under conditions of AMPK activation. We leveraged this data to screen for small molecules to target

ULK1 and autophagy, which could be the first class of drugs to specifically target the cascade at the first step using ATP-competitive kinase inhibitors.

Acknowledgements

This chapter contains excerpts from materials as it appears in Autophagy 2011 Jun;7(6):643-4. On this publication, I was the primary author. Reuben Shaw directed and supervised the writing which formed the basis of this chapter.

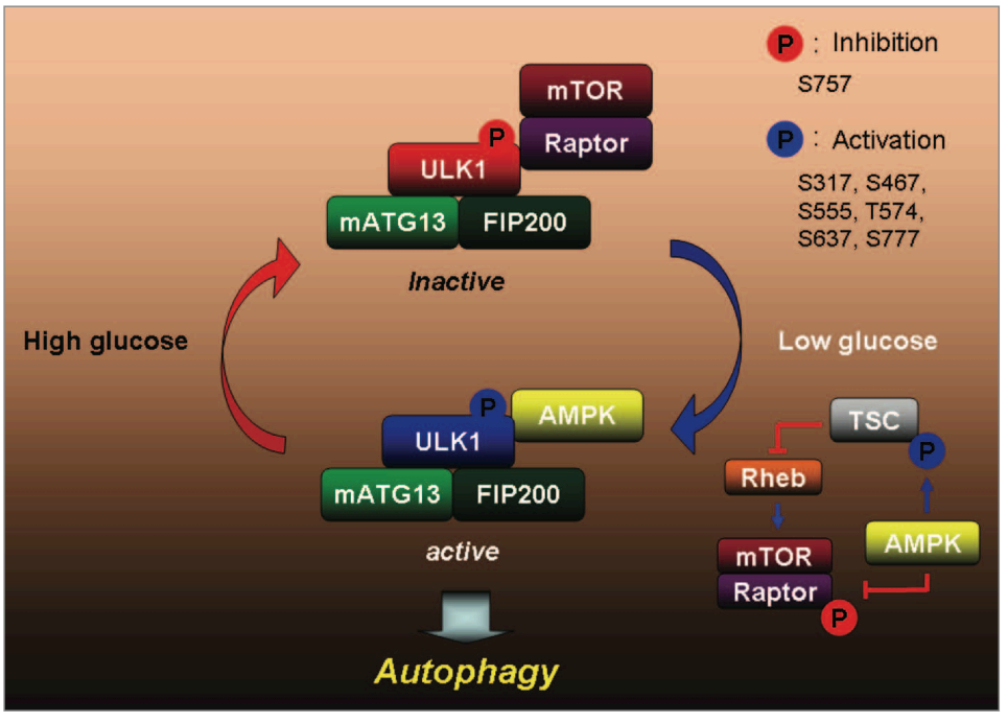

Figure 1.1: A proposed model for ULK1 regulation by AMPK and mTOR
When nutrients are plentiful, mTORC1 is active and inhibits ULK1 by phosphorylation thus preventing its interaction with AMPK. When nutrients are scarce, AMPK is activated and phosphorylates ULK1. The active AMPK inhibits mTORC1 by phosphorylating TSC2 and raptor, and stimulates ULK1 by directly phosphorylating it on multiple sites. The active ULK1 complex then initiates autophagy.

CHAPTER TWO:

Phosphorylation of ULK1 (hATG1) by AMP-Activated Protein Kinase Connects Energy Sensing to Mitophagy

Abstract

Adenosine monophosphate–activated protein kinase (AMPK) is a conserved sensor of intracellular energy activated in response to low nutrient availability and environmental stress. In a screen for conserved substrates of AMPK, we identified ULK1 and ULK2, mammalian orthologs of the yeast protein kinase Atg1, which is required for autophagy. Genetic analysis of AMPK or ULK1 in mammalian liver and Caenorhabditis elegans revealed a requirement for these kinases in autophagy. In mammals, loss of AMPK or ULK1 resulted in aberrant accumulation of the autophagy adaptor p62 and defective mitophagy. Reconstitution of ULK1-deficient cells with a mutant ULK1 that cannot be phosphorylated by AMPK revealed that such phosphorylation is required for mitochondrial homeostasis and cell survival during starvation. These findings uncover a conserved biochemical mechanism coupling nutrient status with autophagy and cell survival.

Introduction

A highly conserved sensor of cellular nutrient status found in all eukaryotes is the adenosine monophosphate (AMP)– activated protein kinase (AMPK). In response to decreases in intracellular ATP, AMPK is activated and serves as a metabolic checkpoint, restoring ATP levels through acute regulation of metabolic enzymes and inhibition of pro-growth anabolic pathways (Hardie, 2007). Inactivation of LKB1, the upstream kinase necessary for activation of AMPK under low-energy conditions, is a frequent event in several forms of human cancer (Shackelford and Shaw, 2009). In

addition, LKB1 signaling is required in the liver for the therapeutic effect of metformin, the most prevalent type 2 diabetes drug worldwide, and LKB1 inactivation in mouse liver results in a type 2 diabetes–like metabolic disease (Shaw et al., 2005). Thus the LKB1-AMPK pathway provides a direct link between tumor suppression and control of cellular and organismal metabolism.

Similar to AMPK activation, the cellular process of autophagy is initiated under nutrient-poor and low-energy conditions as a survival mechanism to ensure availability of critical metabolic intermediates and to eliminate damaged organelles, including mitochondria (Yang and Klionsky, 2009). Autophagy is thought to be initiated under nutrient-limited conditions by a conserved kinase complex containing the serine-threonine kinase Atg1 and its associated subunits, Atg13 and Atg17 (Mizushima, 2010). In mammals, this complex is encoded by two Atg1 homologs, ULK1 and ULK2, and the subunits Atg13 and FIP200, which signal to downstream autophagy regulators through still poorly understood mechanisms. In yeast and mammalian cells, Atg1 or ULK1 activity is suppressed under nutrient-rich conditions by the TOR (target of rapamycin) complex 1 (TORC1) (Chan, 2009). However, biochemical events that activate Atg1 or ULK1 have not yet been identified.

We used a two-part screen to identify substrates of AMPK that mediate its effects on cell growth and metabolism. First, we used an optimal AMPK substrate motif (Gwinn et al., 2008)to search eukaryotic databases for proteins containing conserved candidate target sites. Many in vivo substrates of AMPK not only conform to this motif but also bind to the phospho-binding protein 14-3-3 inducibly upon

phosphorylation by AMPK. We therefore screened for proteins that bound to recombinant 14-3-3 in wild-type (wt) but not AMPK-deficient cells, and only under conditions of energy stress, when AMPK would be active. One protein we identified that contained multiple conserved candidate AMPK phosphorylation sites and associated with 14-3-3 in an AMPK-dependent manner was the mammalian Atg1 homolog ULK1 (Figure 2.1 and Figure 2.2).

Results

ULK1 contains four sites (Ser467, Ser 555, Thr 574, and Ser637) matching the optimal AMPK substrate motif, all of which are conserved in higher eukaryotes. Two of the sites are conserved back to Caenorhabditis elegans (Ser 555 and Ser574) and in the mammalian family member ULK2, though not the more distant family members ULK3 and ULK4, which unlike ULK1 and ULK2 are not thought to function in autophagy. Indeed, endogenous AMPK subunits co-immunoprecipitated with ULK1 and ULK2 but not ULK3 (Figure 2.3), and AMPK subunits were found in unbiased identifications of proteins co- immunoprecipitating with overexpressed ULK2 (Figure 2.4), which is consistent with recent proteomic analyses (Behrends et al., 2010). To examine ULK1 in vivo phosphorylation sites, we used tandem mass spectrometry on epitope-tagged ULK1 isolated from cells treated with or without the mitochondrial complex I inhibitor phenformin (Hardie, 2006). We detected peptides spanning three of the four candidate AMPK sites in ULK1 (Ser 555, Thr 574, and Ser637), and all three were phosphorylated only after phenformin treatment (Figure

2.5 and Figure 2.6). To examine whether ULK1 could serve as a direct substrate for AMPK in vitro, we created a kinase- inactive allele (K46I) (Chang and Neufeld, 2009)to remove its autophosphorylation. AMPK phosphorylated ULK1 to a greater extent than it did an established substrate, Raptor (Figure 2.7), which may reflect the presence of at least four potential AMPK sites in ULK1, as compared with Raptor, which has two reported AMPK sites (Gwinn et al., 2008). We generated phosphospecific antibodies against Ser467 and Ser555 of ULK1. Phosphorylation of both sites was induced by means of phenformin treatment or expression of ULK1 with a constitutively active AMPKa1 allele (Crute et al., 1998)in the absence of energy stress (Figure 2.8). Purified AMPK also induced phosphorylation at these sites in an in vitro kinase assay, which is consistent with their direct phosphorylation (Figure 2.9). Using AMPK- and ULK1-deficient primary mouse embryonic fibroblasts (MEFs) or matched control wt MEFs, we observed phosphorylation of endogenous ULK1 on Ser555 in an AMPK-dependent manner after treatment of cells with the AMP-mimetic 5-Aminoimidazole-4-carboxamide ribonucleotide (AICAR) (Figure 2.10). The phosphorylation of ULK1 in these cells paralleled that of two bona fide AMPK substrates, acetyl-CoA carboxylase (ACC) and Raptor.

We examined the phenotypic consequences of AMPK or ULK1 deficiency on markers of autophagy in mouse liver and primary hepatocytes. Immunoblot and immunohistochemical analysis of AMPK-deficient livers (Andreelli et al., 2006) showed accumulation of the p62 protein (Figure 2.11 and Figure 2.12), whose selective degradation by autophagy has established it as a widely used marker of this

process(Mizushima et al., 2010). p62 contains a ubiquitin-associated (UBA) ubiquitin-binding domain, which mediates binding to ubiquitinated cargo targeted for autophagy-mediated degradation. Consistent with this function, p62 aggregates colocalized with ubiquitin aggregates in AMPK-deficient livers (Figure 2.12). p62 is recruited to mitochondria targeted for mitophagy and is involved in mitochondrial aggregation and clearance (Geisler et al., 2010). ULK1-deficient mice exhibit accumulation of defective mitochondria in mature red blood cells, which are normally devoid of mitochondria (Kundu et al., 2008). Given the aberrant accumulation of p62 in the absence of AMPK in mouse liver and the fact that rodent hepatocytes undergo substantial mitophagy upon culturing(Rodriguez-Enriquez et al., 2009), we examined whether AMPK or ULK1 deficiency in primary hepatocytes might exhibit mitochondrial defects. Protein levels of p62 and the mitochondrial marker protein CoxIV were similarly elevated in lysates from AMPK- or ULK1-deficient hepatocytes cells but not from wt controls (Figure 2.13). Increased phosphorylation of endogenous ULK1 Ser 555 was observed in wt but not AMPK-deficient hepatocytes after AMPK activation by metformin treatment (Figure 2.13). Further analysis of the ULK1 and AMPK hepatocytes by use of transmission electron microscopy (TEM) revealed elevated levels of abnormal mitochondria, which was analyzed quantitatively with morphometric software (Figure 2.14). Similar to findings in other autophagy-mutant hepatocytes (Martinez-Vicente et al., 2010), the number of mitochondria per cell was significantly increased in AMPK- and ULK1- deficient hepatocytes as compared with

that of wt controls (Figure 2.15), which is also seen with immunocytochemical staining for the mitochondrial membrane protein TOM20 (Figure 2.16).

Given the conservation of AMPK sites in ULK1, we examined whether these two proteins function together to play conserved roles in autophagy in the nematode C. elegans (strains in Table 2.1). In a reporter assay based on the C. elegans LC3 homolog LGG-1 (Meléndez et al., 2003), we observed that loss of insulin signaling through genetic mutation [daf-2 (e1370)] or RNA interference (RNAi) against the insulin receptor daf2 resulted in increased numbers of green fluorescent protein (GFP):: LGG-1–positive foci in hypodermal seam cells, which is indicative of increased autophagy and consistent with the established role for insulin signaling in the suppression of autophagy in C. elegans (Meléndez et al., 2003). daf-2 mutant worms treated with RNAi to aak-2 or unc-51, the AMPK and ULK1 orthologs, respectively, resulted in a decrease in abundance of LGG-1–containing puncta (Figure 2.17). daf-2 RNAi failed to increase the number of LGG-1–positive foci in AMPK-deficient worms (Figure 2.18). These data indicate that both AMPK and ULK1 have critical roles in autophagy induced by means of reduced insulin signaling in C. elegans. Transgenic worms expressing constitutively active AMPK exhibited an approximately threefold increase in the number of LGG-1–positive foci in seam cells as compared with the number of foci in controls (Figure 2.19). The number of LGG-1–positive foci was significantly reduced when these animals were fed unc-51 RNAi (Figure 2.20). These observations indicate that AMPK activation is sufficient to induce autophagy in worms, and ULK1 is required for this induction. To test whether

AMPK phosphorylation of ULK1 is required for ULK1 function, we stably introduced wt, catalytically inactive (ki), or the AMPK nonphosphorylatable (4SA) ULK1 cDNA into human osteosarcoma U2OS cells in which we subsequently reduced endogenous ULK1 and ULK2 with lentiviral short hairpin RNAs (shRNAs) against each (Figure 2.21). U2OS cells stably expressing ULK1 and ULK2 shRNA exhibited increased amounts of p62 indicative of defective autophagy as compared with that of parental U2OS cells infected with an empty lentiviral vector (Figure 2.22). Stable retroviral reconstitution of a Myc-tagged wt ULK1 cDNA, but not the 4SA or ki mutant, restored p62 degradation (Figure 22). Furthermore, we reconstituted ULK1$^{-/-}$ MEFs that were also knocked down for endogenous ULK2 (Figure 2.23) with wt, ki, or 4SA ULK1 cDNAs and examined the extent of autophagy after placement of these cell lines into starvation media. MEFs deficient for ULK1 and ULK2 contained elevated levels of p62 upon starvation. Cells reconstituted with wt ULK1 had reduced p62 levels, unlike the ki- or 4SA-expressing cells, which behaved like the ULK-deficient state (Figure 2.24). To test whether the 4SA mutant exhibited effects on mitochondrial homeostasis, we used TEM and mitochondrial-selective dyes on the wt, ki, and 4SA ULK1 stably reconstituted ULK-deficient MEFs. TEM and Mitotracker Red staining revealed that the ki- and 4SA-ULK1– expressing cells had altered mitochondrial homeostasis as compared with that of wt ULK1 cells, denoted by increases in the overall number and aberrant morphology of mitochondria (Figure 2.25 and Figure 2.26). The altered cristae and aberrant morphology of the mitochondria in the ki- and 4SA-ULK1–reconstituted cells was enhanced upon starvation (Figure

2.27). To test whether these mitochondria were functionally impaired, we analyzed the mitochondrial membrane potential with the activity-dependent JC-1 dye, which revealed defects in ki- and 4SA-reconstituted MEFs (Figure 2.28).

A hallmark of cells defective for autophagy is a predisposition to undergo apoptosis after stress stimuli that normally would activate autophagy to promote cell survival (Levine and Kroemer, 2008). We examined how ULK1/2 deficiency would compare with loss of central downstream autophagic regulator such as Atg5 in terms of requirement for cell survival after starvation. wt MEFs were treated with control, Atg5, or combined ULK1 and ULK2 small interfering RNA (siRNA) and analyzed for effects on cell viability after being placed into starvation conditions. Simultaneous depletion of ULK1 and ULK2 (Figure 2.29) mirrored the magnitude and kinetics of cell death observed with Atg5 loss upon starvation (Figure 2.30). We next investigated whether mutation of the AMPK sites in ULK1 might also mimic ULK1/2 loss of function in this cell survival assay. ULK-deficient MEFs reconstituted with wt, but not ki or 4SA ULK1, restored cell survival upon starvation (Figure 2.31). ULK1-deficient cells expressing the ki or 4SA mutant ULK1 showed rates of cell death similar to those of wt MEFs treated with Ulk1 and Ulk2 siRNA. Thus, loss of the AMPK sites in ULK1 mimics complete loss of ULK1 and ULK2 in control of cell survival after nutrient deprivation.

Discussion

Our findings reveal a direct connection between energy sensing and core conserved autophagy proteins. In mammals, phosphorylation of ULK1 by AMPK is

required for ULK1 function in the response to nutrient deprivation. Because AMPK suppresses mammalian TOR (mTOR) activity and mTOR inhibits ULK1 (Hosokawa et al., 2009; Jung et al., 2009), AMPK controls ULK1 via a two-pronged mechanism, ensuring activation only under the appropriate cellular conditions (Figure 2.35). There are a number of physiological and pathological contexts in which this pathway is likely to play a critical role (Nakada et al., 2010). Beyond the conserved nature of these signaling events and the role of some autophagy genes as tumor suppressors (Mathew and White, 2011), AMPK is defective in a variety of human cancers bearing inactivating mutations in its upstream kinase LKB1. Thus, ULK1 may have a central role in the beneficial effects of the LKB1/AMPK pathway on tumor suppression or in treatment of metabolic disease, as observed here with metformin stimulation of ULK1 phosphorylation in liver and the profound defect in autophagy in AMPK-deficient livers. ULK1-dependent effects on mitochondrial homeostasis and cell survival may represent additional beneficial effects of metformin and other AMPK activators in overall organismal health and life span (Fogarty and Hardie, 2010).

Experimental Procedures

Plasmids

The cDNA encoding human Atg13 (KIAA0652/AB014552) was obtained from Kazusa DNA Research Institute in Japan. The cDNAs for human FIP200, mouse ULK1, and mouse ULK2 constructs were obtained from Open Biosystems (clones 3908134, 6834534, and 5709559 respectively). Human Atg101 was obtained from Invitrogen (60673). The Myc tag and attL1 sites (for BP reaction) were PCR'd to the N-term of ULK1 using the standard procedure. cDNAs were subcloned into pDONR221 with BP clonase (Invitrogen), and site-directed mutagenesis was performed using QuikChange II XL (Stratagene). Kinase dead ULK1 was achieved by a K46I mutation. Wild type and mutant alleles in pDONR221 were sequenced in their entirety to verify no additional mutations were introduced during PCR or mutagenesis steps and then put into either mammalian expression pDest15 GST bacterial expression vector, pcDNA3 Myc mammalian expression vector, or pcDNA6.2 V5 dest (Invitrogen), or pQCXIN retroviral destination vector (Addgene 17399) by LR reaction (Invitrogen). AMPK and GST-14-3-3 constructs were described previously.

Antibodies and reagents

Cell Signaling Antibodies used: pAMPK Thr172 (#2535), total AMPK alpha1(#2532), total AMPK beta 1/2 (#4150), pACC Ser79 (#3661), pRaptor Ser792 (#2083), phospho ULK1 (#4634), total ULK1 (#4776), ubiquitin (#3933), pS6K (9205), total S6 (2217), total Raptor (#2280), LKB1 (#3050), Myc (#2278), Myc

(#2276), GST (#2622), LC3B (#3868). Abgent antibodies used: gabarap (PM037). Total ULK1 from Sigma (A7481). Guinea pig anti p62 sequestosome antibody from Progen, Heidelberg Germany (03-GPP62-C). TOM20 antibody from Santa Cruz (FL-145). Phospho ULK1 serine 555 was developed in collaboration with Gary Kasof at Cell Signaling Technology. GSH sepharose from GE Healthcare. Active recombinant AMPK were obtained from Millipore. AICAR was obtained from Toronto Research Chemicals. Phenformin, Chloroquine and Metformin from Sigma. EBSS, Medium199 for primary hepatocytes and Protein G sepharose from Invitrogen. A769662 from Abbot labs. Mitotracker Red CMXRos from Invitrogen. Annexin V-PE Apoptosis Detection Kit from BD Biosciences, and JC-1 dye from Molecular Probes. STO-609 from VWR. TPP plates for primary hepatocytes from Light Lab Systems.

shRNA target sequences:

TRC lentiviral shRNAs targeting ULK1 or ULK2 were obtained from Sigma.

Human ULK1 shRNA #5: TRCN0000000835

Human ULK1 shRNA #6: TRCN0000000836

Human ULK1 shRNA #7: TRCN0000000837

Human ULK1 shRNA #8: TRCN0000000838

Human ULK1 shRNA #9: TRCN0000000839

Human ULK2 shRNA #89: TRCN0000000889

Human ULK2 shRNA #90: TRCN0000000890

Human ULK2 shRNA #91: TRCN0000000891

Human ULK2 shRNA #92: TRCN0000000892

Human ULK2 shRNA #93: TRCN0000000893

Mouse ULK2 shRNA #20: TRCN0000278670

Mouse ULK2 shRNA #38: TRCN0000278671

Mouse ULK2 shRNA #65: TRCN0000026765

Mouse ULK2 shRNA #93: TRCN0000026693

Mouse ULK2 shRNA #95: TRCN0000026695

Cell Culture and Transfection

HEK293T, U2OS, and mouse embryonic fibroblast (MEF) cells were cultured in DMEM containing 10% fetal bovine serum (HyClone) and penicillin/streptomycin at 37°C in 5% CO_2. For transient expression of proteins and packaging of virus, HEK293T cells were transfected with DNA or short hairpin RNA (shRNA) plasmids using Lipofectamine 2000 (Invitrogen) following the manufacturer's protocol. SV40 immortalized wild-type and AMPKa1-/-, a2-/- double knockout MEFs were obtained from Keith Laderoute with permission from Benoit Viollet(Laderoute et al., 2006). SV40 immortalized wild-type and ULK1 knockout MEFs were obtained from Mondira Kundu(Kundu et al., 2008).

Lenti- and retro-viral Preparation and Viral Infection

Lentiviral shRNA transduction and retroviral gene expression was performed as described previously(Gwinn et al., 2008). Briefly, the pQCXIN Myc ULK1 construct was transfected along with the ampho packaging plasmid into growing 293Ts. Virus-containing supernatants were collected 48 hours after transfection, filtered to eliminate cells and target $ULK1^{-/-}$ MEFs or U2OS were infected in the presence of polybrene. 24 hours later, cells were selected with neomcyin. The pLKO shRNA vectors encoding shRNAs were transfected into HEK293T cells with lentiviral packaging plasmids vsvg, GAG/pol, and REV using Lipofectamine 2000. Viruses were collected 48 hours after transfection, and MEFs (shRNA #93 against mULK2) and U2OS (shRNA #8 and #91 against hULK1 and hULK2 respectively) already stably expressing Myc ULK1 were infected with the collected viruses for 4 h in the presence of polybrene to knock down the endogenous human protein, but not Myc ULK, which is mouse.

Cell lysis, immunoprecipitations, and mammalian autophagy analysis

Cells were harvested 24 hours after transfection for coimmunoprecipitation assay and Western blot analysis. Cells were rinsed once with ice-cold PBS and lysed in ice-cold lysis buffer (20mM Tris pH 7.5, 150mM NaCl, 1mM EDTA, 1 mM EGTA, 1% Triton X-100, 2.5 mM pyrophosphate, 50 mM NaF, 5 mM b-glycero-phosphate, 50 nM calyculin A, 1 mM Na3VO4, and proteased inhibitors (Roche). The soluble fractions of cell lysates were isolated by centrifugation at 13,000 rpm for 10 minutes. For immunoprecipitations, primary antibodies were added to the lysates and

incubated with rotation for 1.5 hours at 4°C. 60 µl of a 50% slurry of protein G-sepharose was then added and the incubation continued for an additional 1 hour. Immunoprecipitates were washed three times with cold lysis buffer before addition of sample buffer. Immunoprecipitated proteins were denatured by the addition of 20 µl of sample buffer and boiling for 5 minutes, resolved by 8%–16% SDS-PAGE, and analyzed by immunoblotting as described. For analysis of autophagy by western blots, cells were plated at a density of $2.0x10^5$ per dish in 6cm dishes and grown in DMEM plus 10% FBS, penicillin, and streptomycin. Twenty hours after plating, cells were then treated with vehicle (fresh media), 5 mM phenformin (Sigma), 100uM A769662, 1 mM metformin or starvation (EBSS) for the indicated times with or without chloroquine and lysed in boiling lysis buffer (10mM Tris pH7.5, 100mM NaCl, 1% SDS). After trituration, lysates were equilibrated for protein levels using the BCA method (Pierce) and resolved on 6 to 12% SDS-PAGE gels, depending on the experiment.

AMPK and ULK1 Kinase Assays

Gamma 32P assays to measure ULK1 kinase activity were performed as previously described(Jung et al., 2009). Briefly, Myc ULK1 was transfected into 293Ts and 20 hours later treated as indicated. The immmunoprecipitate was washed in IP buffer 3 times, and washed in kinase buffer (25 mM MOPS, pH 7.5, 1 mM EGTA, 0.1 mM Na_3VO_4, 15 mM $MgCl_2$,). Hot and cold ATP were added at a 100 µM final concentration. As substrates, GST or the recombinant protein GST-Atg101

purified from *E. coli* were used at 1 μg for each reaction. Reactions were boiled, run out on SDS page gel. The gel was dried, and imaged using PhosphoImager software. For cold assays to asses AMPK activity on ULK1, recombinant, active AMPK (Millipore) added to Myc ULK1 which was transiently overexpressed and immunoprecipited from 293T cells. Reactions were then run out on SDS page gel, transferred to PVDF membrane and blotted with a phospho-specific antibody against either serine 467 or 555 of ULK1.

Fluorescence Microscopy

MEFs reconstituted with Myc ULK1 were plated on glass coverslips at a density of $3x10^5$ cells per well in 6-well tissue culture plates. 18h later, cells were fixed in 4% PFA in PBS for 10 minutes and permeabilized in 0.2% Triton in PBS for 10 minutes. The following primary antibodies were used: mouse anti-Myc epitope and LC3B XP antibody (2276 and 3868 respectively, Cell Signaling Technologies). Secondary antibodies were anti-rabbit Alexa488 and anti-mouse Alexa594 (Molecular Probes, 1:1000). Mitotracker Red (Invitrogen) used at 50 nM for 15 minutes to stain live cells. Cells were then fixed and counter stained with DAPI. Coverslips were mounted in FluoromountG (SouthernBiothech). Images were acquired on a Zeiss Axioplan2 epifluorescence microscope coupled to the Openlab software. Confocal images of mitotracker were taken on Zeiss LSM 710 laser scanning confocal microscope. 10 random fields per condition were acquired using the 100x objective and representative images shown. Primary hepatocytes were isolated from $ULK1^{-/-}$,

AMPKa1$^{-/-}$, a2$^{-/-}$ double knockout, or matched wt littermates and the cells were plated to confluency on TPP plates, grown for 48 hours and washed with PBS and fixed in 4% cold PFA 20 hours later. TOM20 (FL-145) used according to the manufacturers instructions at 1:200 overnight incubation at 4 degrees. Glass coverslips were mounted directly on plate with FluoromountG and images taken on Zeiss Axioplan2 epifluorescence microscope.

Electron Microscopy

Primary hepatocytes grown on TPP plates or MEFs grown in 60mm plastic culture dishes were fixed in 2.5% glutaraldehyde in 0.1M Na cacodylate buffer (pH7.3), washed and fixed in 1% osmium tetroxide in 0.1M Na cacodylate buffer. They were subsequently treated with 0.5% tannic acid followed by 1% sodium sulfate in cacodylate buffer and then dehydrated in graded ethanol series. The cells were transitioned in HPMA (2-hydroxypropyl methacrylate: Ladd Research, Williston VT) and embedded in LX112 resin. Following overnight polymerization at 60 degrees C, small pieces of resin were attached to blank blocks using SuperGlue. Thin sections (70nm) were cut on a Reichert Ultracut E (Leica, Deerfield, IL) using a diamond knife (Diatome, Electron Microscopy Sciences, Hatfield PA), mounted on parlodion coated, copper, slot grids and stained in uranyl acetate and lead citrate. Sections were examined on a Philips CM100 TEM (FEI, Hillsbrough, OR) and data documented on Kodak SO-163 film for later analysis. Alternatively the samples were documented on an Olympus- SIS Megaview III CCD camera (Lakewood, CO).

Mass Spectrometry

Myc ULK1 overexpressed in 293T cells was treated with either vehicle, A769662, or phenformin, IP'd with anti Myc antibody (Cell Signaling), run out on SDS page gel and coomassie stained. Bands on the gel corresponding to ULK1 were cut out and subjected to reduction with dithiothreitol, alkylation with iodoacetamide, and in-gel digestion with trypsin or chymotrypsin overnight at pH 8.3, followed by reversed-phase microcapillary/tandem mass spectrometry (LC/MS/MS). LC/MS/MS was performed using an Easy-nLC nanoflow HPLC (Proxeon Biosciences) with a self-packed 75 μm id x 15 cm C_{18} column coupled to a LTQ-Orbitrap XL mass spectrometer (Thermo Scientific) in the data-dependent acquisition and positive ion mode at 300 nL/min. Peptide ions from AMPK predicted phosphorylation sites were also targeted in MS/MS mode for quantitative analyses. MS/MS spectra collected via collision induced dissociation in the ion trap were searched against the concatenated target and decoy (reversed) single entry ULK1 and full Swiss-Prot protein databases using Sequest (Proteomics Browser Software, Thermo Scientific) with differential modifications for Ser/Thr/Tyr phosphorylation (+79.97) and the sample processing artifacts Met oxidation (+15.99), deamidation of Asn and Gln (+0.984) and Cys alkylation (+57.02). Phosphorylated and unphosphorylated peptide sequences were identified if they initially passed the following Sequest scoring thresholds against the target database: 1+ ions, Xcorr ≥ 2.0 Sf ≥ 0.4, P ≥ 5; 2+ ions, Xcorr ≥ 2.0, Sf ≥ 0.4, P ≥ 5; 3+ ions, Xcorr ≥ 2.60, Sf ≥ 0.4, P ≥ 5 against the target protein database. Passing MS/MS spectra were manually inspected to be sure that all b- and y- fragment ions

aligned with the assigned sequence and modification sites. Determination of the exact sites of phosphorylation was aided using FuzzyIons and GraphMod and phosphorylation site maps were created using ProteinReport software (Proteomics Browser Software suite, Thermo Scientific). False discovery rates (FDR) of peptide hits (phosphorylated and unphosphorylated) were estimated below 1.5% based on reversed database hits.

Relative Quantification of Phosphorylation Sites

For relative quantification of phosphorylated peptide signal levels, an isotope-free (label-free) method was used by first integrating the total ion counts (TIC) for each MS/MS sequencing event during a targeted ion MS/MS (TIMM) experiment or a data-dependant acquisition. For each targeted phosphorylation site, a ratio of phosphorylated peptide signal (TIC of phosphorylated form) to the total peptide signal (TIC of phosphorylated form + TIC of non-phosphorylated form) for both the insulin and insulin plus rapamycin treated samples were calculated according to the following equation:

$TIC_{PO4}/(TIC_{PO4}+TIC_{nonPO4})$ = *Ratio of phosphopeptide signal* (R_{PO4})

These ratios of phosphopeptide signal were then compared to the same phosphopeptide ratios from the unstimulated samples according to the following equation:

$[(R_{PO4}Unstimulated/R_{PO4}Stimulated)-1] \times 100$ = *% change in phosphorylation level upon treatment*

While a direct comparison of phosphopeptide signals between different experimental conditions is not accurate due to differences in sample content, a comparison of the relative ratios of the phosphorylated to non-phosphorylated peptide forms between samples is an accurate measure of signal-level change since the total peptide signal (modified and unmodified) is measured. The above calculations were performed manually using Microsoft Excel and with automated in-house developed software named Protein Modification Quantifier v1.0 (Beth Israel Deaconess Medical Center, Boston, MA).

Tissue Isolation

Experimental mice were cervically dislocated and liver and muscle were harvested immediately and either processed for histological analysis (10% formalin) or frozen in liquid nitrogen for molecular studies. These samples were then placed frozen into Nunc tubes, pulverized in liquid nitrogen, and homogenized in lysis buffer (20mM Tris pH 7.5, 150mM NaCl, 1mM EDTA, 1 mM EGTA, 1% Triton X-100, 2.5 mM pyrophosphate, 50 mM NaF, 5 mM -glycero-phosphate, 50 nM calyculin A, 1 mM Na3VO4, 10 mM PMSF, 4 μg/ml leupeptin, 4 μg/ml pepstatin, 4 μg/ml aprotinin) on ice for 30s using a tissue homogenizer. Total protein was normalized using BCA protein kit (Pierce) and lysates resolved on SDS-PAGE gel.

Flow Cytometry:

Cells were seeded at a concentration of 2.5 x 10^5 cells/mL, grown overnight (18hrs) and treated with Vehicle (DMEM + 10%FBS) or EBSS. Cells were collected at the appropriate time point, washed once in PBS, trypsinized and spun. For the JC-1 staining cells were resuspended in 1mL DMEM + 10% FBS, and stained with 2μM JC-1 dye (Molecular Probes) at 37°C for 20 minutes in the dark. Cells were washed once and resuspended in 500μL staining buffer (PBS + 3% FBS). For Annexin V staining, cells were washed in 1x Annexin V buffer and treated as described by the Annexin V staining protocol (BD Pharmingen, San Diego, CA). Briefly, cells were resuspended in Annexin V buffer to a concentration of one million per mL, 100,000 cells were then stained with 5 μL of phycoerythrin (PE)-conjugated Annexin V antibody (BD Pharmingen, San Diego, CA) and 5 μL of 7-amino-actinomycin D (7AAD) and then incubated at room temperature for 15 minutes. 400μL of Annexin V buffer was then added to each sample with gentle mixing. Stained cells were analyzed using a FACScan flow cytometer (Becton Dickinson, San Jose, CA). Flow cytometry data was analyzed using FlowJo 8.6 software (Tree Star Inc., Ashland, OR).

Histology and Immunohistochemistry.

Mouse tissues were fixed in 10% formalin overnight and embedded in paraffin. For immunohistochemistry, slides were deparaffinized in xylene and ethanol and rehydrated in water. Heat mediated antigen retrieval using sodium citrate pH 6.0 buffer and slides were quenched in hydrogen peroxide (3%) to block endogenous peroxidase activity and washed in TBST buffer. Slides were blocked in 5% normal

serum for 1 hr at room temperature and incubated with primary antibody diluted in blocking buffer, washed and a secondary biotinylated goat-anti mouse IgG antibody was applied. The avidin-biotin peroxidase complex method (Vector, Birlingame, CA) was used and staining was visualized using the DAB chromophore (Vector ABC; DAB). Slides were counterstained with hematoxylin and mounted with Fluoromount (SoutherBiotech, Birmingham, AL). The anti-ubiquitin (P4D1) (Cell Signaling Technology, Beverly, MA 1:750) and anti-p62 (Progen, Heidelberg Germany 1:200) antibodies were diluted according to manufacturer's suggestions.

Analysis of autophagic events in *C. elegans.*

The level of autophagy in various mutant strains was assessed using a GFP::LGG-1/LC3 translational reporter, which was originally constructed and described in (Meléndez et al., 2003). The strains used in this study were MAH14 (*daf-2(e1370) III; adIs2122[lgg-1p::GFP:LGG-1 + rol-6]),* MAH28 *(aak-2(ok524) X; adIs2122[lgg-1p::GFP::LGG-1 + rol-6],* and AGD383 (*uthIs202[aak-2cp::AAK-2(aa1-321)::Tomato + rol-6*]) crossed to DA2123(Kang et al., 2007)to obtain F1 heterozygous animals. AAK-2 gain of function expression construct consisted of the 3KB putative promoter region 5' to the *aak-2*c (T01C8.1c) start site driving cDNA sequence corresponding to AAK-2 aa 1-321. Expression construct backbone was based upon pPD95.77 from the Fire lab *C. elegans* vector kit with tdTOMATO in place of GFP. Transgenic strains were generated via microinjection into the gonad of adult hermaphrodites using standard techniques with pRF4 *rol-6 (su1006)* a

transformation marker. Integrated transgenic lines were generated using gamma irradiation and out-crossed to wild type (N2) animals four times. GFP-positive foci/puncta were counted as described earlier(Hansen et al., 2008). In brief, GFP-positive foci were counted (using 1000-fold magnification on a Zeiss Axioplan II microscope) in the seam (lateral epidermal) cells of L3 transgenic animals, which were staged by gonad morphology and germline developmental phenotype. Between 3-10 seam cells were examined in each of 8-30 animals from at least two independent trials and averaged. Data analysis was done using unpaired, two-tailed *t*-test. When performing RNAi experiments to count GFP-positive foci, young adults were fed the RNAi bacteria, and the L3 progeny of their progeny ("F2 generation") were examined. In all cases, animals were raised at 20ºC. RNAi clones were from Julie Ahringer's RNAi library(Kamath et al., 2003)or Marc Vidal's RNAi library(Rual et al., 2004).

Acknowledgements

We thank L. Gerken for mouse colony assistance, F. Esterman for confocal assistance, C. Chu for assistance in scoring LGG-1 assays, M. Wood at The Scripps Research Institute EM facility, X. Yang in the Beth Israel Deaconess Medical Center mass spectometry facility, R. Chitta from St. Jude's proteomic core, and K. Lamia for comments on the manuscript. D.F.E., D.M.G., and M.M.M. were supported through the T32 CMG training grant to the UCSD-Salk Biological Sciences Graduate Program. D.B.S. was funded by T32 CA009370 to the Salk Institute Center for Cancer Research. R.J.S. is funded by the NIH grants R01 DK080425 and 1P01CA120964, National Cancer Institute grant P30CA014195, an American Cancer Society Research Scholar Award, the American Diabetes Association Junior Faculty Award 1-08-JF-47, and a Howard Hughes Medical Institute Early Career Scientist Award. J.M.A. is supported by grants 5P30CA006516-43 and 1P01CA120964-01A. M.K. is funded by grant NHBLI K08, Burroughs Welcome Fund, and the American Lebanese Syrian Association. B.V. is supported by Agence Nationale de la Recherche (ANR). M.H. is an Ellison Medical Foundation New Scholar in Aging. We also thank the Leona M. and Harry B. Helmsley Charitable Trust for their generous support. Several of the authors (D.F.E., D.B.S., M.M.M, and R.J.S.) have filed a patent related to this work (U.S. patent application 61/325361). Chapter Two contains excerpts from material as it appears in: Egan, D.F., Shackelford, D.B., Mihaylova, M.M., Gelino, S., Kohnz, R.A., Mair, W., Vasquez, D.S., Joshi, A., Gwinn, D.M., Taylor, R., Asara, J.M., Fitzpatrick, J., Dillin, A., Viollet, B., Kundu, M., Hansen, M.,

Shaw, R.J. (2011). Phosphorylation of ULK1 (hATG1) by AMP-activated protein kinase connect energy sensing to mitophagy. Science 331(6016), 456-461. On this publication, I was the primary author. Reuben Shaw directed and supervised the writing and oversaw the project which formed the basis of this chapter.

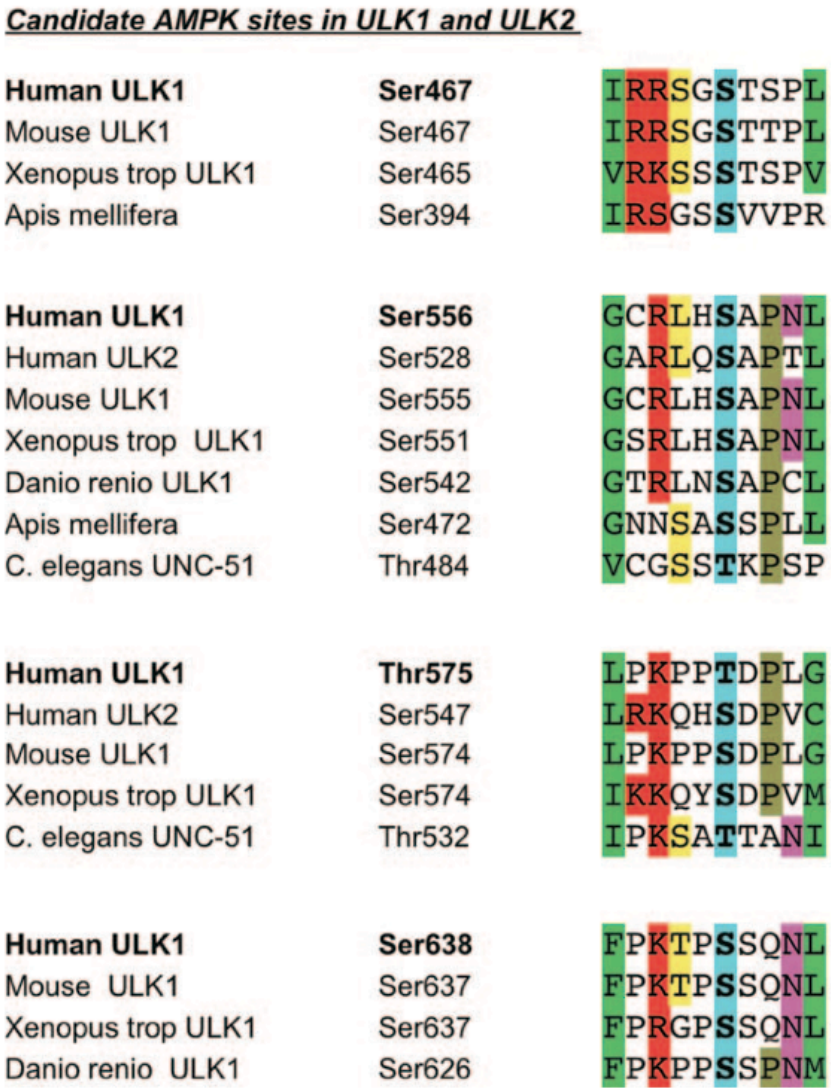

Figure 2.1: Putative AMPK sites in ULK1 are conserved across evolution
Clustal alignment of four conserved sites in ULK1 and two sites in ULK2 matching the optimal AMPK substrate motif.

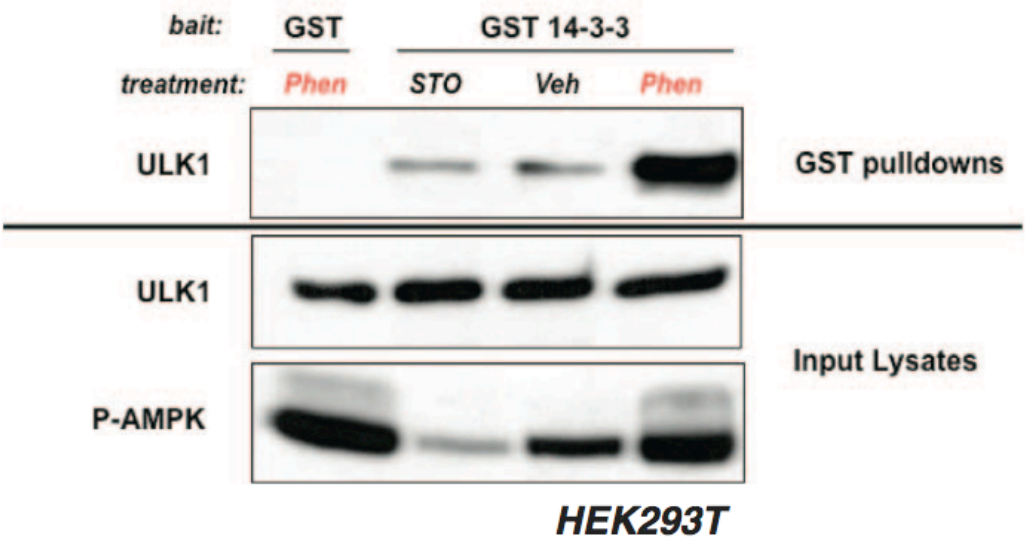

Figure 2.2: Activation of AMPK with mitochondrial inhibitor phenformin induces ULK1 binding to 14-3-3

ULK1 and glutathione S-transferase (GST) or GST- 14-3-3 expression vectors were transfected into human embryonic kidney (HEK) 293T cells, and placed in media containing 20 mM STO-609 (STO), vehicle (veh), or 5 mM phenformin (Phen) for 1 hour. Cell lysates and GST pulldowns were immunoblotted as indicated.

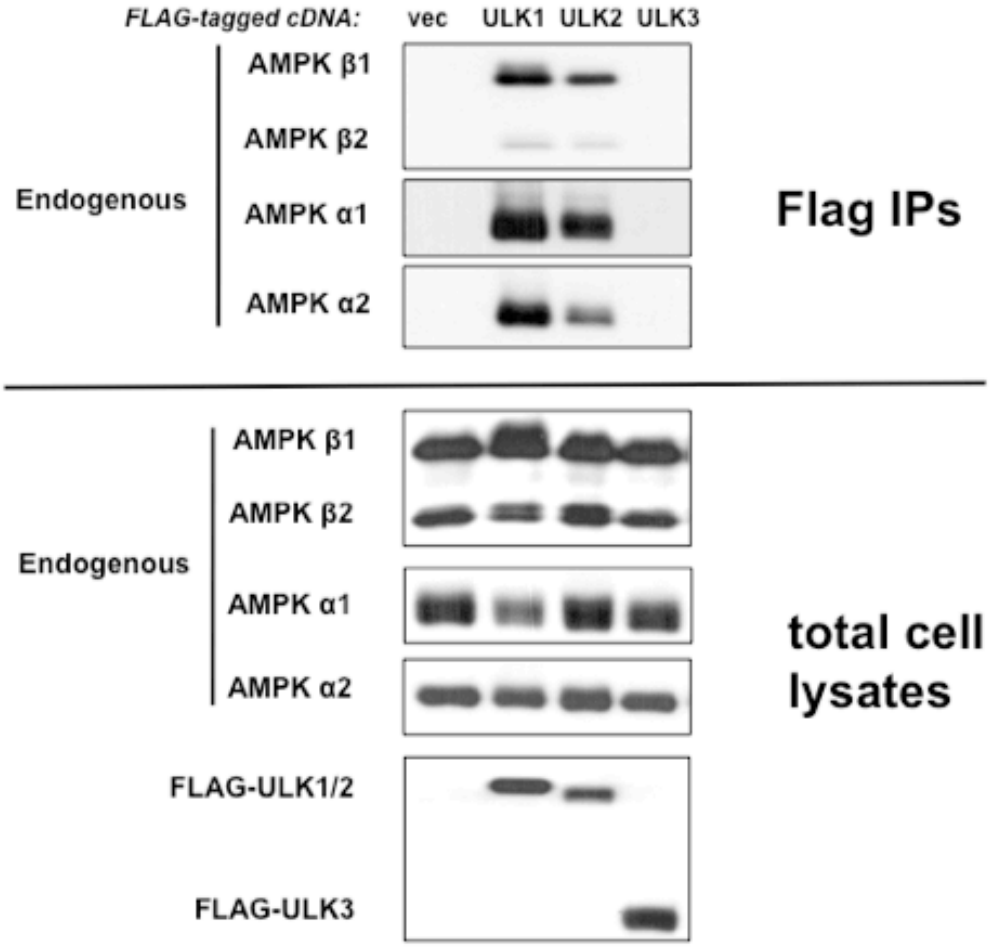

Figure 2.3: ULK1 and ULK2, but not ULK3 co-immunoprecipitate with endogenous AMPK

Immunoprecipitates of Flag-tagged ULK1, ULK2, ULK3 or empty Flag- tagged vector (vec) transfected in HEK-293T cells were immunoblotted for endogenous AMPK subunits as indicated.

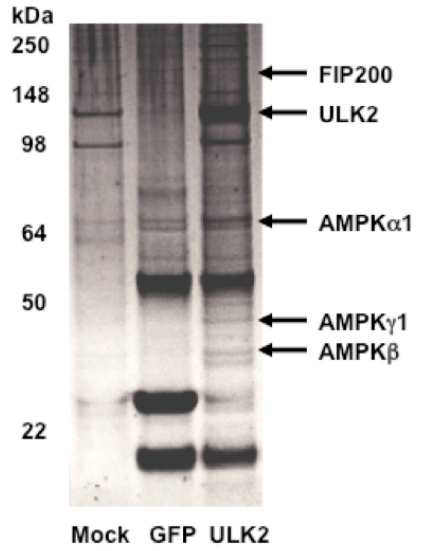

Protein ID by MS	Mascot score	# peptides
ULK2	3873	29 peptides
FIP200	138	5 peptides
AMPKα1	182	2 peptides
AMPKβ1	118	3 peptides
AMPKβ2	53	1 peptide
AMPKγ1	288	4 peptides

Figure 2.4: Identification of endogenous AMPK as an interacting partner of ULK2

Eluted Flag-tagged ULK2 immunoprecipitates from HEK-293T cells were resolved on SDS- PAGE and lanes 1 (mock transfected) and 3 (ULK2) of SuproRuby stained gel shown were sliced into 25 fragments each and analyzed by tandem mass spectrometry. Endogenous FIP200 as well as the indicated AMPK subunits were uniquely found in the ULK2 immunoprecipitates and bands corresponding to each in the ULK2 lanes are indicated. Mascot scores are indicated as well as number of unique peptides analyzed.

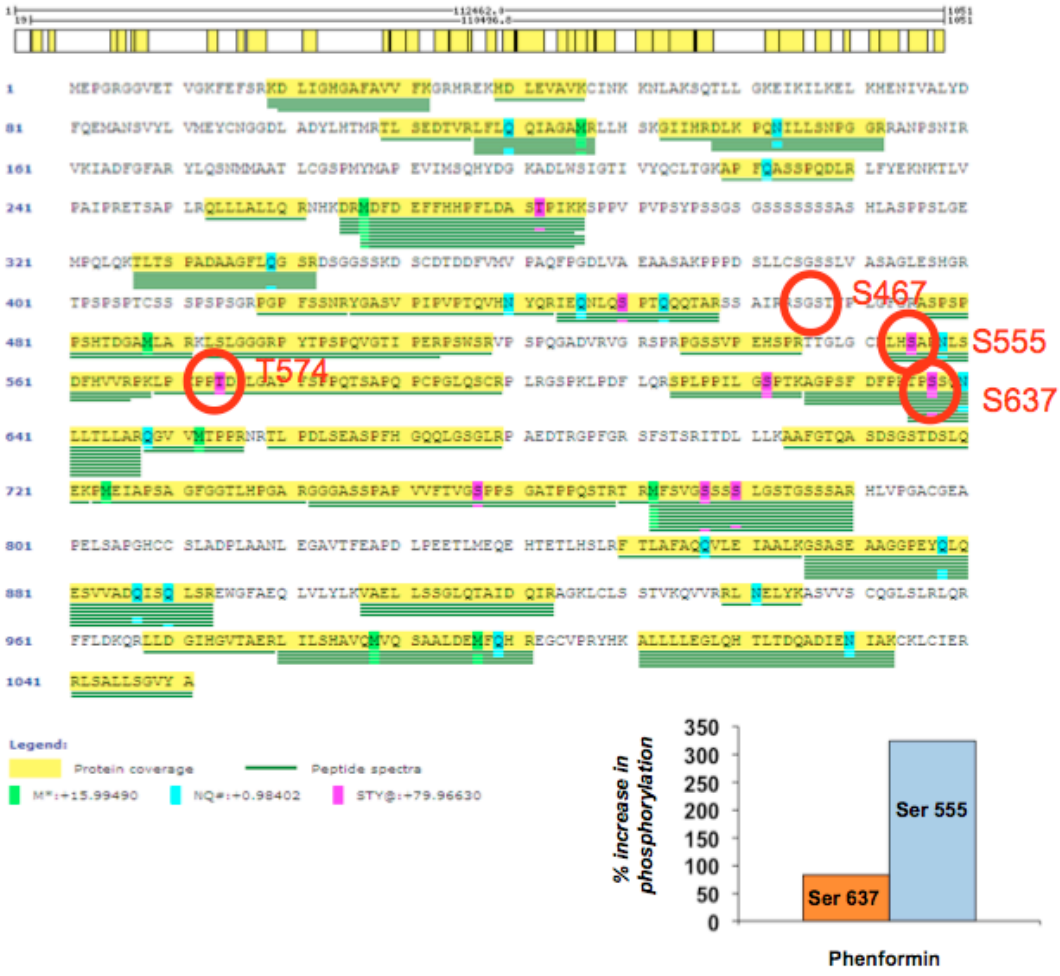

Figure 2.5: Diagram of all LC/MS/MS identified in vivo phosphorylation sites in human ULK1

Top: Myc-ULK1 was transfected into human embryonic kidney (HEK)-293T cells, treated with 5 mM phenformin to reduce cellular ATP for 1 hour and immunoprecipitated with anti Myc antibody. The IP was run out on SDS PAGE, stained with coomassie, and the band corresponding to Myc- ULK1 was cut out, isolated and subjected to tryptic digest and LC/MS/MS analysis. Three indicated sites matching the AMPK substrate motif were identified, all mapping to the serine – rich unstructured region between the N-terminal kinase domain and the conserved C-terminus that mediates ULK1 binding to its subunits Atg13 and FIP200. Bottom: Quantitative mass spec spectrometry (MS/MS TIC ratio quantification) reveals that tryptic peptides containing Phospho- Ser555 and Phospho-Ser637 of ULK1 are induced by treatment of HEK-293T cells with 5mM phenformin for 1h.

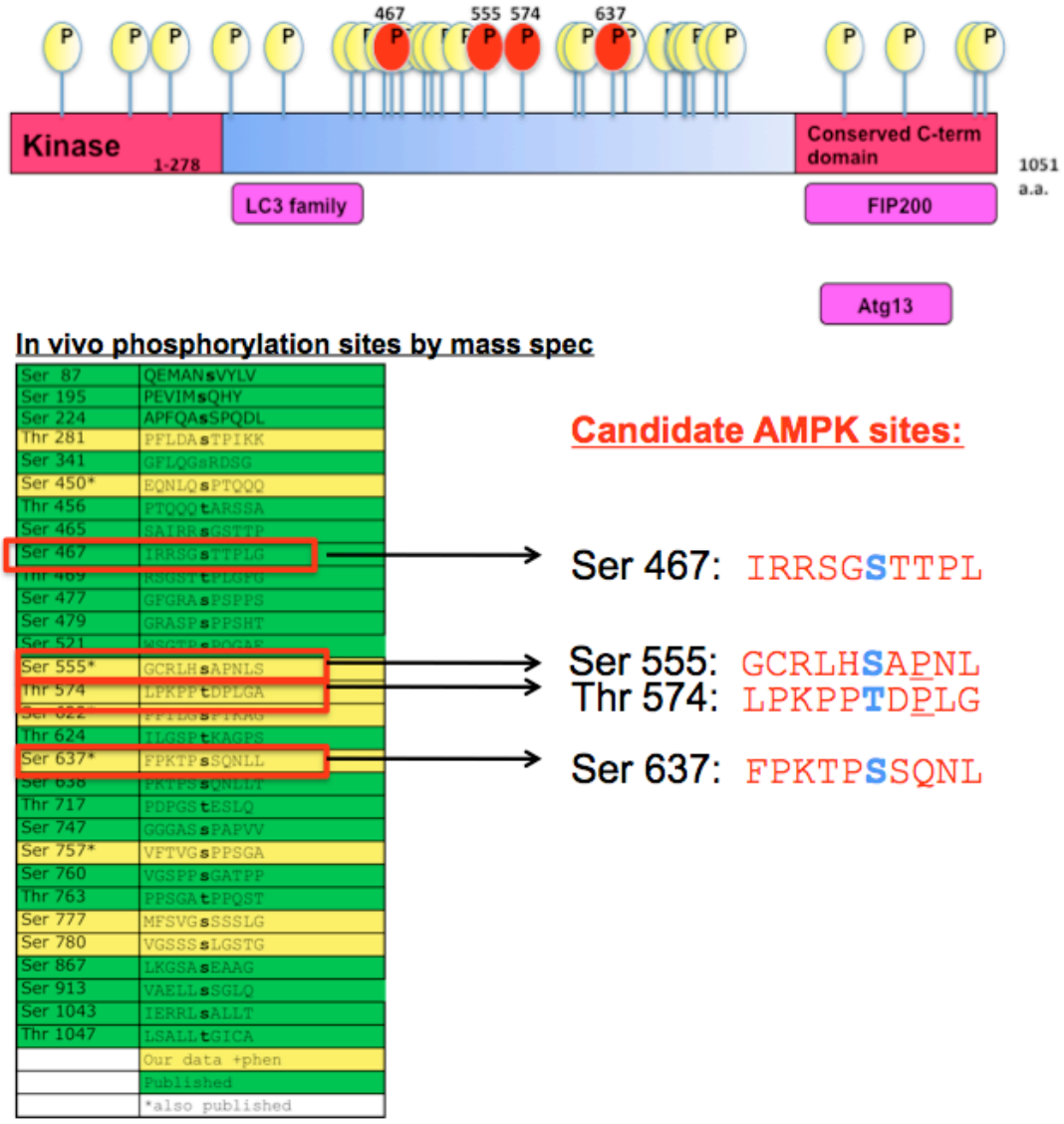

Figure 2.6: Schematic of potential AMPK-dependent phosphorylation sites in ULK1

Results from Figure 9 shown along with previously published data. Previously published sites (www.Phosphosite.org) indicated in green and sites identified in this work as being enriched in phenformin treated samples in yellow.

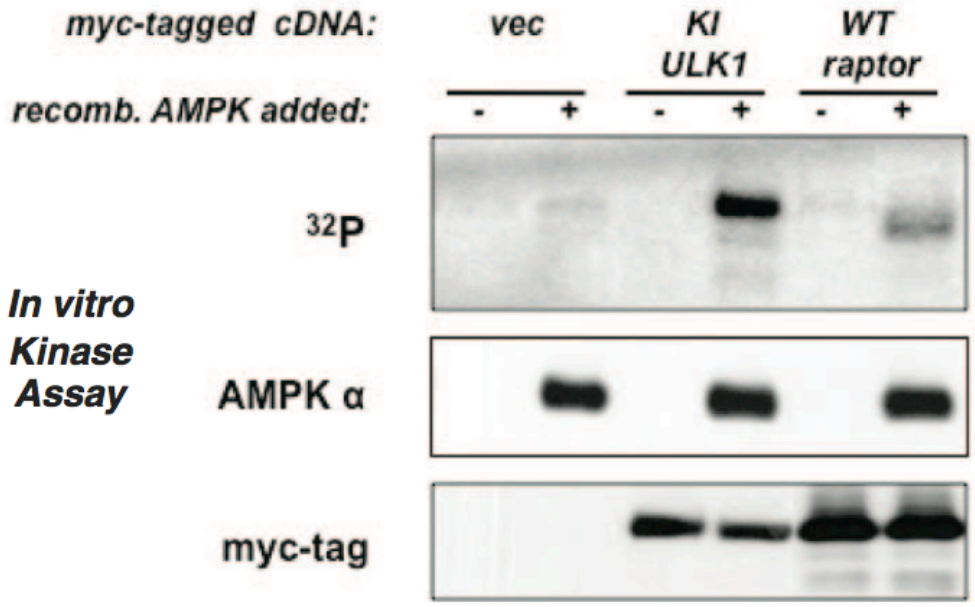

Figure 2.7: AMPK directly phosphorylates ULK1
In vitro kinase assays with Myc-tagged catalytically inactive (ki: K46I) ULK1 or Myc-tagged wt raptor that were immunoprecipitated from HEK293T cells and used as substrates for purified active AMPK in the presence of 32P-(C)-ATP.

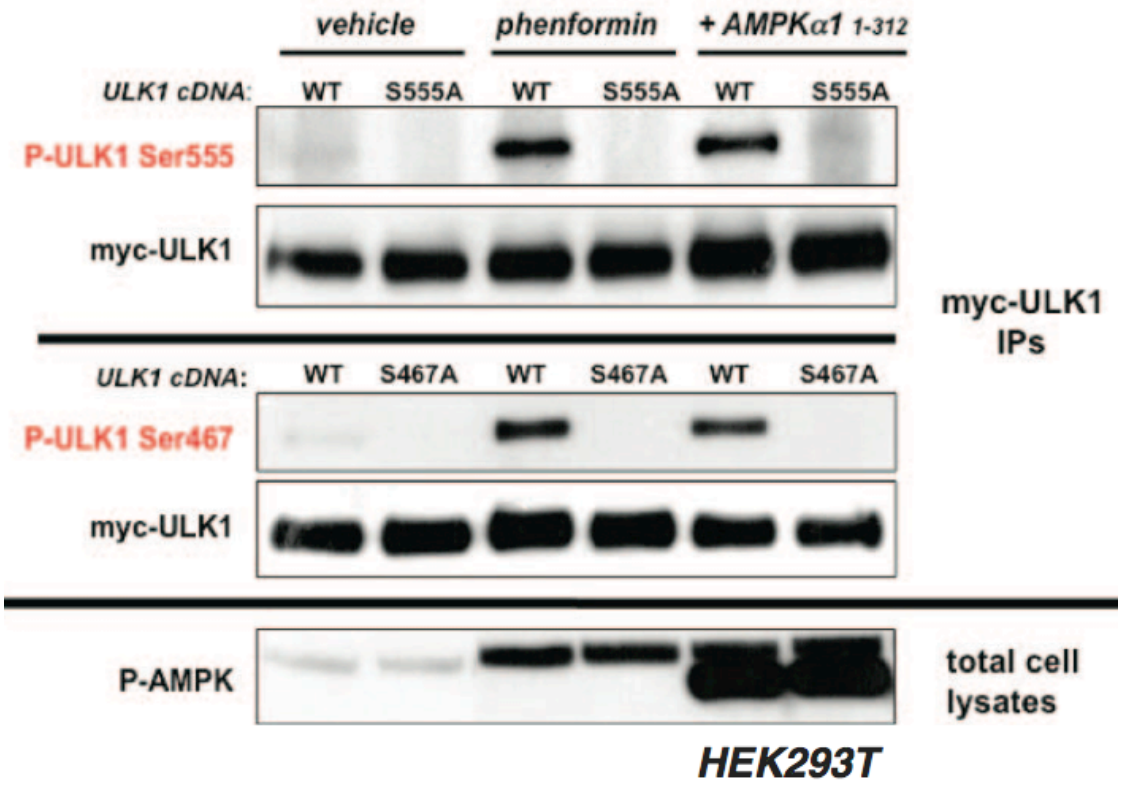

Figure 2.8: AMPK phosphorylates ULK1 in HEK293T cells
HEK293T cells transfected with Myc- tagged wt ULK1 or indicated serine-to-alanine ULK1 mutants were treated with either vehicle or 1 mM phenformin for 1 hour or were cotransfected with a constitutively active AMPKa1 (aa1-312) mammalian expression vector. Proteins from lysates were immunoblotted with phospho-specific antibodies as indicated.

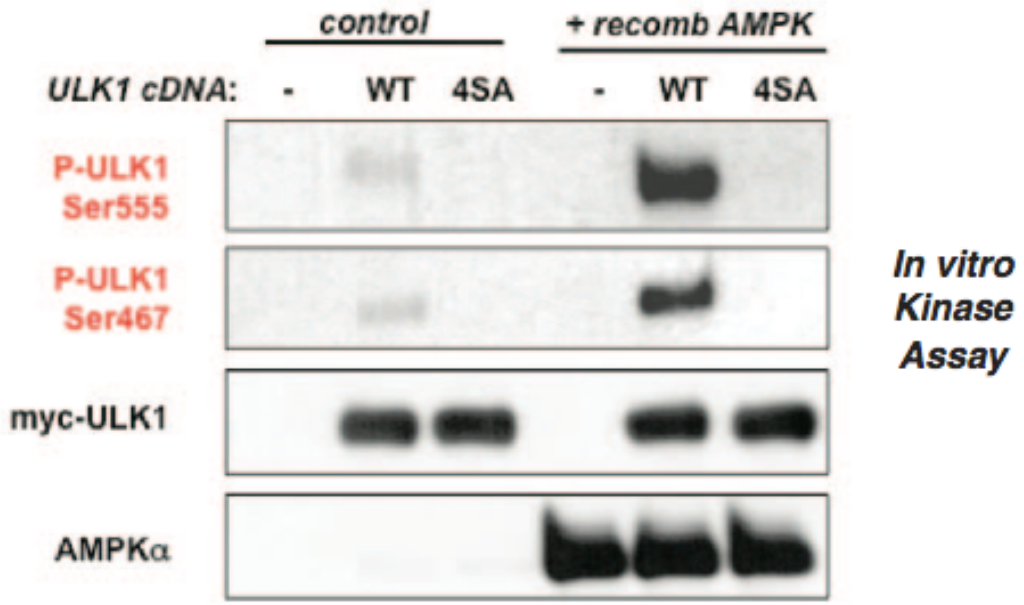

Figure 2.9: AMPK directly phosphorylates ULK1 on ser555 and ser467 in vitro. In vitro kinase assays using Myc-ULK1 and purified AMPK as above. Phosphorylation of Myc-ULK1 detected through immunoblotting with indicated phospho- specific antibodies.

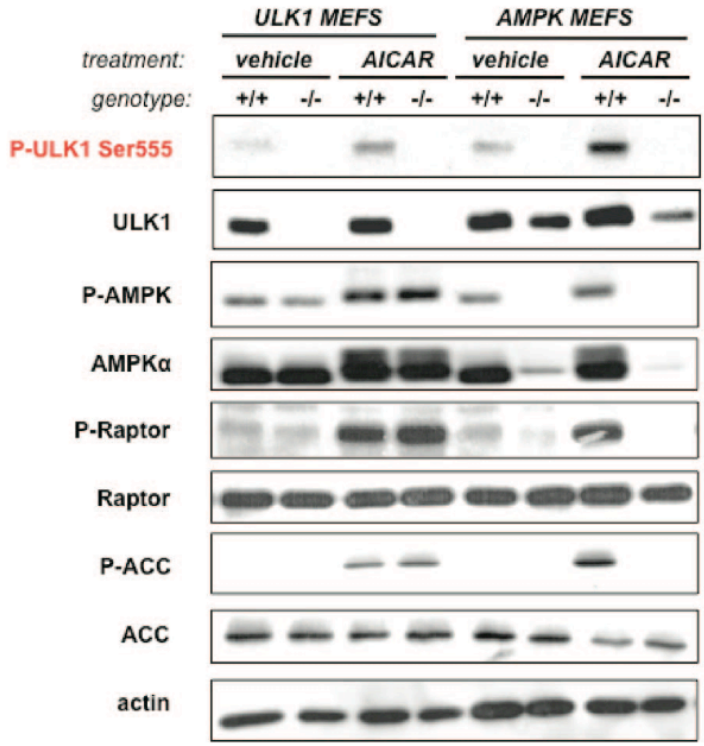

Figure 2.10: AMPK is required for ULK1 phosphorylation on ser555 in primary MEFs

Primary MEFs were treated with 2 mM AICAR or vehicle for 1 hour. Lysates were immunoblotted as indicated, including detection of endogenous ULK1 P-Ser555.

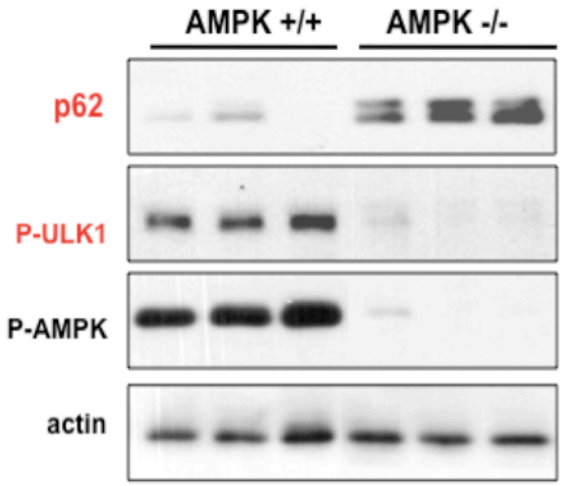

Figure 2.11: p62 is elevated in AMPK deficient livers compared to littermate controls as visualized by western blot
Liver lysates from littermate-matched mice were immunoblotted for the indicated antibodies.

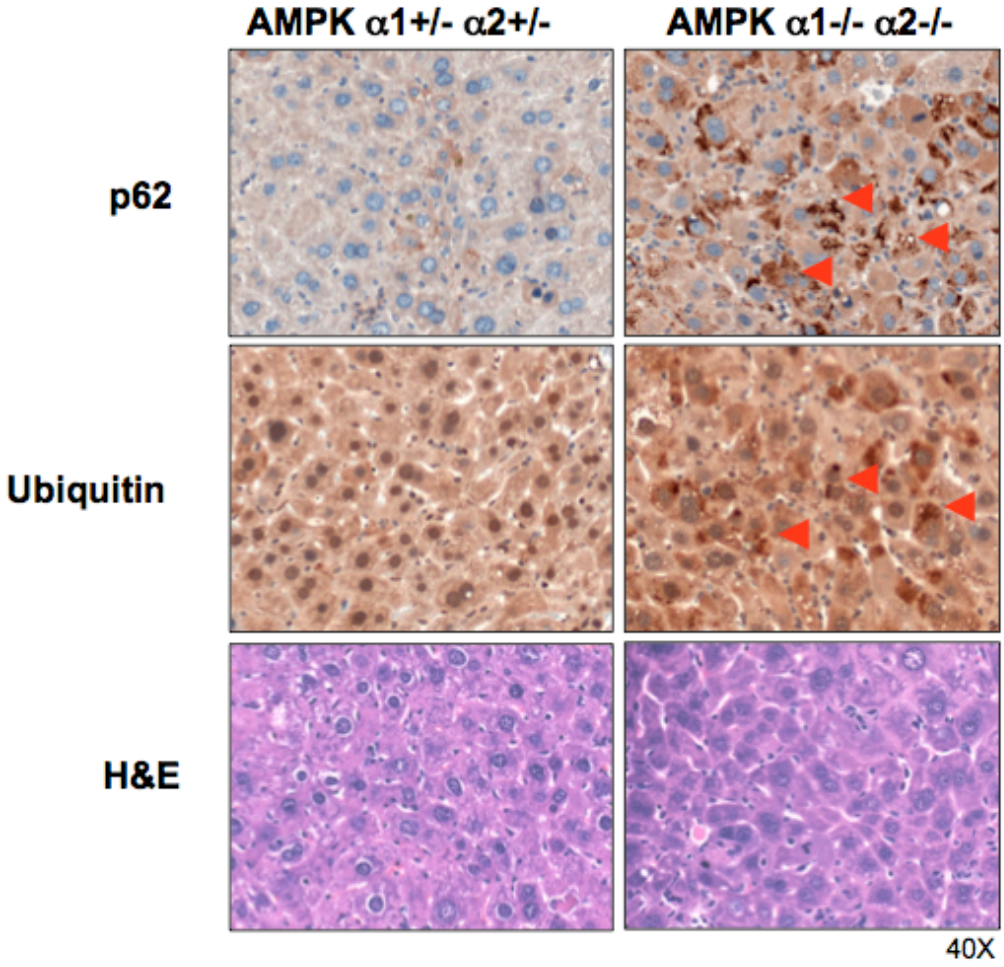

Figure 2.12: p62 and ubiquitin are elevated in AMPK deficient livers compared to littermate controls as visualized by immunohistochemistry
AMPK deficient (a1-/-; a2lox/lox; tail-vein adenovirus cre-injected) livers or control (a1+/-; a2lox/+; tail vein adenovirus cre injected) livers were subjected to immunohistochemistry for the p62 autophagy marker or ubiquitin. Note elevated p62 and ubiquitin levels in the AMPK double knockout (DKO) liver. Overlapping aggregates of p62 and ubiquitin from serial sections indicated with red arrowheads. H&E is shown illustrating normal liver architecture. Data are representative of 2 independent experiments and 5 mice of each genotype analyzed.

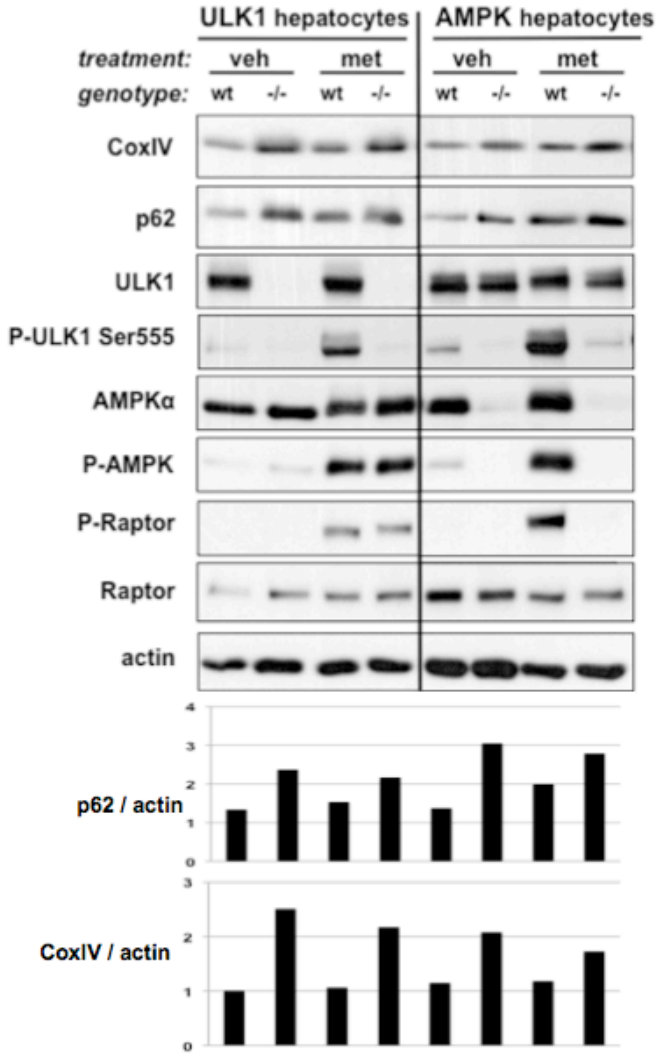

Figure 2.13: p62 and the mitochondrial protein COXIV are elevated with loss of ULK1 or AMPK in primary murine hepatocytes

Primary hepatocytes were derived from ULK1+/+ or ULK1-/- mice or aforementioned AMPK mice 7 days after tail-vein injection of adenovirus-cre. Cells were treated with 2mM metformin (met) or vehicle (veh) for 2h and immunoblotted with the indicated antibodies including p62 and the mitochondrial marker CoxIV, which are densitometrically quantified relative to actin below.

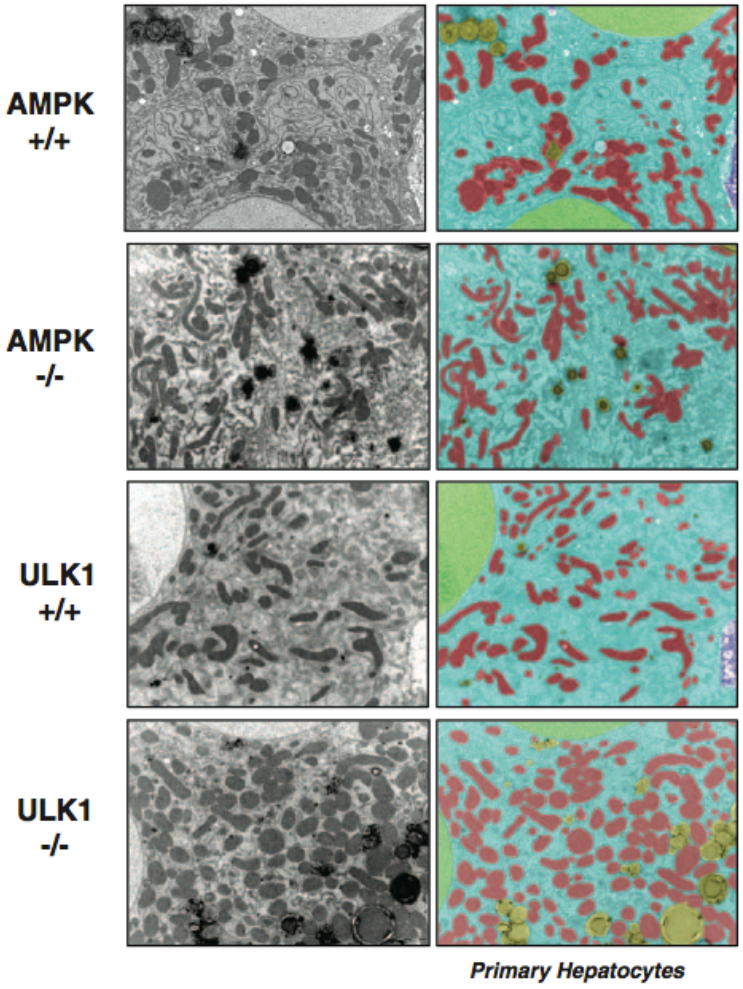

Figure 2.14: Enlarged, abnormal mitchondria accumulate in AMPK and ULK1 deficient hepatocytes

TEM was performed on primary mouse hepatocytes of the indicated genotypes, revealing accumulation of mitochondria in both AMPK- and ULK1- deficient cells. Red, mitochondria; blue, cytoplasm; green, nuclei; yellow, lipid droplets.

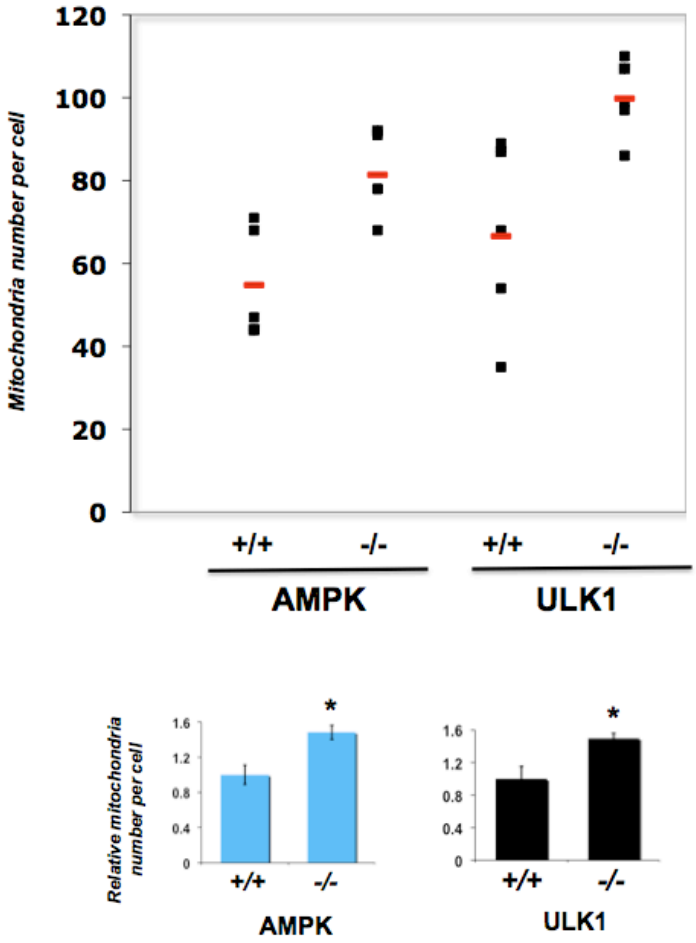

Figure 2.15: Relative number of mitochondria is increased with loss of ULK1 or AMPK in primary murine hepatocytes

Quantification of TEM from primary murine hepatocytes from Figure 2.14. Top: boxwhisker plot of number of mitochondria per cell from 5 independent TEM fields. Below: The number of mitochondria per cell as expressed relative to levels seen in littermate matched control hepatocytes (set to 1.0). Data shown as mean +/- SEM. *P< .01 student's unpaired *t*-test.

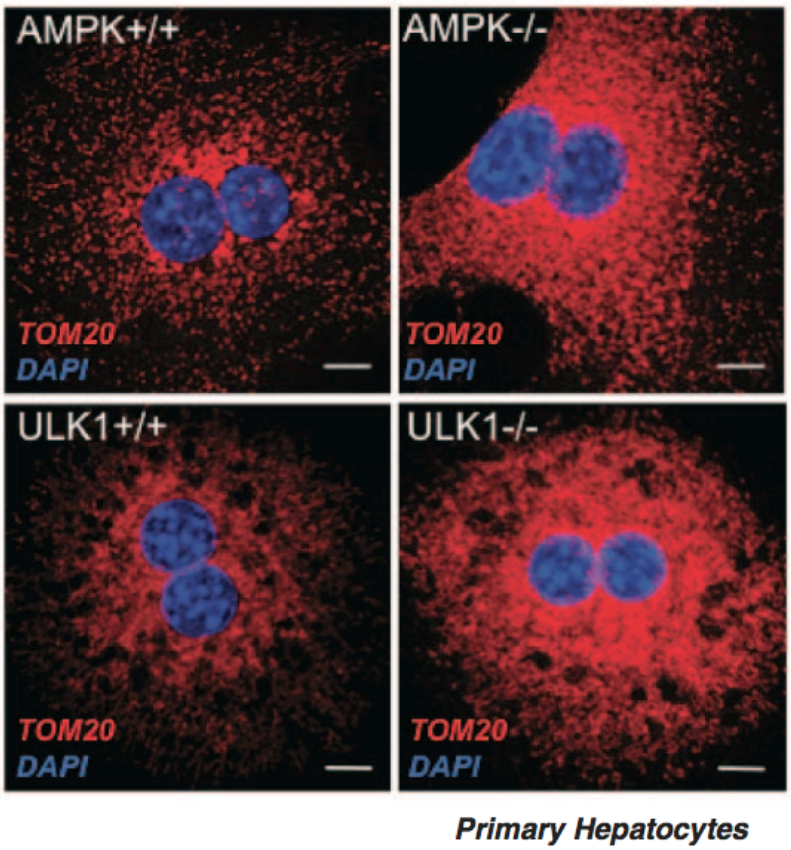

Figure 2.16: Enlarged, abnormal mitchondria accumulate in AMPK and ULK1 deficient hepatocytes

Primary mouse hepatocytes of the indicated genotypes stained by means of immunocytochemistry for the mitochondrial marker TOM20 (red) and nuclei (blue). Scale bar, 10 mm.

Table 2.1: Analysis of strains expressing the transgene LGG-1::GFP
Summary of LGG-1::GFP positive puncta in L3 larvae of different genetic backgrounds using the LGG-1::GFP reporter (described in ref.15, and integrated in ref. 16). The average number of puncta per seam cell was calculated from two-three independent trials. Nseam cells, number of seam cells analyzed, Nanimals, number of animals in which seam cells were analyzed. P values were calculated as unpaired, two-tailed t-test. N/A, animals were grown on regular OP50 E. coli bacteria. "hets' refer to F1 animals analyzed from cross between DA2123 and AGD383. Animals were raised at 20 degrees Celsius.

Data from Fig.Panel#	Strain	LGG-1::GFP expressing strain	RNAi treatment	Average # puncta/ seam cell	SEM	$N_{seam\ cells}$	$N_{animals}$	*P* value
3A1	MAH14	*daf-2(e1370)*	-	2.44	0.14	127	30	
			bec-1	0.67	0.08	155	17	<0.0001
			aak-2	0.82	0.12	135	16	<0.0001
			unc-51	1.08	0.11	181	25	<0.0001
3B2	DA2123	N2 wild-type	-	0.43	0.06	168	19	
			daf-2	1.41	0.14	112	16	<0.0001
	MAH28	*aak-2(ok524)*	-	0.57	0.06	237	29	
			daf-2	0.68	0.12	253	26	0.20
3C	DA2123	N2 wild-type	N/A	0.48	0.07	137	16	
	AGD383 'hets'	AAK-2::TOMATO	N/A	1.57	0.11	207	26	<0.0001
3D4	DA2123	N2 wild-type	-	1.07	0.14	74	8	
	AGD383 'hets'	AAK-2::TOMATO	-	3.37	0.15	223	34	
			unc-51	2.13	0.11	277	33	<0.0001

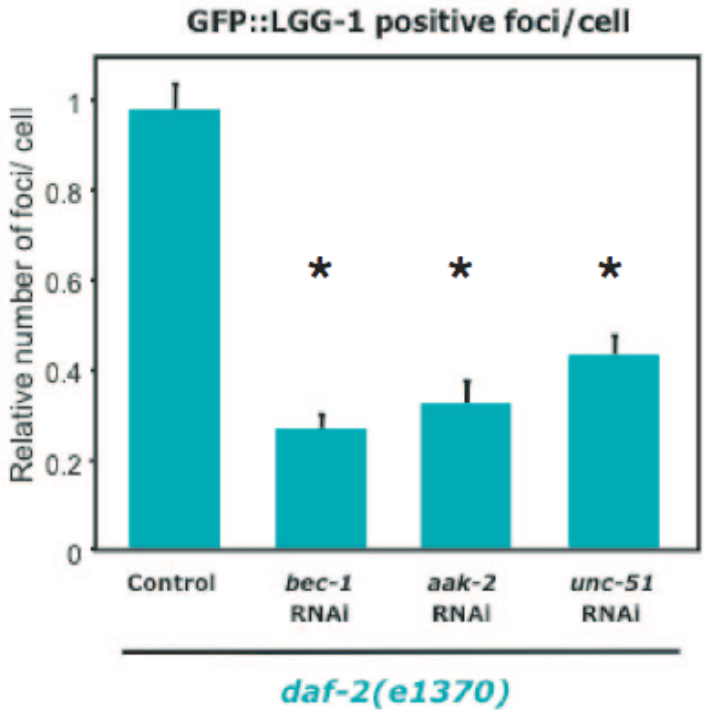

Figure 2.17: AMPK is required for autophagy induction in C. elegans
Insulin receptor daf-2(e1370) mutant worms expressing GFP::LGG-1 (equivalent to GFP-LC3) were treated with control RNAi or RNAi against bec-1 (Beclin), aak-2 (AMPKa2), or unc- 51 (ULK1), and the number of LGG-1/LC3–positive puncta per hypodermal seam cell were quantified.

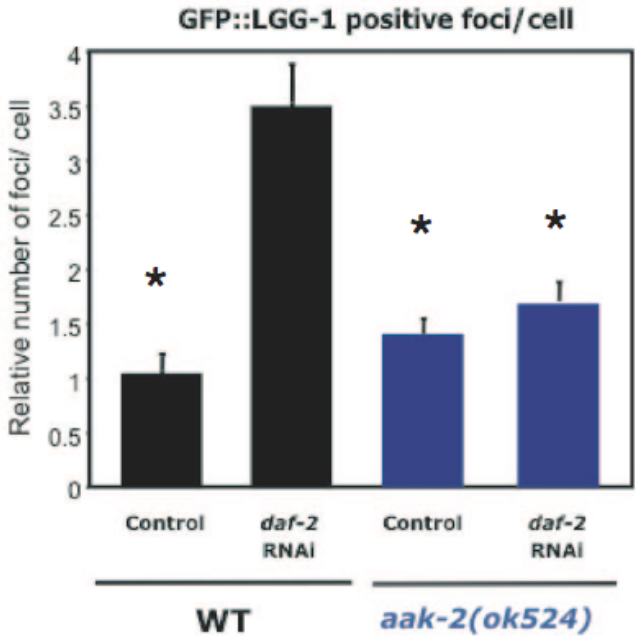

Figure 2.18: Overexpression of a dominant negative AMPK (aak-2(ok524)) attenuates the daf-2 mediated autophagy induction
aak-2(ok524) mutants or wt N2 (wt) animals expressing GFP::LGG-1 were treated with control or daf-2 RNAi and scored for LGG-1 positive puncta per seam cell.

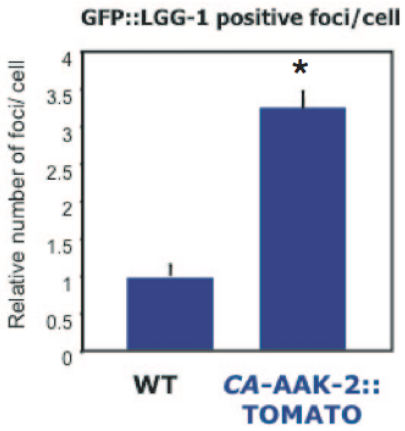

Figure 2.19: AMPK is sufficient for autophagy induction in C. elegans
Transgenic worms expressing constitutively active AAK-2 (12) (amino acids 1-321)::TOMATO (CA- AAK-2::TOMATO) fusion or controls (wt) were analyzed for LGG-1–positive puncta per seam cell.

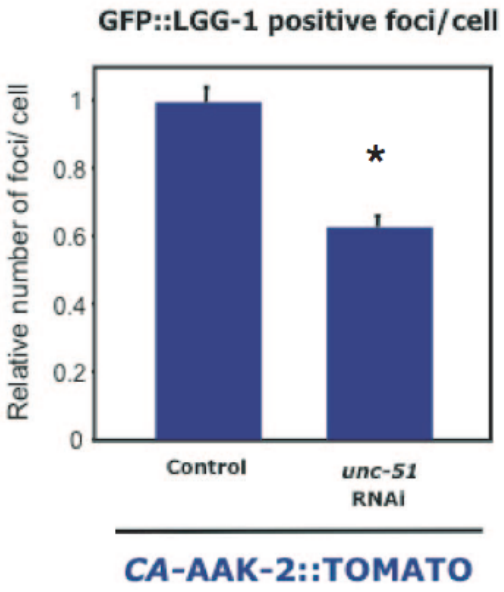

Figure 2.20: Unc51 is required for AMPK mediated autophagy induction in C. elegans

Animals expressing both CA-AAK-2(1-321)::TOMATO and GFP:: LGG-1 were treated with control or unc-51 RNAi and scored for LGG-1/LC3–positive puncta per seam cell. All panels show relative counts. Data shown as mean T SEM. *P < 0.0001.

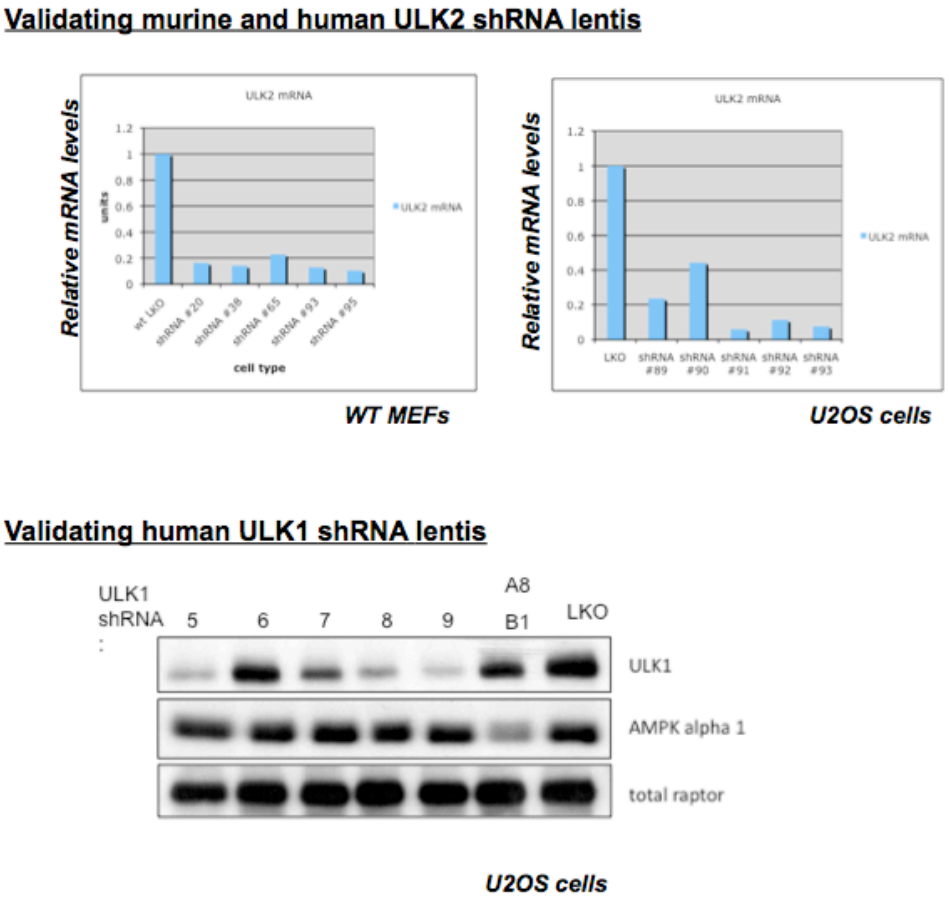

Figure 2.21: Validation of lentiviral shRNAs against human and murine ULK1 and ULK2

Top: Quantitative RT-PCR was used to validate the effectiveness of lentiviruses bearing hairpin shRNAs against murine and human ULK2 in cell types indicated. mRNA levels were normalized to GAPDH mRNA levels. Bottom: Immunoblotting was used to validate the effectiveness of lentiviruses bearing hairpin shRNAs against human ULK1. Lentivirus shRNAs A8/B10 directed against AMPKalpha served as a positive control for viral tittering and LKO is the empty lentiviral vector negative control. Raptor served as a loading control here.

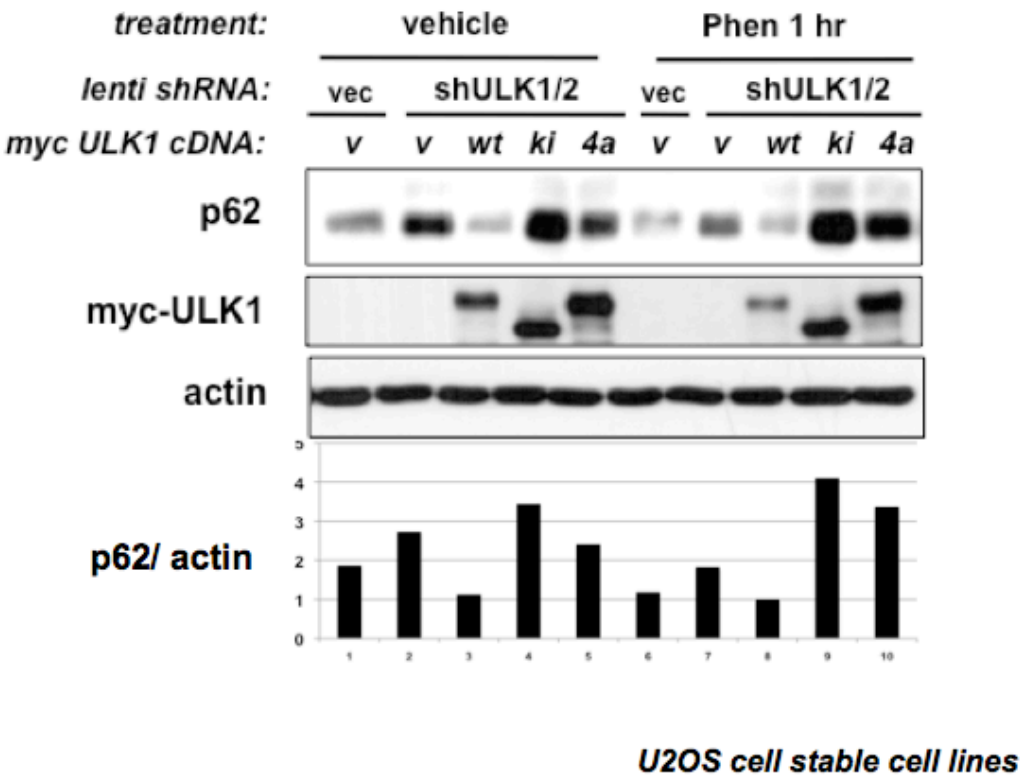

Figure 2.22: AMPK-dependent sites in ULK1 are required for ULK1 function in U2OS cells

U2OS cells were stably infected with empty lentiviral vector pLKO (vec) or human ULK1 and ULK2 shRNA-expressing lentiviruses and then stably reconstituted with retroviruses bearing wild-type (wt) or kinase-inactive (ki) or AMPK non-phosphosphorylatable (4SA) ULK1 cDNA or the empty retroviral vector (v). wt ULK1, but not ki or 4SA ULK1 was able to restore p62 degradation to the ULK1/2-deficient U2OS cells, which is quantified by densitometry below (detailed in methods). Cells were treated with 5mM Phenformin (Phen) or vehicle for 1h. Results are representative of 3 independent experiments.

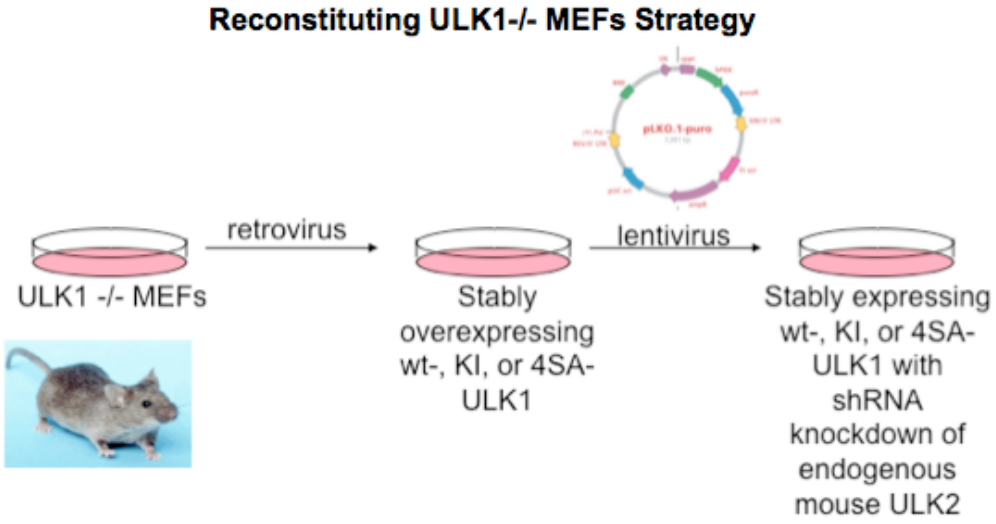

Figure 2.23: Reconstitution strategy for ULK1$^{-/-}$ MEFs
Retroviruses bearing Myc-tagged wild-type or kinase inactive or non-phosphorylatable ULK1 were introduced into ULK1$^{-/-}$ MEFs and after selection these cells were next infected with lentiviruses bearing shRNAs for murine ULK2. The same strategy was used for replacing ULK1/2 function in U2OS cells except there after the retroviral selection, cells were co-infected with lentiviruses bearing shRNAs against human ULK1 and ULK2.

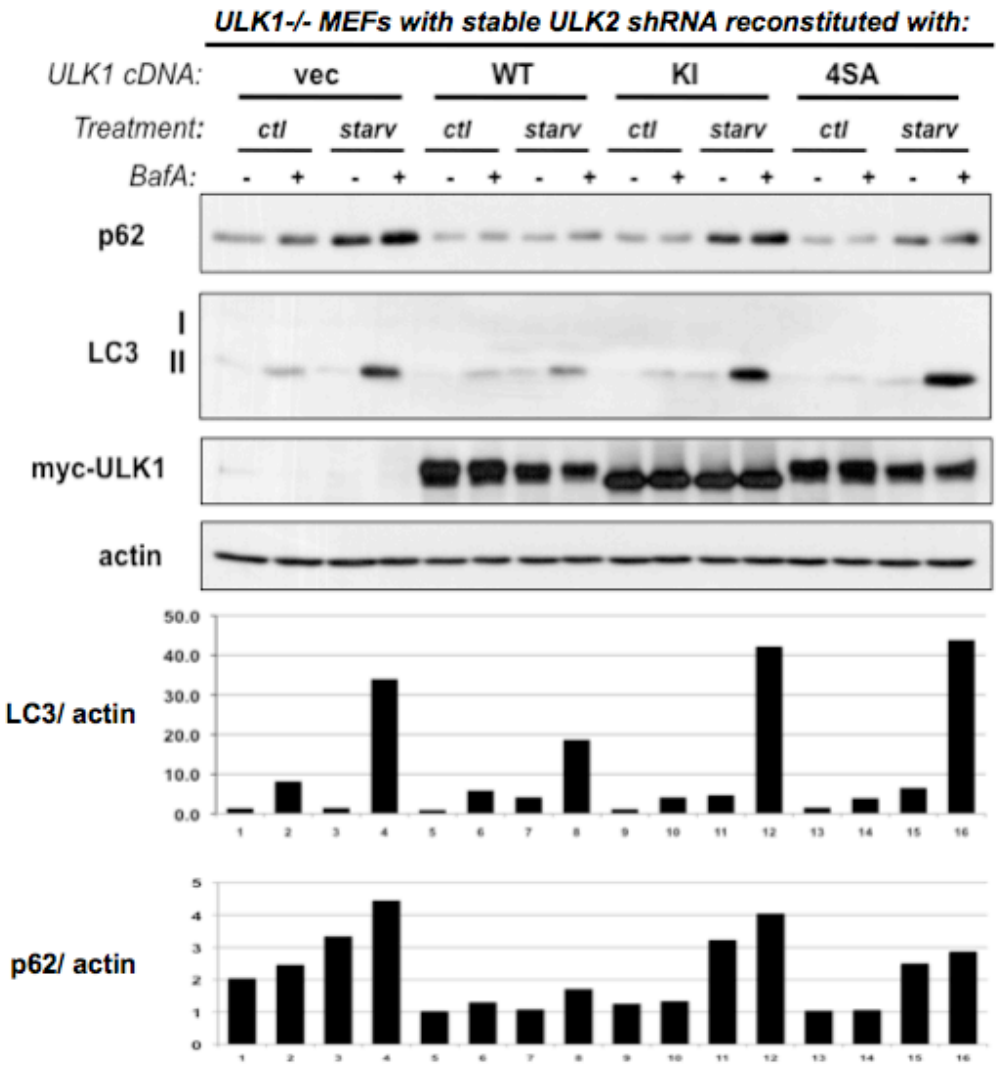

Figure 2.24: AMPK-dependent sites in ULK1 are required for ULK1 function in MEFs

ULK1$^{-/-}$ MEFs bearing stable murine ULK2 shRNA lentiviruses were stably reconstituted with retroviral vectors bearing wt, ki, or 4SA ULK1 or no cDNA (vec) and then placed in starvation media (starv – EBSS: Earle's buffered salt solution) or control media (ctl: standard media for these cells: DMEM + 10% FBS) for 6h in the presence of BafilomycinA (BafA) as indicated. Lipidated LC3 (II) and p62 levels were quantified by densitometry and shown at bottom. Results are representative of 3 independent experiments.

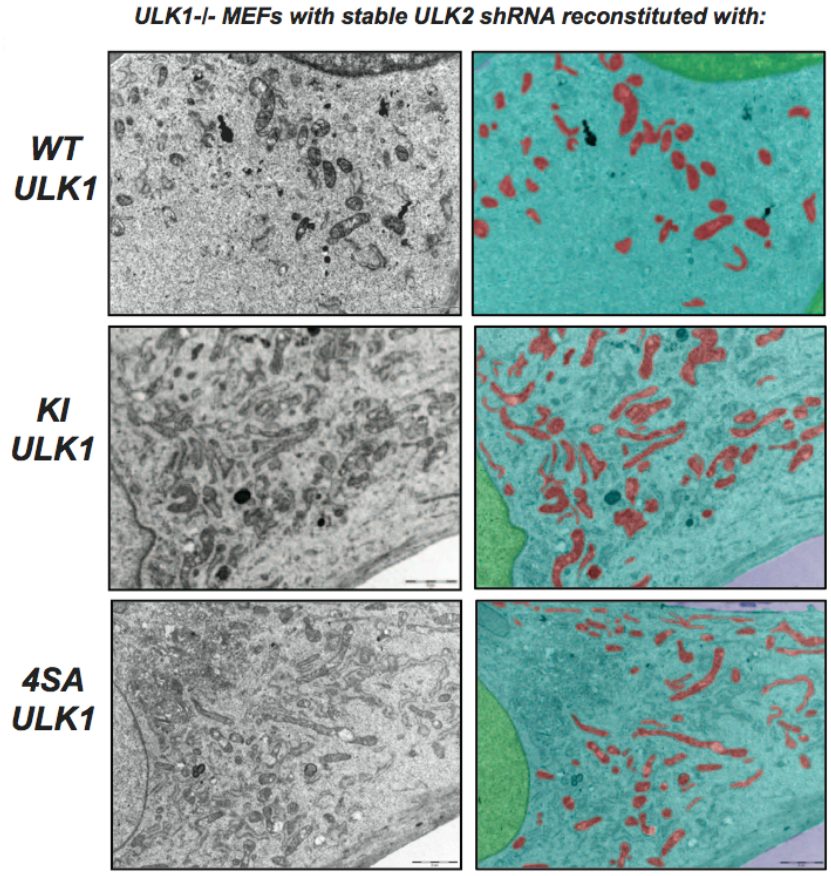

Figure 2.25: Electron microscopy of ULK1 cDNA-reconstituted ULK1$^{-/-}$ MEFs
Cells from Figure 2.24 analyzed with TEM and Inform morphometric software. Red, mitochondria; blue, cytoplasm; green, nuclei.

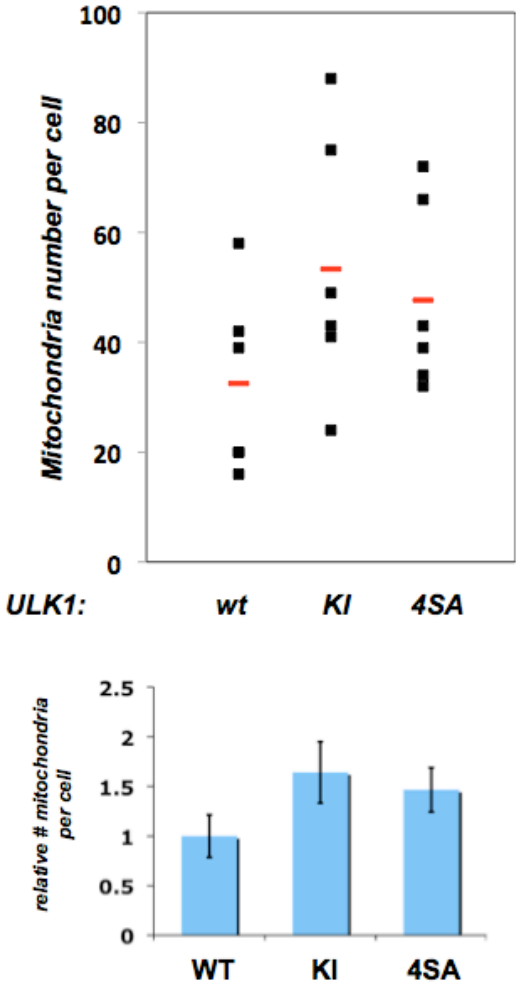

Figure 2.26: Relative number of mitochondria is increased with loss of ULK1/2 function

Quantification of the number of mitochondria per cell from Figure 2.25 as analyzed using Inform morphometric software. Cells expressing wt ULK1 were set to 1.0 (=avg 32.5 mito/cell).

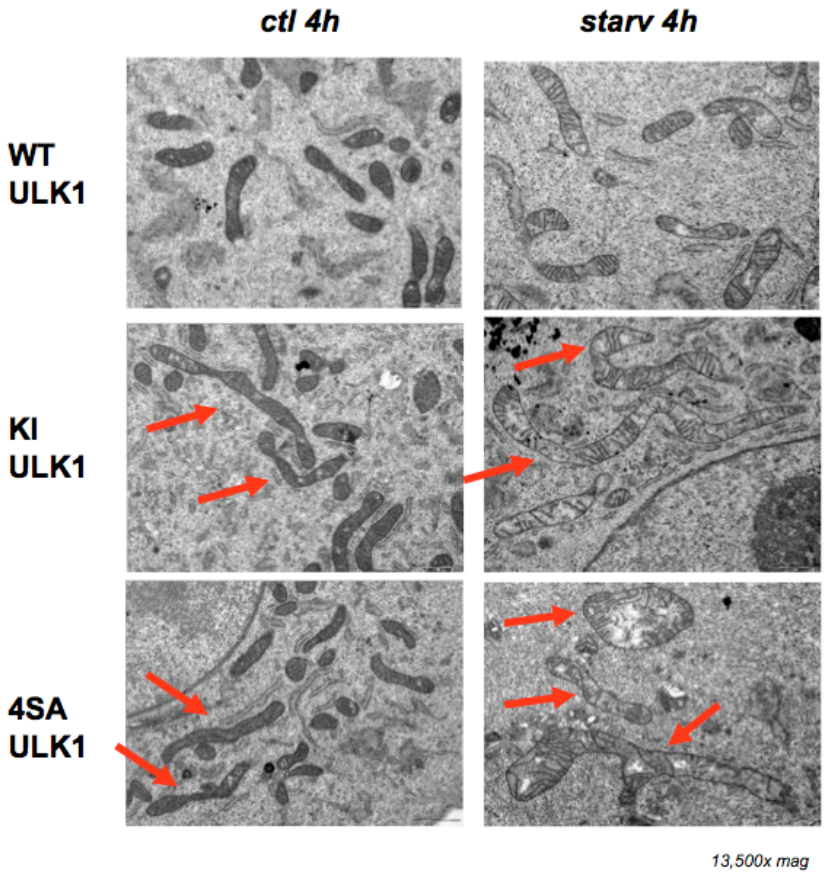

Figure 2.27: Mitochondrial morphological defects in ULK-deficient MEFs reconstituted with ki or 4SA mutant ULK1

Transmitting Electron Microscopy images from wt, ki, or 4SA reconstituted ULK1-/- MEFs bearing ULK2 shRNA. Cells were placed into fresh growth media (ctl) or EBSS (starvation) at time zero and fixed at 4h. Note the aberrant elongated mitochondria in the ki and 4SA cells, and the altered mitochondrial cristae in the ki or 4SA reconstituted cells following starvation. Images taken at 13,500x.

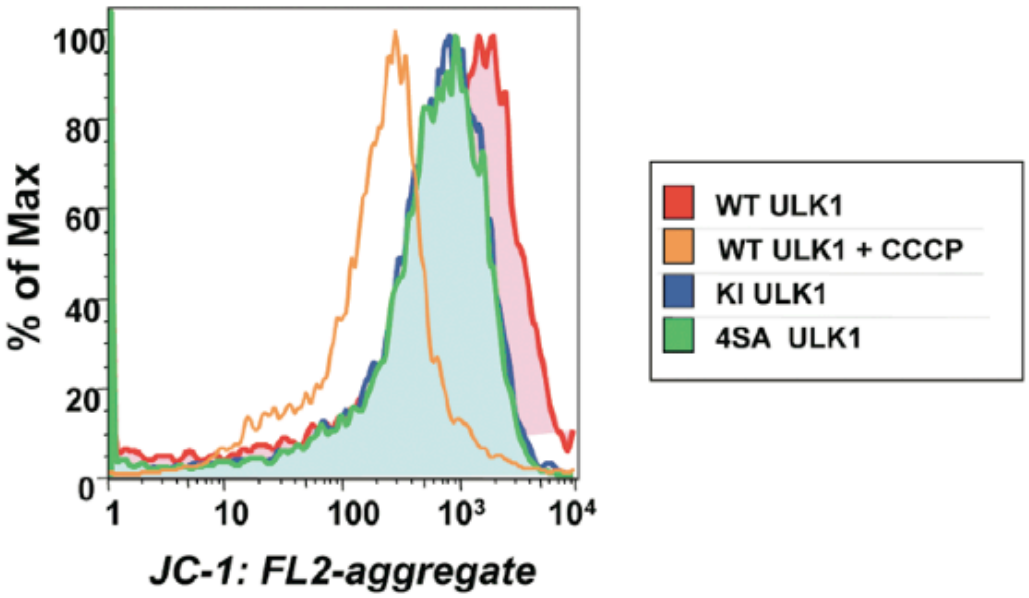

Figure 2.28: Mitochondrial membrane potential defects in ULK-deficient MEFs reconstituted with ki or 4SA mutant ULK1

Flourescence-activated cell sorting (FACS) analysis on cells from Figure 2.27, which were stained with JC-1 under basal conditions or with the mitochondrial uncoupler carbonyl cyanide m-chloro phenyl hydrazone (CCCP) as a control in order to measure mitochondrial membrane potential. Compromised mitochondrial membrane potential is shifted to the left, as observed in cells treated with CCCP.

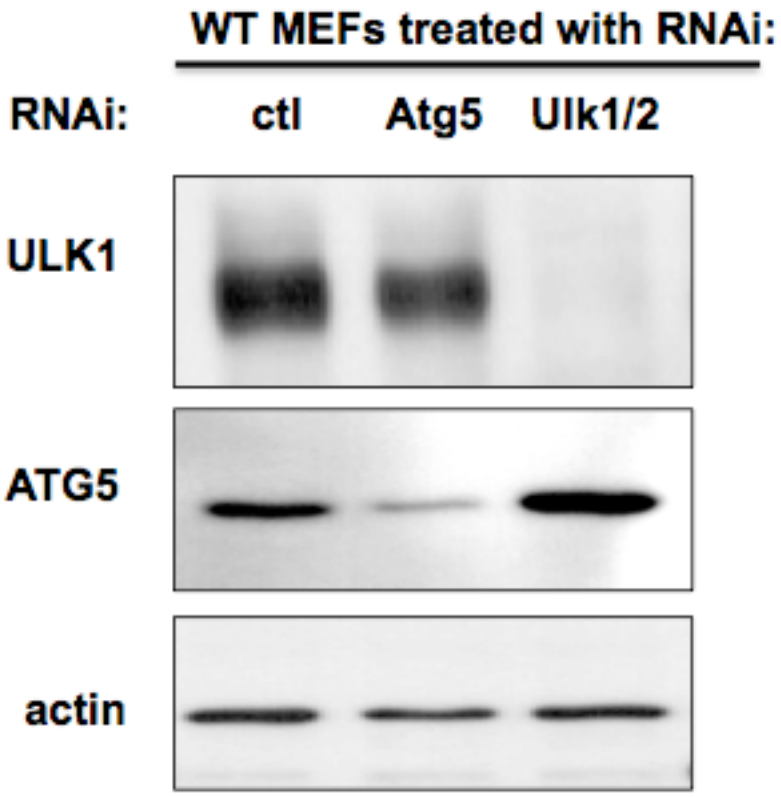

Figure 2.29: Validation of Dharmacon SMARTPool siRNAs against murine ULK1, ULK2, and Atg5
Wild-type (wt) MEFs transfected with 20nM siRNA pools to a universal control (ctl), murine Atg5, or murine ULK1 and ULK2 for 72 hours. Proteins from lysates were immunoblotted with indicated total antibody.

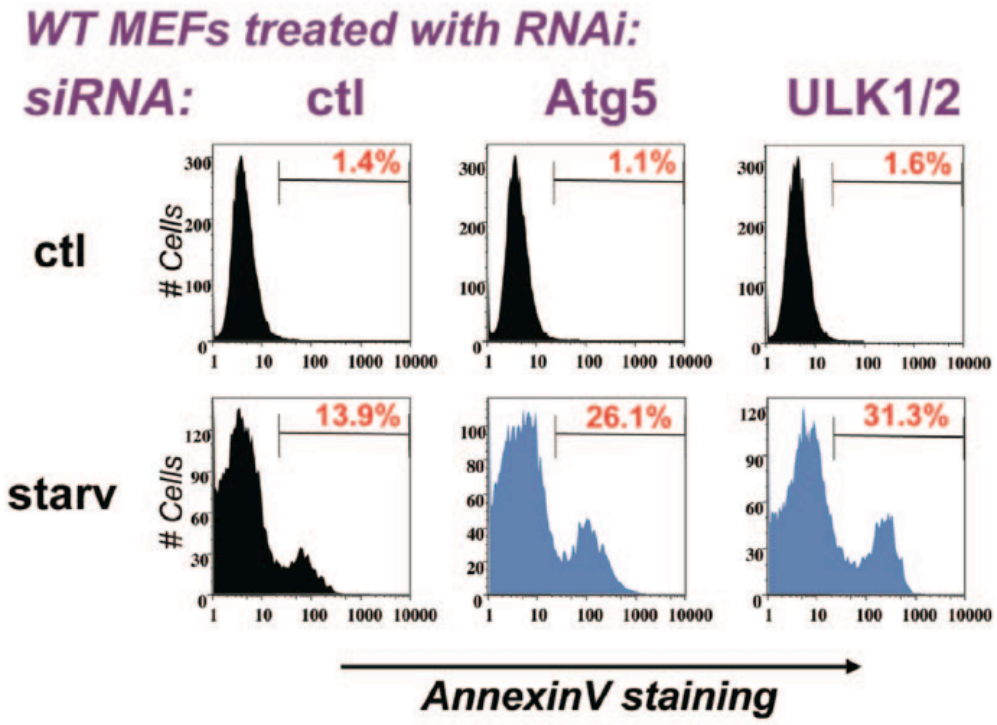

Figure 2.30: ULK1/2 is required to survive starvation induced cell death
wt MEFs transfected with 20 nM siRNA pools to a universal control (ctl), mouse Atg5, or mouse ULK1 and ULK2 for 72 hours were then placed in starvation medium (starv) or standard media (ctl) for 12 hours, and cell death was scored by means of AnnexinV-FACS.

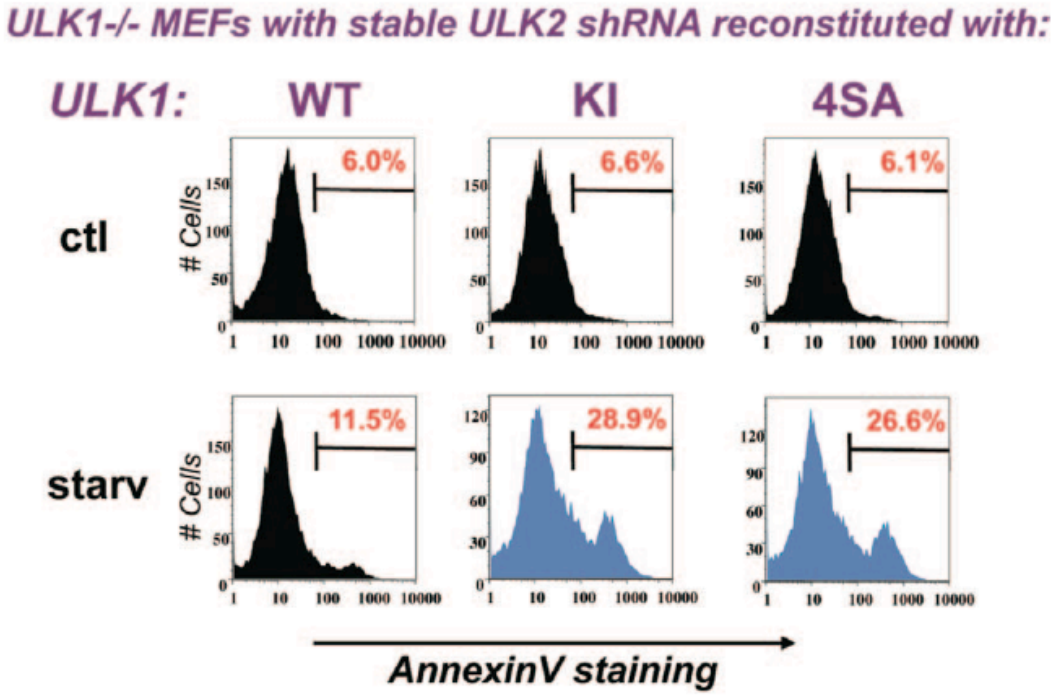

Figure 2.31: The AMPK-dependent phosphorylation sites in ULK1 are required to survive starvation induced death

Cells from Figure 31 were placed in starvation medium (starv) or standard media (ctl) for 12 hours, and cell death was scored by means of AnnexinV-FACS.

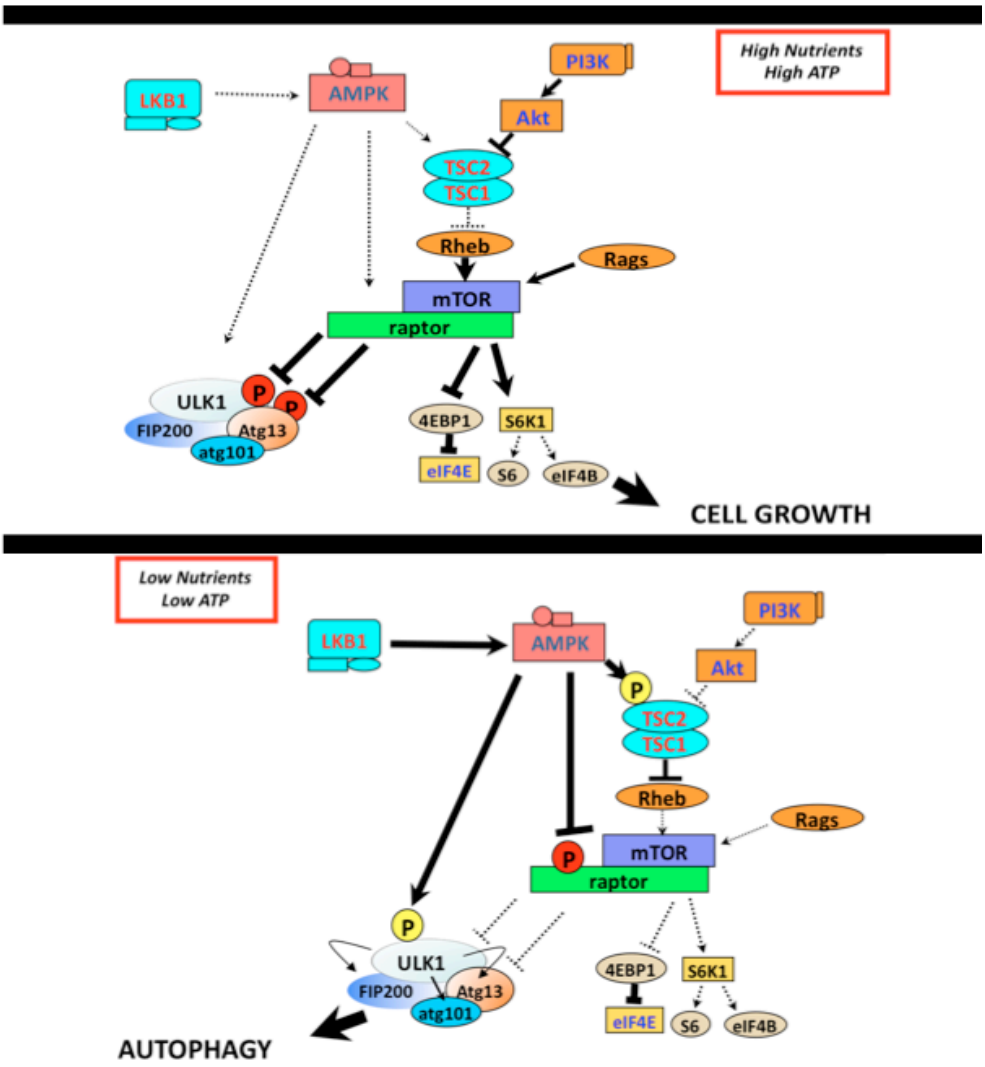

Figure 2.32: Model for AMPK activation of ULK1 in a two-pronged mechanism via direct phosphorylation of ULK1 and inhibition of mTORC1 suppression of ULK1

Schematic of intersection of mTOR, AMPK, and ULK1 pathways. Top: Under nutrient replete conditions. Bottom: Under nutrient deprived conditions.

CHAPTER THREE:

Development of an ATP-competitive inhibitor of the ULK1 autophagy kinase and systems analysis of its downstream substrates

Abstract

The conserved autophagy gene ULK1/Atg1 is the only serine/threonine kinase in the core conserved autophagy pathway. Despite recent breakthroughs in the understanding of how ULK1 is activated by nutrient deprivation, the molecular details of how ULK1 initiates autophagy remain poorly understood. Here we have screened degenerate peptide libraries to deduce the optimal substrate specificity for ULK1. Utilizing this motif, we identified more than ten in vivo ULK1 phosphorylation sites in seven components of the upstream autophagy complexes. As autophagy is a mechanism for cells to survive when nutrients are limited, inhibition of autophagy has been suggested as a therapeutic approach for the treatment of cancers whose cells are reliant on autophagy for survival, under nutrient poor conditions or following the stress of therapeutic treatment. We utilized our newly defined ULK1 substrates to in cellulo screen lead compounds of ATP-competitive kinase inhibitors showing in vitro specificity for ULK1. From these efforts a tool compound SBI-02096965 was identified which shows great specificity and which mimics RNAi for ULK1 in its effects on cell survival. We provide proof of principle experiments that this ULK1 inhibitor synergizes strongly with mTOR catalytic inhibitors, providing a rationale for use in future studies.

Introduction

Autophagy is a central cellular mechanism for elimination of damaged proteins, protein complexes, and organelles. This conserved process plays crucial roles

in the cellular response to nutrient deprivation as well as other stresses, in addition to being required for proper cellular and tissue homeostasis during embryonic development and in defense against pathogens. Defects in autophagy pathways have been associated with a number of human pathologies, including infectious diseases, neurodegenerative disorders, and cancer (Green and Levine, 2014). In spite of these highly conserved fundamental cellular functions, the molecular and biochemical details of how autophagy is initiated for different cargoes, and the coordination of steps starting from autophagosome initiation to ultimate fusion with the lysosome remain poorly understood.

Pioneering studies in budding yeast first defined 36 core AuTophaGy ("ATG") genes required for this process, of which most are conserved with mammals (Tsukada and Ohsumi, 1993). One of the most upstream components of the pathway in yeast is the Atg1 gene, which is notable for being the only core ATG gene to encode a serine/threonine kinase. Atg1 forms a complex with multiple regulatory subunits, including Atg13 and Atg17. In mammals, there appear to be two Atg1 homologs, ULK1 and ULK2, which similarly bind to an Atg13 homolog and a Atg17 like protein, FIP200. The ULK1 kinase complex is activated in response to nutrient deprivation and as such is thought to serve as a critical initiator of starvation-induced autophagy. Whether the ULK1 complex is needed for bulk steady-state autophagy that some cell types undergo remains unclear, as well as whether certain forms of selective autophagy may also proceed without involvement of the ULK1 complex. In the context of starvation induced autophagy, ULK1 receives inputs from the cellular

energy sensor AMP-activated protein kinase (AMPK), which is activated following cellular stresses that lower intracellular ATP levels, including glucose or oxygen deprivation as well as following mitochondrial insults (Egan et al., 2011b). Another critical input to ULK1 is the mechanistic target of rapamycin complex 1 (mTORC1). Some nutrient stresses like amino acid withdrawal do not result in acute AMPK activation, but do trigger rapid mTORC1 inactivation, thereby resulting in ULK1 activation even without the stimulatory input from AMPK (Kim et al., 2011). ULK1 is directly phosphorylated on at least one serine, Ser757, by mTORC1, and is phosphorylated on at least four different serines by AMPK to activate it. As most of the aforementioned stresses result in both AMPK activation and mTOR inhibition, starvation should result in an increase in phosphorylation of the AMPK sites in ULK1 and loss of the mTORC1 site (Egan et al., 2011a).

In addition, a recent study suggests that AMPK may directly phosphorylate both Beclin-1 and Vps34, the two central components of the Vps34/Beclin complex which is responsible for localized PI3P production required for autophagosome biogenesis (Kim et al., 2013) thus positively mediating autophagic flux. The relative contributions of AMPK dependent phosphorylation of the Beclin complex versus the ULk1 complex remains to be investigated.

Despite many studies identifying molecular details of how nutrients regulate ULK1 via opposing effects from mTORC1 and AMPK, the critical downstream targets of the ULK1 kinase complex in the initiation of autophagy remain largely unknown. In spite of a lack of molecular details of how ULK1 mediates initiation of

autophagy, genetic disruption of ULK1, similar to genetic disruption of any core autophagy gene results in loss of cell viability under nutrient-poor conditions. The ability of autophagy to promote cell survival following a variety of cellular stresses has led to the direct examination of autophagy inhibitors for the treatment of cancer (Guo et al., 2013b). However, to date, potent and selective autophagy inhibitors have remained elusive as most of the core autophagy proteins are not druggable enzymes. As ULK1 is the only conserved serine/threonine kinase in the autophagy pathway, using our new identified ULK1-dependent phosphorylation events in vivo, we report here the first small molecule ATP-competitive kinase inhibitors to ULK1. We report here the ability of these compounds to ameliorate cell survival following different stresses, including therapeutic treatment of cancer cells.

Results

Determination of the ULK1 kinase Consensus Phosphorylation Site

To identify novel substrates of ULK1 that may be important for its function, we identified an optimal ULK1 phosphorylation site consensus motif using arrayed degenerate peptide libraries, as we have done previously for AMPK (Gwinn et al., 2008). To generate active ULK1 for these experiments, Flag-tagged ULK1 was co-expressed with its subunits FIP200 and Atg13 in HEK293T cells and peptide eluted from affinity resin. Previous studies have demonstrated that association of FIP200 and Atg13 is required for proper ULK1 activity (Hara et al., 2008). To examine the in vitro kinase activity of our immunoprecipitated ULK1/FIP200/Atg13 complexes, we

utilized Atg13 as an in vitro kinase substrate, as it is a conserved ULK1 substrate across evolution, and one of the earliest ULK1 substrates reported in mammalian cells (Chan, 2009). The purified ULK1 complex exhibited robust kinase activity towards Atg13 in a dose-response fashion (Figure 3.1). This source of purified ULK1 complex was subjected to in vitro kinase assays on arrayed degenerate peptide libraries, revealing selective transfer of $^{32}\gamma$-ATP to specific peptide libraries reflecting the sequence preferences of ULK1 towards its substrates.

The mammalian ULK1 consensus motif determined here matches the recent data on the yeast Atg1 consensus motif (Papinski et al., 2014) having a unique substrate motif sequence specificity compared to most kinases studied to date (Ubersax and Ferrell, 2007). Unique amongst most kinases, ULK1 prefers hydrophobic residues at position -3, particularly methionine and leucine. In addition, hydrophobic residues, especially bulky resides like phenylalanine and tyrosine are enriched in the +1 position, correlating well with the Atg1 optimal motif (Figure 3.2). We generated an optimal peptide, Ulktide, based on the optimal ULK1 substrate consensus sequence, validating its efficient use as a surrogate for ULK1 kinase activity in vitro (Figure 3.3). Starting with this peptide, substitutions in key residues including the -3 and +1 positions were tested for activity as a substrate in an in vitro kinase assays revealing that both positions are important for optimal sequence specificity (Figure 3.4).

Identification of novel ULK1 substrates

A matrix of the position-specific selectivities of ULK1 (Figure 3.5) was used to bioinformatically search the human proteome for sites closely matching the ULK1 substrate consensus (Obenauer et al., 2003). We chose to focus first on those candidate substrates with well-established highly conserved roles in autophagy. To define ULK1 phosphorylation sites in vivo, we took advantage of the fact that wild-type ULK1 is constitutively active when overexpressed, thus we compared global phosphorylation events on epitope-tagged candidate targets when co-expressed with wild-type, or kinase-dead, ULK1 in HEK293T cells. Using mass spectrometry to determine all phospho-peptides in candidate proteins under these conditions revealed that several candidate proteins bearing multiple ULK1 consensus sites contained peptides which were highly phosphorylated in the presence of wild-type but not kinase-dead ULK1.

Interestingly, focusing on the core autophagy proteins bearing a consensus candidate ULK1 phosphorylation site, it was notable that none of the downstream ATG components contained this consensus (e.g. ATG5, ATG7, ATG3, ATG12), yet many of the upstream components (FIP200, ATG13, ATG14, Beclin) did bear such sequences. We first focused on the components of the ULK1 kinase complex itself, including FIP200, ATG13, and ATG101.

Atg101 was first identified by mass spectrometry on ULK1 and found to encode a highly conserved integral component of the ULK1-AT13-FIP200 complex in mammalian cells immunoprecipitations (Mercer et al., 2009). ATG101 was found to

bind directly to Atg13, and is critical for Atg13 stabilization and its resultant stimulation of ULK1 kinase activity. To map potential ULK1-dependent phosphorylation events in Atg101, we co-expressed Flag-tagged ATG101 with wild-type or kinase-dead ULK1 and performed MS/MS analysis of total peptide in the Flag-Atg101 immunoprecipitates to map total phosphorylation sites in Atg101 under the two conditions. We observed that two specific serine sites (Ser11, Ser203) within human Atg101 were stoichimetrically phosphorylated in cells bearing a wild-type ULK1 but not in cells co-expressing kinase-dead ULK1 (Figure 3.6). Notably these two ULK1-dependent phosphorylation sites conform to the optimal ULK1 substrate motif, suggesting they may be direct ULK1 substrates in vivo. To further explore ULK1 phosphorylation in vivo, we examined its migration on a Phos-tag SDS-PAGE gel, which uses a phosphate binding dinuclear metal complex to accentuate mobility shifts on proteins containing phosphorylation events (Kinoshita et al., 2006). Comparing the pattern of ATG101 on a Phostag containing gel when overexpressed in HEK293 cells with wild-type or kinase-dead ULK1 or vector controls, revealed a robust mobility change indictive of phosphorylation (Figure 3.7). Mutation of ATG101 Ser11 abolished a large extent of the mobility change, which was further enhanced in a Ser11/Ser203 double mutant, thus corroborating their identification as potential ULK1-dependent sits by mass spectrometry. We next performed similar mass spectrometry analysis of FIP200 and ATG13 phosphorylation events, discovering multiple serine sites in FIP200 and Atg13 bearing the ULK1 substrate

consensus whose phosphorylation was induced by overexpressed ULK1 in vivo (Figure 3.8 and Figure 3.9).

Next we examined components of the Beclin/Vps34 complex which lies downstream of the ULK1 complex in autophagy initiation. Here we identified multiple serines in Beclin which conform to the optimal Ulk1 consensus and contribute to Beclin mobility change on Phostag gels (Figure 3.10 and Figure 3.11). An additional site, Ser15, which was recently discovered and reported to play a conserved role in autophagy induction (Russell et al., 2013)was not identified by our mass spectrometry. Our data examining Beclin mobility on Phostag gels suggests that when co-expressed with active ULK1, only when three serines are abolished (Ser15, Ser30, Ser337), does one reduce the mobility back to control levels. Examination of another component of the Beclin complex, Ambra1 revealed multiple ULK1-dependent phosphorylation events in vivo (Figure 3.12). Finally, we examined a known ULK1 interactor, Syntenin-1, which was also recently reported as a ULK1 substrate (Rajesh et al., 2011). Here we find the previously reported in vitro phosphorylation site, Ser6, along with a second site Ser61, are responsible for altered mobility of Syntenin-1 in the presence of ULK1 in vivo (Figure 3.13). Notably, both of these sites match the ULK1 consensus we defined using peptide libraries.

In contrast to many of the substrates examined which contain between 2 and 4 ULK1-dependent phosphorylation sites, we only found a single protein with an apparent single site regulated: Vps34. The highly conserved Ser249 of Vps34 was stoichimetrically phosphorylated in HEK293 cells when co-expressed with wild-type

but not kinase dead ULK1 (Figure 3.14 and Figure 3.15). In vitro kinase assays using Vps34 as a substrate revealed that a single serine-to- alanine substitution at Ser249 abolished in vitro phosphorylation of Vps34 by ULK1 (Figure 3.16), which was paralleled by abolition of a significant mobility shift of Vps34 protein with the Ser249Ala mutant even on a regular SDS-PAGE gel when co-expressed with ULK1 (Figure 3.17).

We explored the potential function for Vps34 phosphorylation by ULK1 by introducing non-phosphorylatable (Ser249Ala) or phospho-mimetic (Ser249Asp) mutants into conditional Vps34 floxed murine embryonic fibroblasts (Jaber et al., 2012). After first corroborating the requirement of Vps34 for proper autophagy and ultimate cell viability (Figure 3.18), we tested the effects of the mutants in four assays of Vps34 function in autophagy: LC3 and p62 turnover in MEF following starvation (Figure 3.19), PI3P production in vivo as detected by p40FX-GFP immunolocalization (Figure 3.20), autophagosome formation as detected by GFP-DFCP1 immunolocalization in vivo (Figure 3.21), cell viability following starvation (Figure 3.22), and EGFR turnover as a measure of general Vps34 function independent of autophagy (Figure 3.23). Vps34 Ser249 did not appear to control any of these activities under the conditions we examined. Given that ULK1 is also regulating multiple phosphorylation events in Beclin and Ambra1 at the same time it is inducing Ser249, this suggests that the sum effects of Ulk1 on the different Beclin-Vps34 subcomplexes will be a highly regulated series of events requiring further study.

We next developed a phospho-specific antibody to Vps34 Ser249, whose signal was increased when ULK1 or ULK2, but not ULK3, was co-expressed with a wild-type but not Ser-249Ala mutant in HEK293T cells (Figure 3.24). Using this phospho-Ser249 Vps34 antibody, we next directly compared its sensitivity to a commercially available phospho-Ser15 Beclin antibody, demonstrating parallel induction of each site when wild-type but not kinase ULK1 was co-expressed in HEK293T cells (Figure 3.25). Notably, the residues flanking Ser15 of Beclin and Ser249 of Vps34 share extensive sequence homology, beyond the ULK1 selective sites at -3 and +1 (Figure 3.25).

Development of novel ATP-competitive inhibitors of ULK1

To further examine how ULK1 regulates autophagy, we sought to identify small molecule ATP competitive kinase inhibitors of ULK1. Screening a library of heterocyclic chemical compounds for inhibitors of ULK1 kinase activity in vitro, we identified a lead compound that was further elaborated through a medicinal chemistry effort to produce SBI-0206965. Dose-response analysis of SBI-0206965 revealed an in vitro IC_{50} of 107nM for ULK1 and 711nM for ULK2 kinase activity (Figure 3.26). To further characterize the ability of SBI-0206965 and related derivatives to inhibit ULK1 in cells, we tested the ability of these compounds to inhibit the phosphorylation of Vps34 Ser249 when epitope-tagged Vps34 was co-expressed in HEK293T cells with a wild-type ULK1 cDNA. Screening 40 compounds, we found SBI-0206965 inhibited P-Vps34 on overexpressed Vps34 when used at ~5uM (Figure 3.27). We

next examined the sensitivity of phosphorylation of Vps34 Serine 249 versus Beclin Serine 15 to a dose response of ULK1 inhibitors, when cDNAs bearing each were introduced into HEK293T cells. We found that in HEK293Ts, SBI-0206965 inhibited Beclin Ser15 and Vps34 Ser249 to comparable extents and with similar kinetics (Figure 3.28).

SBI-0206965 is a highly selective ULK1 inhibitor

We next examined the specificity of SBI-0206965 using the DiscoveRx KINOMEscan panel of 456 purified human kinases and subsequent competition binding assay (Fabian et al., 2005; Karaman et al., 2008). As seen in Figures 3.29 and 3.30, SBI-0206965 was very selective, only inhibiting 8 kinases >95% and 19 kinases > 90% when tested at 10uM. The S(35) selectivity index of SBI-0206965 = 0.123 where S(35) = (number of non-mutant kinases with %Ctrl <35)/(number of non-mutant kinases tested) (Table 3.1), as measured by the % of the kinome inhibited below 35% of control comparable to several kinase inhibitors in widespread use in clinical oncology, including Gleevac and Lapatinib (Karaman et al., 2008). Notably, by this ATP binding pocket competition assay, SBI-0206965 inhibited FAK, Src, Abl, and Jak3 with similar IC50 to Ulk1 (Table 3.2), which is notable as other than ULK1, all of the other kinases hit by the compound act on tyrosine residues.

To use a more well-established measure of the selectivity of SBI-0206965 against its top binding kinases, we examined dose-response curves for its inhibition of these kinases in a classic in vitro kinase assays. Here we tested the ten kinases most

suppressed by SBI-0206965 by the competition binding assay. From this analysis, FAK, ULK1, JAK2, and AuroraA kinase emerged as being equivalently inhibited by SBI-0206965 (Table 3.3). It is important to note that even though SBI-0206965 inhibits these 4 kinase quite equivalently across all of the different assays we have examined, this is still greater selectivity than all but a handful of widely used ATP-competitive kinases inhibitors widely used in clinical oncology today (Karaman et al., 2008). We next examined the ability of SBI-0206965 to suppress signaling downstream of various kinases in cells in culture. We found that at 1uM, SBI-0206965 reduced FAK and AuroraA kinase signaling to an extent comparable to inhibition of Ulk1 (Figure 3.31) in HEK293T cells.

SBI-0206965 following nutrient deprivation prevents ULK1-dependent cell survival

One of the best-established functions of autophagy is to promote cell survival under conditions of nutrient deprivation. Indeed, genetic deletion of ATG5 in MEFs has no effect on cell survival of cells in normal media conditions, but when such cells are placed into starvation media, they undergo apoptosis at an accelerated rate compared to control cells (Guo et al., 2011). Similarly, we previously demonstrated that RNAi to ULK1 and ULK2 phenocopied RNAi to ATG5 in the loss of cell viability under nutrient deprived conditions (Egan et al., 2011b). To examine whether our small molecule ULK1 inhibitor would similarly control cell survival under nutrient deprived conditions, we treated MEFs with SBI-0206965 in the context of

normal media, amino-acid deprived media, or glucose-deprived media. At 24h after amino-acid deprivation, 20% of the vehicle treated MEFs were positive for AnnexinV, a classic apoptotic marker (Figure 3.32), whereas 50% of the SBI-0206965 treated cells were AnnexinV positive. An immunoblot timecourse analysis of amino-acid starved cells revealed that active cleaved caspase-3 and the cleavage of its target PARP was observed only appreciably in starved, SBI-0206965 co-treated cells (Figure 3.33). Interestingly, the immunoblot analysis revealed that SBI-0206965 treatment induced loss of ULK1 and Atg13 protein levels, but only in nutrient-deprived, and not nutrient replete, conditions. Perhaps only in this context when ULK1 is activated, does the direct binding of SBI-0206965 stimulate ULK1 turnover (Figure 3.33).

Small molecule ULK1 inhibitor converts the cytostatic response to catalytic mTOR inhibitors into a cytotoxic response

There has been great interest in the role of autophagy in the survival of tumor cells, particular tumor cells faced with metabolic stress from chemotherapies or targeted therapeutics. We next examined whether SBI-0206965 would promote apoptosis in tumor cells similar to the MEFs, selectively under conditions in which autophagy is actively engaged. Given that mTOR activity is a dominant regulator of ULK1 activity, and we previously noted that treatment of cells with mTOR catalytic inhibitors was sufficient to induce ULK1 activity, we examined the effect of adding in the ULK1 inhibitor in the context of treatment with mTOR catalytic inhibitors. Using a cell line well-established to be sensitive to mTORC1 inhibition, A549 lung cancer

cells, we treated with escalating doses of ULK1 inhibitor while keeping a constant cytostatic growth arrest-inducing 1 micromolar dose of the mTOR catalytic inhibitor AZD8055 (Figure 3.34). We observed that 5uM SBI-0206965 in combination with AZD8055 triggered apoptosis in 22% of A549 cells compared to 9% of the 5uM SBI-0206965 alone or 6% of those cells treated with AZD8055 alone. The induction of Annexin-V+ apoptotic A549 cells was even more dramatically heightened at 10 or 20uM dosing of SBI-0206965. As observed in MEFs with nutrient deprivation combined with the ULK1 inhibitor, immunoblot analysis revealed that only the combination of ULK1 and mTOR inhibitors triggered caspase activation in A549 cells, paralleling the FACS analysis of cell death (Figure 3.35). Degradation of total ULK1 levels and Atg13 levels was observed as before, only in the presence of the autophagy activating stimulus (AZD8055) and the ULK1 inhibitor.

Discussion

Autophagy has been best understood as a cellular response to loss of nutrients in which cells cannibalize various proteins and organelles to provide building blocks and critical metabolites needed for cell survival. In addition, autophagy plays a critical homeostatic role in many tissues by removing protein aggregates and defective organelles that accumulate with cellular damage over time. While genetics first defined the core components of autophagy conserved across all eukaryotes, the molecular details of how the different autophagy complexes regulate one another and

the precise temporal and spatial ordering of biochemical events involved in autophagy induction are poorly understood currently.

Given that the most upstream component of the conserved autophagy cascade encodes the only serine/threonine kinase in the cascade, it has been assumed that ULK1-dependent phosphorylation of other components of the pathway must instruct and provide proper temporal and spatial cues. While a detailed understanding of how ULK1 is controlled by opposing phosphorylation events by AMPK and mTORC1 has become appreciated, the absolute requirement for ULK1/2 in different forms of mammalian autophagy has become less clear given recent findings that AMPK and mTOR also regulate multiple components of the downstream Beclin-Vps34 complex which directly initiates the PI3P lipid formation which incorporates into the omegasome and is held to represent a direct physical initiation of autophagosomes. If AMPK and mTORC1 control Beclin/Vps34 complexes directly, what is the function of the ULK1 kinase complex in autophagy initiation, and autophagy components is it targeting?

Here we shed additional light on the complexities involved by identifying multiple ULK1-dependent phosphorylation sites in Beclin, Ambra1, and Vps34. Though not studied here, it is also notably that Atg14 contains a conserved ULK1 consensus site as well (Ser29). Recent reports that AMPK phosphorylates distinct sites from these ULK1 sites in both Beclin and Vps34 reveals that additional tools including sensitive phospho-specific antibodies against these sites which can be used to determine if spatial or temporal differences for these targets.

The induction of ULK1 kinase activity following catalytic mTORC1 inhibition alone is consistent with amino acid deprivation induction of ULK1 kinase activity, which does not appear to involve AMPK. mTORC1 phosphorylates one now well-established serine site in ULK1, Ser757(Kang et al., 2013; Kim et al., 2011) and mTOR inhibitors are being widely testing in clinical trials for oncology, and rapamycin analogs are the approved standard of care for advanced kidney cancer and other solid tumors. Given that ULK1 is a kinase inhibited by mTORC1, further delineation of ULK1 substrate phosphorylation sites may yield important biomarkers for mTOR inhibitors as their signal will increase under the exact conditions when mTORC1-substrates phosphorylation is decreasing.

Moreover, autophagy provides a survival signal to cells faced with mTORC1 inhibition and this effect may greatly rely on ULK1 as the primary mechanism by which mTORC1 suppresses autophagy, unlike board nutrient loss which may engage the autophagy pathways via ULK1-dependent and ULK1-independent means (including direct phosphorylation of Beclin-Vps34 complexes by stress kinases like AMPK and p38, etc). ULK1 inhibition would be expected to convert the cytostatic response to mTOR inhibition to a cytotoxic response due to loss of ability of autophagy to promote cell survival, a hypothesis we directly test and demonstrate is true in A549 NSCLC cells in Figure 3.34 and Figure 3.35.

The fact that ULK1 is the only conserved serine/threonine kinase in the autophagy cascade makes it a very unique and attractive target for therapeutic development. Our findings that SBI-0206965 potently synergizes with nutrient

deprivation to trigger cell death in tumor cells, yet has minimal effects on cells growing in full media corroborates findings with genetic loss of ULK1/2. The finding that ULK1 and its binding partner Atg13 are selectively degraded by co-treatment of starvation and SBI-0206965, but not following either alone, indicates that the active pool of the ULK1 kinase complex may be uniquely sensitive to SBI-0206965-induced degradation. This provides additional biomarkers for ULK1 inhibition in vivo, as it suggests that when cells rely on ULK1 for survival, their ULK1 will be degraded when effectively inhibited by on-target ATP-competitive inhibitors. This suggests that total ULK1 or total Atg13 levels could serve as a biomarker for effective targeting and suppression of ULK1 in contexts where it is turned on to act as a survival promoting mechanism. The development of additional ULK1-selective ATP-competitive inhibitors will allow for the full examination of the pathological contexts which autophagy inhibition stimulates clearance of damaged cells and expedites resolution of damaged and tumorigenic cells.

Experimental Procedures

Plasmids

The cDNA encoding human Atg13 (KIAA0652/AB014552) was obtained from Kazusa DNA Research Institute in Japan. The cDNAs for human FIP200, mouse ULK1, and mouse ULK2 constructs were obtained from Open Biosystems (clones 3908134, 6834534, and 5709559 respectively). Human Atg101, human VPS34, human Ambra1 and human Beclin-1 were obtained from Invitrogen. The cDNA for mouse Syntenin-1 was cloned from a cDNA library prepared from mouse embryonic fibroblasts (MEFs) and sequence verified to match the sequence of the transcript variant 1 of mouse Syntenin-1 (NM_001098227.1).

The Flag tag and attL1 sites (for BP reaction) were PCR'd using the standard procedure. cDNAs were subcloned into pDONR221 with BP clonase (Invitrogen), and site-directed mutagenesis was performed using QuikChange II XL (Stratagene). Kinase dead ULK1 was achieved by a K46I mutation. Kinase dead VPS34 was achieved by D747N/N748K double mutation. Wild type and mutant alleles in pDONR221 were sequenced in their entirety to verify no additional mutations were introduced during PCR or mutagenesis steps and then put into either pcDNA3 Myc or Flag mammalian expression vector, or pcDNA6.2 V5 dest (Invitrogen), or pQCXIN retroviral destination vector (Addgene 17399) by LR reaction (Invitrogen). pMXspuro-GFP-DFCP1 was a kind gift from Noboru Mizushima and pEGFP-p40PX was a kind gift from Seth Field (UCSD).

Antibodies and reagents

Cell Signaling Antibodies used: total 4EBP-1 (#9452), total Beclin (#3495), Parp (#9542), total Atg13 (#6940), pAMPK Thr172 (#2535), total AMPK alpha1(#2532), pACC Ser79 (#3661), total ACC (#4190), pAurora (#2914), pRaptor Ser792 (#2083), total raptor (#4978), phospho ULK1 ser555 (#5869), pS6 (#4858), Myc (#2278), LC3B (#3868), total VPS34 (#4263), pJak2 (#4406). Phospho VPS34 ser249 antibody was developed in collaboration with Gary Kasof at Cell Signaling Technology.

Abgent antibodies used: gabarap (PM037). pFAK Y397 from Abcam (ab4803). Total FAK from Epitomics (2146-1). Sigma antibodies used: Total ULK1(A7481) tubulin (T5168), and Flag polyclonal (F7425). Guinea pig anti p62 sequestosome antibody from Progen, Heidelberg Germany (03-GPP62-C). pBeclin-1 ser15 from Abbiotec (254515).

EBSS (14155-063) and Glucose-free media (11966-025) from Gibco/Life Technologies. Chloroquine from Sigma. AZD-8055 (A-1008) from Active Biochem. Annexin V-PE Apoptosis Detection Kit from BD Biosciences. Phos-tag^{TM} AAL-107 from NARD (#304-93521). Adeno-Cre purchased from University of Iowa adenoviral core.

Cell Culture, Transient Transfections, Cell lysis and Phos-tag^{TM} mobility shift analysis

HEK293T, U87MG, PC3, A549 and SV40 immortalized wild-type mouse embryonic fibroblast (MEF) cells were cultured in DMEM (Mediatech, Manassas,

VA) containing 10% fetal bovine serum (Hyclone, Thermo Scientific) and penicillin/streptomycin at 37°C in 10% CO_2. $FAK^{-/-}$ MEFs were a kind gift from David Schlaepfer (UCSD), $ULK1^{-/-}$ and $ULK1/2^{-/-}$ MEFs from Craig Thompson (MSKCC) $VPS34^{flox/flox}$ MEFs from Wei-Xing Zong (SUNYSB) and $Atg5^{-/-}$ MEFs from Jay Debnath (UCSF).

For transient expression in HEK293T cells were transfected with 2ug each DNA plasmid per 6cm dish using Lipofectamine 2000 (Invitrogen) following the manufacturer's protocol. Cells were harvested 24 hours after transfection and rinsed once with ice-cold PBS and lysed in boiling SDS lysis buffer (10mM Tris pH7.5, 100mM NaCl, 1% SDS). After trituration, lysates were equilibrated for protein levels using the BCA method (Pierce) and resolved on 8 to 15% SDS-PAGE Phos-tag™ gels according to the manufacturers instructions. Briefly, Phos-tag™ AAL-107 (NARD #304-93521) was added to SDS-PAGE acryamide mixture at a final concentration of 50 μM along with $MnCl_2$ at a final concentration of 100 μM. Prior to transfer, the gel is soaked in transfer buffer containing 1 mmol/L EDTA for 30 min with gentle agitation to eliminate the manganese ions from the gel. The gel is transfered to PVDF membrane and probed with indictated antibodies according to the manufacturers instructions.

Lenti- and retro-viral Preparation and Viral Infection

Lentiviral shRNA transduction and retroviral gene expression was performed as described previously(Gwinn et al., 2008). Briefly, the pQCXIN Flag ULK1

construct was transfected along with the ampho packaging plasmid into growing 293Ts. Virus-containing supernatants were collected 48 hours after transfection, filtered to eliminate cells and target ULK1 -/- MEFs or A549s were infected in the presence of polybrene. 24 hours later, cells were selected with neomcyin. The pLKO shRNA vectors encoding shRNAs were transfected into HEK293T cells with lentiviral packaging plasmids vsvg, GAG/pol, and REV using Lipofectamine 2000. Viruses were collected 48 hours after transfection, and MEFs (shRNA #93 against mULK2) and U2OS (shRNA #8 and #91 against hULK1 and hULK2 respectively) already stably expressing Myc ULK1 were infected with the collected viruses for 4 h in the presence of polybrene to knock down the endogenous human protein, but not Myc ULK1, which is mouse.

Apoptosis Analysis - Western Blot and Flow Cytometry:

A549 cells (ATCC #CCL185) and MEFs were seeded at a concentration of 2.5 x 10^5 cells/mL (ie. 750,000 cells per 6cm dish), grown overnight (18hrs) and treated as indicted in the figure legends. Unless otherwise indicated, "starvation" is EBSS and "control" is DMEM with full serum for indicated timepoints. Samples for western blot were washed once in 1x ice cold PBS and lysed in boiling SDS lysis buffer (10mM Tris pH7.5, 100mM NaCl, 1% SDS). After trituration, lysates were equilibrated for protein levels using the BCA method (Pierce) and resolved on 8 to 15% SDS-PAGE gels, depending on the size of the protein. PVDF membranes were probed with indicated antibodies overnight according to the manufacturers

instructions.

For flow cytometry analysis, cells were collected at the appropriate time point, washed once in PBS, trypsinized and pelleted. For Annexin V staining, cells were washed in 1x Annexin V buffer and treated as described by the Annexin V staining protocol (BD Pharmingen, San Diego, CA). Briefly, cells were resuspended in Annexin V buffer to a concentration of one million per mL, 100,000 cells were then stained with 5 μL of phycoerythrin (PE)-conjugated Annexin V antibody (BD Pharmingen, San Diego, CA) and 5 μL of 7-amino-actinomycin D (7AAD) and then incubated at room temperature for 15 minutes. 400μL of Annexin V buffer was then added to each sample with gentle mixing. Stained cells were analyzed using a FACScan flow cytometer (Becton Dickinson, San Jose, CA). Flow cytometry data was analyzed using FlowJo 8.6 software (Tree Star Inc., Ashland, OR).

ULK1 Kinase Assays

Gamma 32P assays to measure ULK1 kinase activity were performed as previously described(Jung et al., 2009). Briefly, Flag ULK1 was transfected into 293Ts and 20 hours later treated as indicated. The immmunoprecipitate was washed in IP buffer 3 times, and washed in kinase buffer (25 mM MOPS, pH 7.5, 1 mM EGTA, 0.1 mM Na_3VO_4, 15 mM $MgCl_2$,). Hot and cold ATP were added at a 100 μM final concentration. As substrates, GST or the recombinant protein GST-Atg101 purified from *E. coli* were used at 1 μg for each reaction. Reactions were boiled, run out on SDS page gel. The gel was dried, and imaged using PhosphoImager software.

For cold assays to asses ULK1, Flag ULK1 which was transiently overexpressed and immunoprecipited from 293T cells. Reactions were then run out on SDS page gel, transferred to PVDF membrane and blotted for total levels

Fluorescence Microscopy

VPS34$^{flox/flox}$ MEFs were reconstituted with Flag VPS34 and either p40FX or GFP DFCP1. 48 hours post ad-Cre (MOI of 100), cells were plated on glass coverslips at a density of $3x10^5$ cells per well in 6-well tissue culture plates. 18h later, cells were fixed in 4% PFA in PBS for 10 minutes and permeabilized in 0.2% Triton in PBS for 10 minutes. The following primary antibodies were used: mouse anti-Myc epitope and LC3B XP antibody (2276 and 3868 respectively, Cell Signaling Technologies). Secondary antibodies were anti-rabbit Alexa488 and anti-mouse Alexa594 (Molecular Probes, 1:1000. Cells were then fixed and counter stained with DAPI. Coverslips were mounted in FluoromountG (SouthernBiothech). Confocal images were taken on Zeiss LSM 710 laser scanning confocal microscope. 10 random fields per condition were acquired using the 100x objective and representative images shown. Glass coverslips were mounted directly on plate with FluoromountG.

Peptide library screening

Peptide mixtures (50 mM) were incubated 2 hours at 30 oC in multiwell plates in the presence of the indicated kinase in 50 mM HEPES, pH 7.4, 25 mM MgCl2, 0.25 mM DTT, 12.5 mM b-glycerophosphate, 5 mM EGTA, 2 mM EDTA, 0.1% Tween

20, and 50 mM ATP (0.03 mCi/ml). Aliquots of each reaction were transferred to streptavidin-coated membrane (Promega), which was quenched, washed and dried as described previously (Hutti et al., 2004). Membranes were exposed to a phosphor imager screen to quantify radiolabel incorporation. Heat maps were generated using Microsoft Excel.

Mass Spectrometry

Myc ULK1 overexpressed in 293T cells was treated with either vehicle, A769662, or phenformin, IP'd with anti Myc antibody (Cell Signaling), run out on SDS page gel and coomassie stained. Bands on the gel corresponding to ULK1 were cut out and subjected to reduction with dithiothreitol, alkylation with iodoacetamide, and in-gel digestion with trypsin or chymotrypsin overnight at pH 8.3, followed by reversed-phase microcapillary/tandem mass spectrometry (LC/MS/MS). LC/MS/MS was performed using an Easy-nLC nanoflow HPLC (Proxeon Biosciences) with a self-packed 75 μm id x 15 cm C_{18} column coupled to a LTQ-Orbitrap XL mass spectrometer (Thermo Scientific) in the data-dependent acquisition and positive ion mode at 300 nL/min. Peptide ions from AMPK predicted phosphorylation sites were also targeted in MS/MS mode for quantitative analyses. MS/MS spectra collected via collision induced dissociation in the ion trap were searched against the concatenated target and decoy (reversed) single entry ULK1 and full Swiss-Prot protein databases using Sequest (Proteomics Browser Software, Thermo Scientific) with differential modifications for Ser/Thr/Tyr phosphorylation (+79.97) and the sample processing

artifacts Met oxidation (+15.99), deamidation of Asn and Gln (+0.984) and Cys alkylation (+57.02). Phosphorylated and unphosphorylated peptide sequences were identified if they initially passed the following Sequest scoring thresholds against the target database: 1+ ions, Xcorr ≥ 2.0 Sf ≥ 0.4, P ≥ 5; 2+ ions, Xcorr ≥ 2.0, Sf ≥ 0.4, P ≥ 5; 3+ ions, Xcorr ≥ 2.60, Sf ≥ 0.4, P ≥ 5 against the target protein database. Passing MS/MS spectra were manually inspected to be sure that all **b-** and **y-** fragment ions aligned with the assigned sequence and modification sites. Determination of the exact sites of phosphorylation was aided using FuzzyIons and GraphMod and phosphorylation site maps were created using ProteinReport software (Proteomics Browser Software suite, Thermo Scientific). False discovery rates (FDR) of peptide hits (phosphorylated and unphosphorylated) were estimated below 1.5% based on reversed database hits.

Selectivity profiling

Kinase inhibitor specificity profiling assays were first carried out using DiscoveRx KINOMEscan competition binding assay against a panel of 456 kinases (www.discoverx.com) using 1uM SBI-0206965. Kinases that potentially interacted with SBI-0206965 (inhibited to less than 10% DMSO control) were then tested in classic in vitro kinase assays with a dose curve of SBI-0206965 to monitor enzymatic activity and determine IC_{50} curves using Reaction Biology (www.reactionbiology.com).

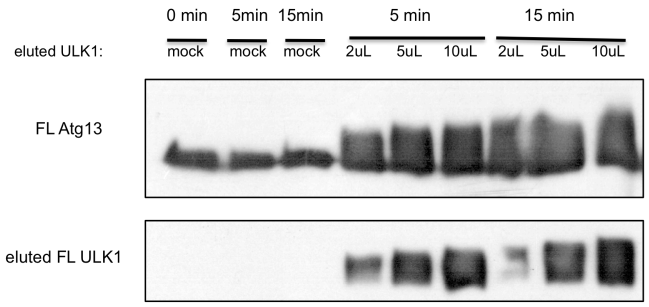

Figure 3.1: Flag tagged ULK1 is catalytically active as determined by in vitro kinase assay using Atg13 as a substrate

Wt Flag ULK1 was transfected into HEK293Ts and immunoprecipitated 24 hours later with M2 agarose. The immunoprecipitated ULK1 was eluted with 3X Flag peptide and used in an in vitro kinase assay with Flag Atg13 which was IP'd by the same manner from HEK293Ts from parallel plates. Mobility shift is indicative of phosphorylation.

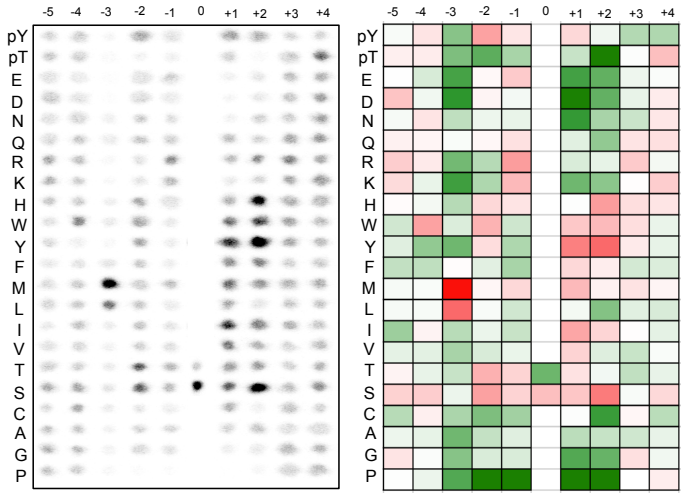

Figure 3.2:
Definition of optimal ULK1 consensus motif
Miniaturized peptide array approach enables high-throughput analysis of kinase consensus phosphorylation motifs. Capillary pin–based liquid transfer devices were used to add components to reactions (2 µl per well) and spot 0.2-µl aliquots onto the streptavidin-coated membrane after incubation. Flag ULK1 was immunoprecipitated from transiently transfected HEK293T cells, eluted with 3X Flag peptide for use in assay. Representative peptide screening results for ULK1. A heat map representing the quantified peptide array is shown on left.

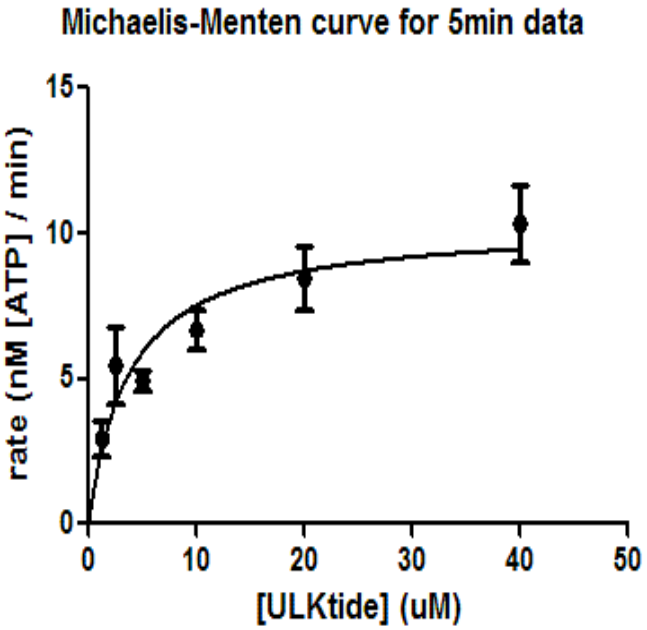

Figure 3.3: Optimizing conditions for ULKtide phosphorylation
Defining the in vitro conditions for in vitro kinase assays of ULK1 and the optimal peptide, named "ULKtide". Michaelis-Menten curve for ULK1 and the ULKtide at 5 minutes. K_m=5uM.

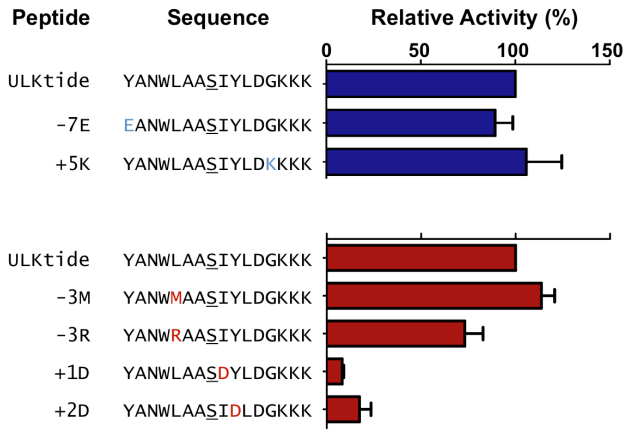

Figure 3.4: Requirement of amino acids relative to phosphoacceptor site
Rates of ULK1 phosphorylation of ULKtide variants with individual point substitutions. Peptide phosphorylation was assayed at 5 μM concentration by radiolabeled kinase assay. Incorporation of radiolabeled phosphate into peptides was determined by phosphocellulose filter binding assay.

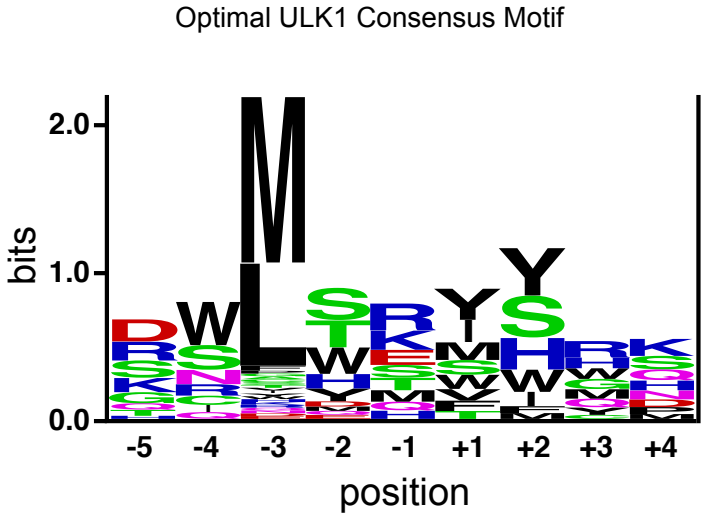

Figure 3.5: Consensus log of ULK1 motif
A consensus logo was generated using Phosphosite (http://www.phosphosite.org/sequenceLogoAction.do)

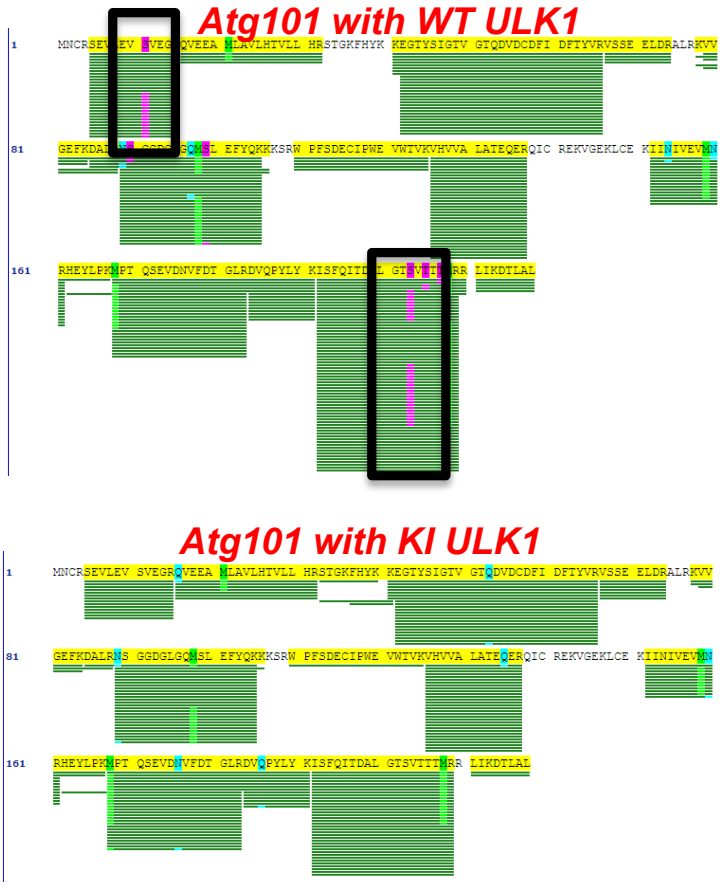

Figure 3.6: Diagram of all LC/MS/MS identified in vivo phosphorylation sites in human Atg101

Either Myc- wt ULK1 (top) or Myc kinsase dead ULK1(bottom) and Flag wt Atg101 were transfected into human embryonic kidney (HEK)-293T cells and immunoprecipitated with M2 agarose. The IP was run out on SDS PAGE, stained with coomassie, and the band corresponding to Flag Atg101 was cut out, isolated and subjected to tryptic digest and LC/MS/MS analysis. The sites matching the ULK1 substrate motif that were identified, are boxed. Green bars indicate peptide coverage, and purple highlights are phosphorylation.

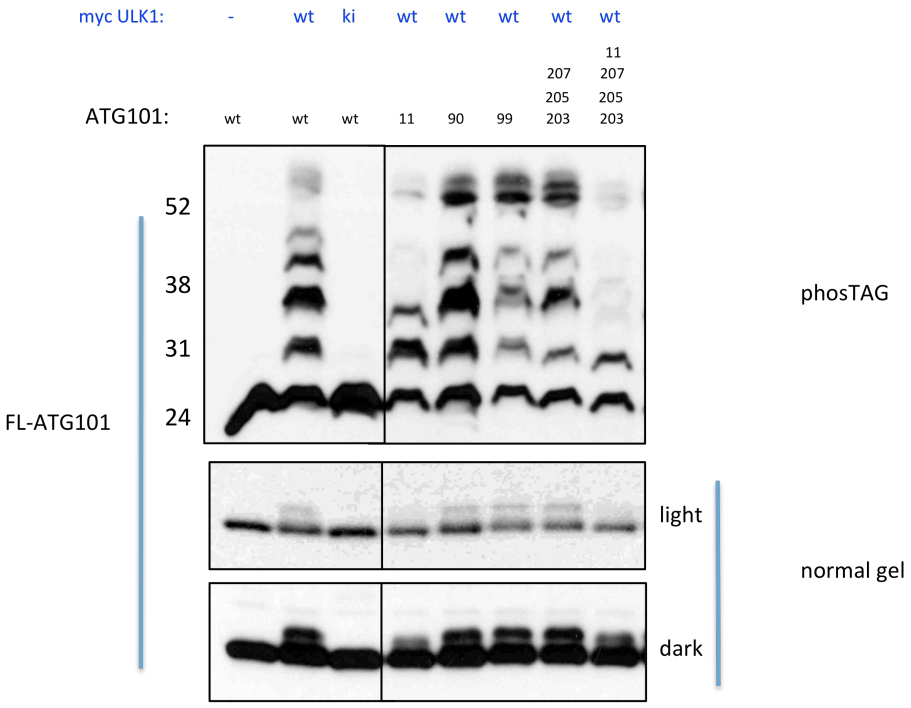

Figure 3.7: ULK1-dependent bandshifts in Atg101
Flag wt Atg101 and indicated Serine to Alanine pointmutants and either Myc ULK1 wt or Kinase dead (ki) ULK1 were transfected in HEK293T cells. Cells were lysed in boiling SDS buffer 24 hours after transfection, run on SDS-PAGE PhosTag® and probed with indicated antibodies.

Figure 3.8: Diagram of all LC/MS/MS identified in vivo phosphorylation sites in human FIP200

Myc- wt ULK1 and Flag wt FIP200 were transfected into human embryonic kidney HEK293T cells and immunoprecipitated with M2 agarose. The IP was run out on SDS PAGE, stained with coomassie, and the band corresponding to Flag FIP200 was cut out, isolated and subjected to tryptic digest and LC/MS/MS analysis.

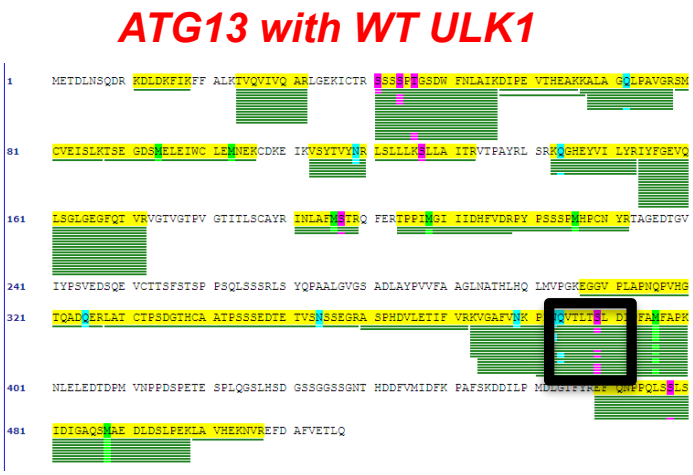

Figure 3.9: Diagram of all LC/MS/MS identified in vivo phosphorylation sites in human Atg13

Myc- wt ULK1 and Flag wt Atg13 were transfected into human embryonic kidney HEK293T cells and immunoprecipitated with M2 agarose. The IP was run out on SDS PAGE, stained with coomassie, and the band corresponding to Flag Atg13 was cut out, isolated and subjected to tryptic digest and LC/MS/MS analysis.

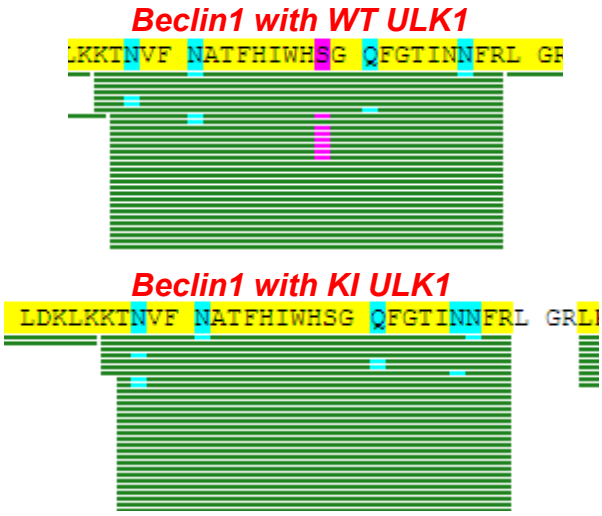

Figure 3.10: Diagram of all LC/MS/MS identified in vivo phosphorylation sites in human Beclin-1

Either Myc- wt ULK1 (top) or Myc kinsase dead ULK1(bottom) and Flag wt Beclin-1 were transfected into human embryonic kidney HEK293T cells and immunoprecipitated with M2 agarose. The IP was run out on SDS PAGE, stained with coomassie, and the band corresponding to Flag Beclin-1 was cut out, isolated and subjected to tryptic digest and LC/MS/MS analysis.

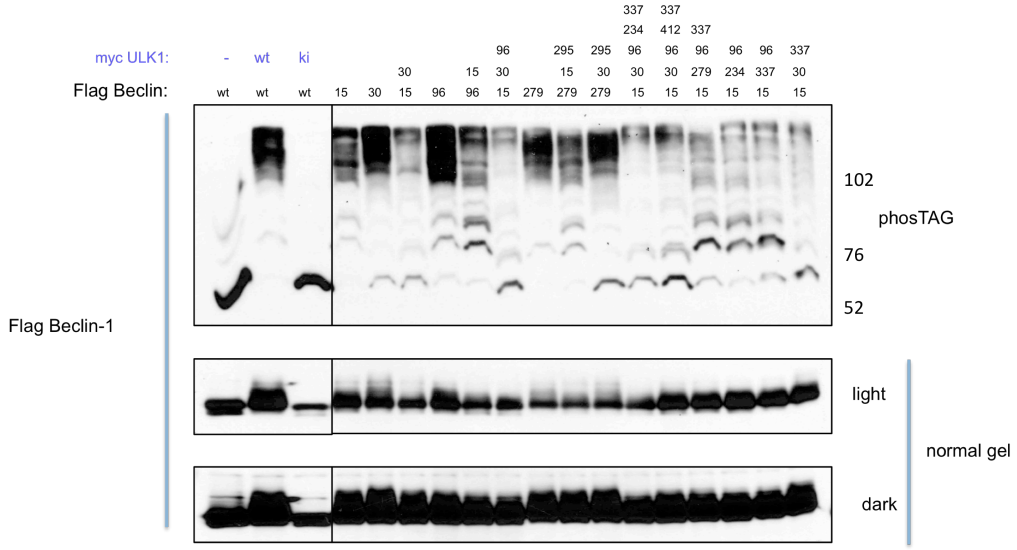

Figure 3.11: ULK1-dependent bandshifts in Beclin-1
Flag wt Beclin-1 and indicated Serine to Alanine pointmutants and either Myc ULK1 wt or Kinase dead (ki) ULK1 were transfected in HEK293T cells. Cells were lysed in boiling SDS buffer 24 hours after transfection, run on SDS-PAGE PhosTag® and probed with indicated antibodies.

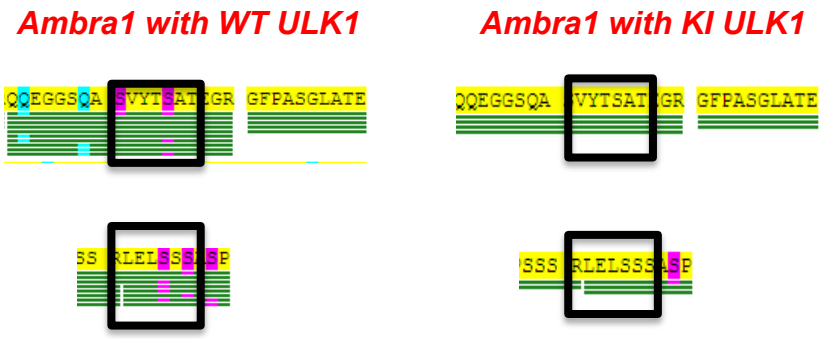

Figure 3.12: Diagram of all LC/MS/MS identified in vivo phosphorylation sites in human Ambra-1

Either Myc- wt ULK1 (left) or Myc kinsase dead ULK1(right) and Flag wt Ambra-1 were transfected into human embryonic kidney HEK293T cells and immunoprecipitated with M2 agarose. The IP was run out on SDS PAGE, stained with coomassie, and the band corresponding to Flag Ambra-1 was cut out, isolated and subjected to tryptic digest and LC/MS/MS analysis.

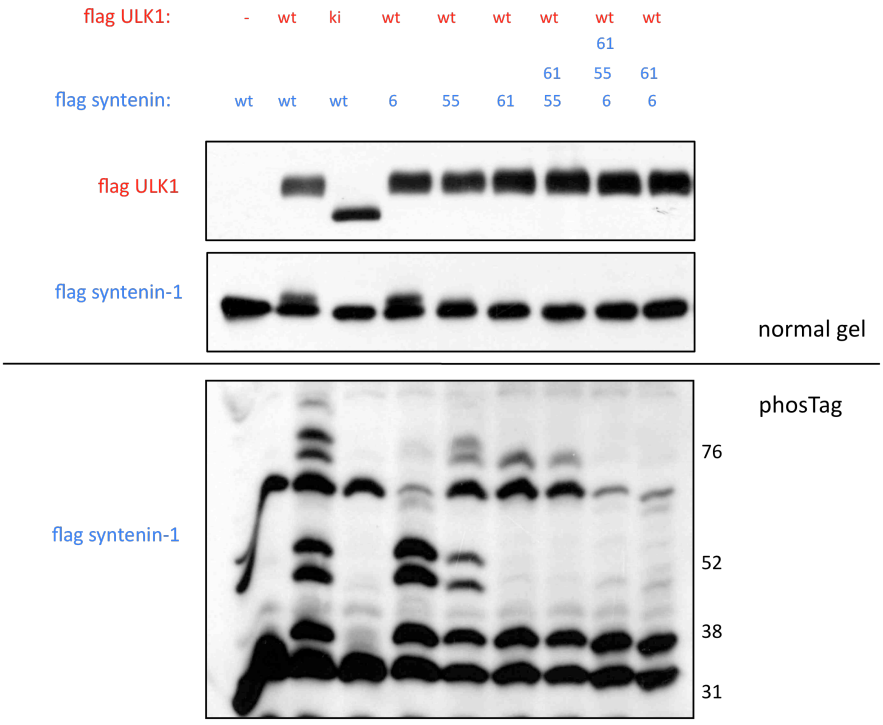

Figure 3.13: ULK1-dependent bandshifts in Syntenin-1
Flag wt Syntenin-1 and indicated serine to alanine point mutants and either Myc ULK1 wt or Kinase dead (ki) ULK1 were transfected in HEK293T cells. Cells were lysed in boiling SDS buffer 24 hours after transfection, run on SDS-PAGE PhosTag® and probed with indicated antibodies.

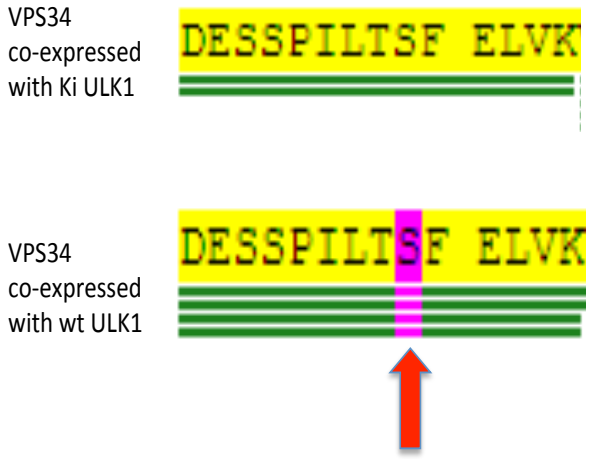

Figure 3.14: Diagram of in vivo LC/MS/MS surrounding serine 249 of VPS34
Either Myc- wt ULK1 (top) or Myc kinsase dead ULK1(bottom) and Flag wt VPS34 were transfected into human embryonic kidney HEK293T cells and immunoprecipitated with M2 agarose. The IP was run out on SDS PAGE, stained with coomassie, and the band corresponding to Flag VPS34 was cut out, isolated and subjected to tryptic digest and LC/MS/MS analysis.

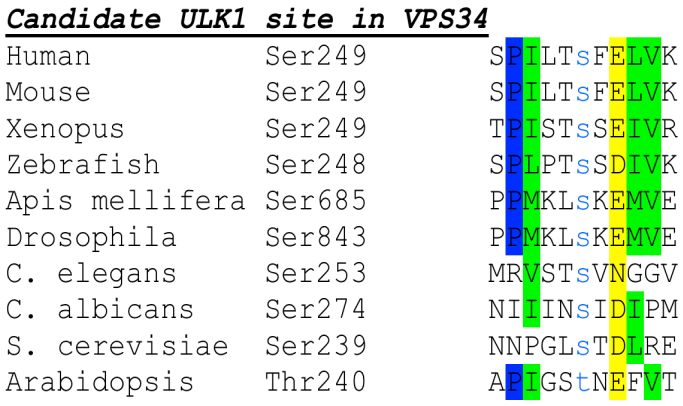

Figure 3.15: Serine 249 of VPS34 is highly conserved
Clustal alignment of serine249 of VPS34 shows it is conserved across evolution and matches the ULK1 consensus motif.

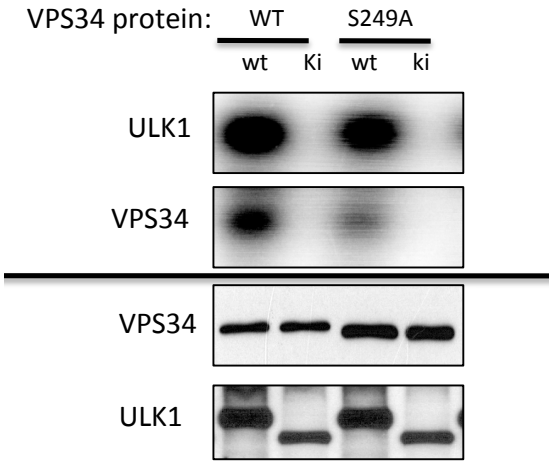

Figure 3.16: ULK1 directly phosphorylates VPS34 on serine 249
In vitro kinase assays with Flag-tagged VPS34 that was immunoprecipitated from HEK293T cells and used as substrates for either wt or catalytically inactive (ki: K46I) ULK1 in the presence of 32P-(C)-ATP.

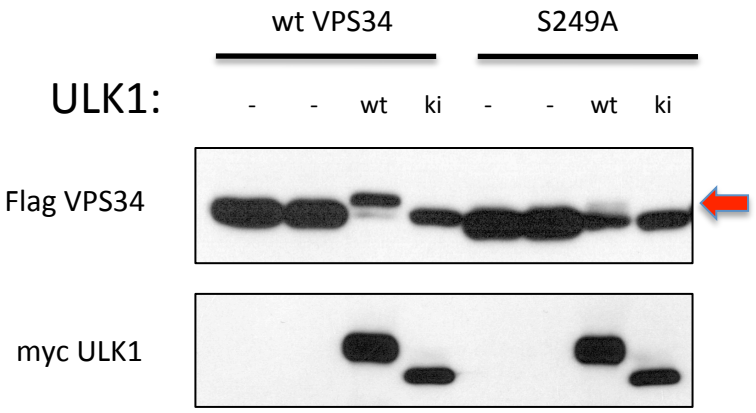

Figure 3.17: ULK1 phosphorylates VPS34 on serine 249 in cells
Flag wt VPS34 or Ser249A VPS34 and either Myc ULK1 wt or Kinase dead (ki) ULK1 were transfected in HEK293T cells. Cells were lysed in boiling SDS buffer 24 hours after transfection, run on SDS-PAGE and probed with indicated antibodies.

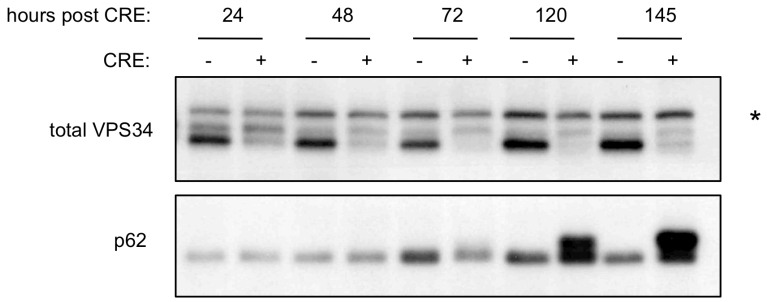

Figure 3.18: Conditional deletion of VPS34 in MEFs results in reduced autophagic flux
VPS34$^{flox/flox}$ MEFs were treated with Ad-Cre (MOI of 100) for indicated times. Cells were lysed, run on SDS-PAGE and immunoblotted as indicated.

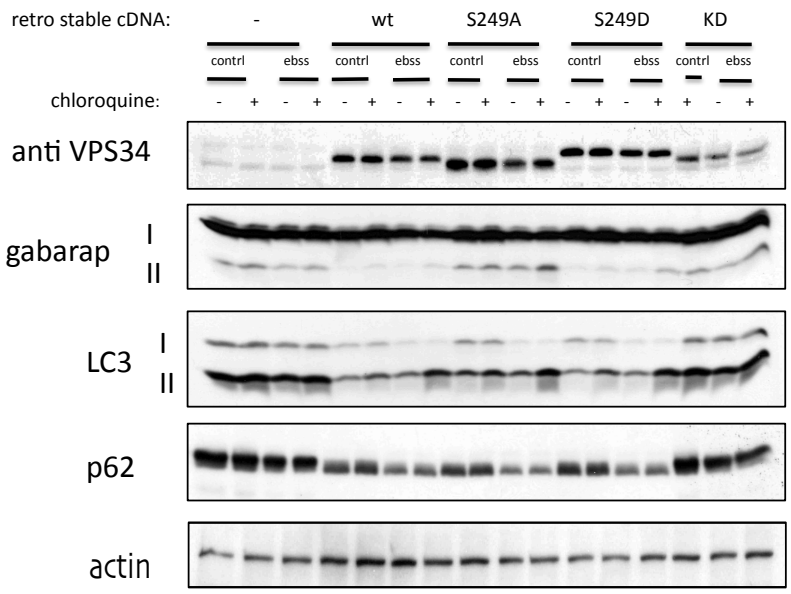

Figure 3.19: VPS34 ser249 is not required for LC3 lipidation or p62 degradation during starvation conditions

VPS34$^{flox/flox}$ MEFs reconstituted with retroviral Flag VPS34 and indicated serine-to-alanine mutants were starved (EBSS) for 2 hours, lysed and probed with indicated antibodies 48 hours post Ad-Cre infection. Cells were lysed in boiling SDS buffer, run out on SDS PAGE and probed with indicated antibodies.

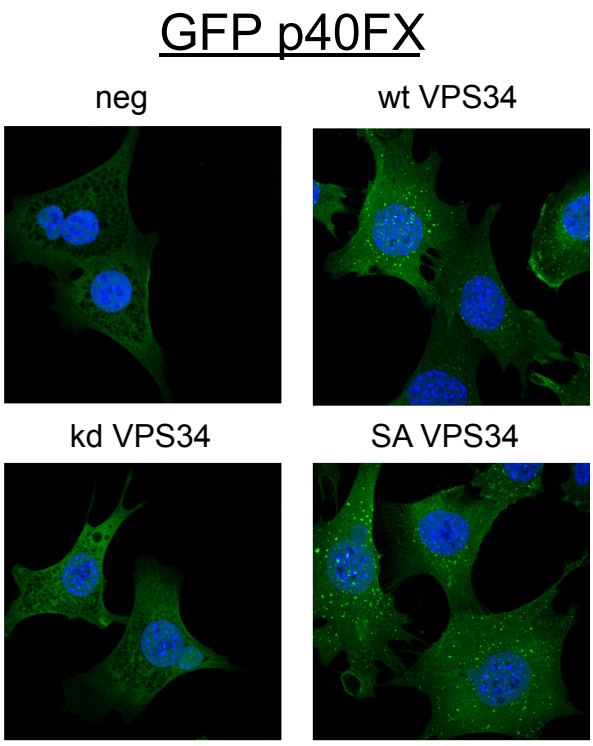

Figure 3.20: VPS34 ser249 is not required for p40FX punctae
VPS34$^{flox/flox}$ MEFs reconstituted with retroviral Flag VPS34 or indicated serine-to-alanine mutants and lenti viral transduction of GFP-p40FX were fixed in 4% PFA and analyzed by confocal microscopy 48 hours post Ad-Cre infection.

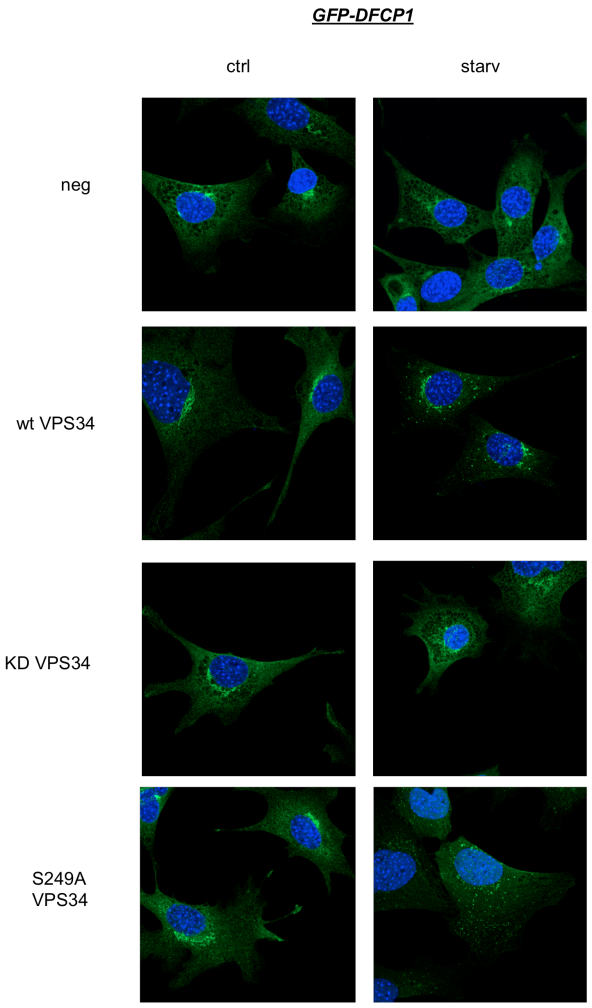

Figure 3.21: VPS34 ser249 is not required for DFCP1 punctae
VPS34$^{flox/flox}$ MEFs reconstituted with retroviral Flag VPS34 or indicated serine-to-alanine mutants and lenti viral transduction of GFP-DFCP1 were treated with fresh media or starvation media (EBSS) for two hours and fixed in 4% PFA and analyzed by confocal microscopy 48 hours post Ad-Cre infection.

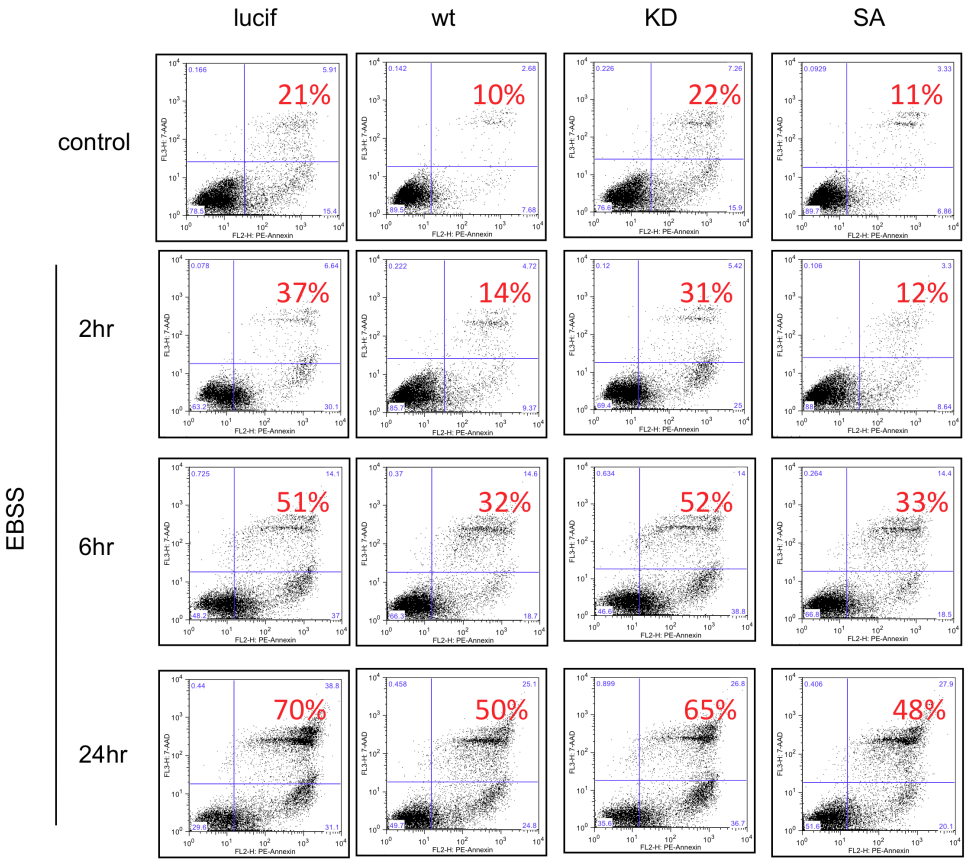

Figure 3.22: VPS34 ser249 is not required for MEFs to survive periods of starvation

VPS34$^{flox/flox}$ MEFs reconstituted with retroviral Flag VPS34 and indicated serine-to-alanine mutants were placed in normal DMEM or starvation media (EBSS) for indicated time periods 48 hours post Ad-Cre infection. Cells were collected and stained for 7-AAD and PE Annexin V and quantified using FACS.

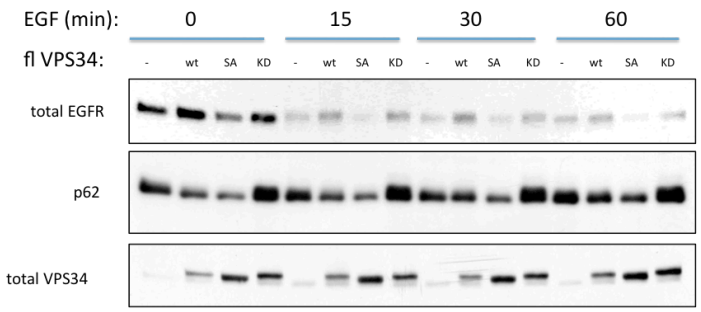

Figure 3.23: VPS34 ser249 is not required for endocytic EGFR degradation in MEFs

VPS34$^{flox/flox}$ MEFs reconstituted with retroviral Flag VPS34 and indicated serine-to-alanine mutants which were serum-starved overnight and stimulated with EGF (100 ng/mL) for the indicated times 48 hours post Ad-Cre infection. Cells were lysed run on SDS-PAGE and immunoblotted as indicated.

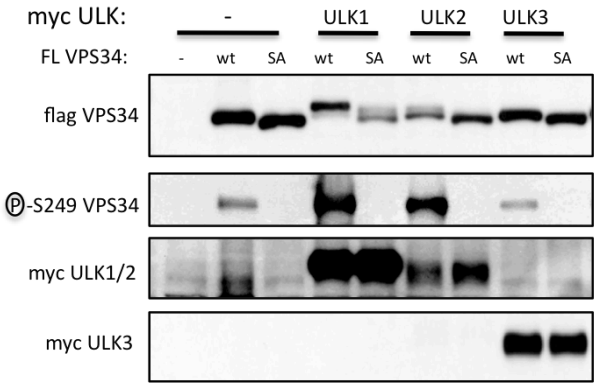

Figure 3.24: ULK1 and ULK2, but not ULK3 phosphorylate VPS34 on ser 249 in cells

HEK293T cells transfected with Flag-tagged wt VPS34 or indicated serine-to-alanine VPS34 mutants were cotransfected with a wt ULK1, wt ULK2 or wt ULK3, lysed 24 hours later, and run on SDS PAGE.

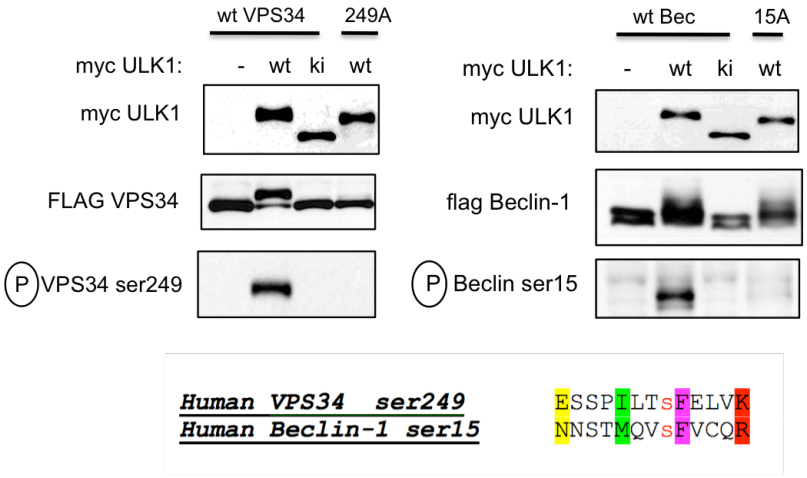

Figure 3.25: Beclin-1 ser15 and VPS34 ser249 are phosphorylated by ULK1 with similar kinetics and both match the ULK1 consensus motif
HEK293T cells transfected with Flag-tagged wt VPS34, or wt Beclin-1 or indicated serine-to-alanine mutants were cotransfected with wt ULK1 or ki ULK1and blotted with indicated antibodies.

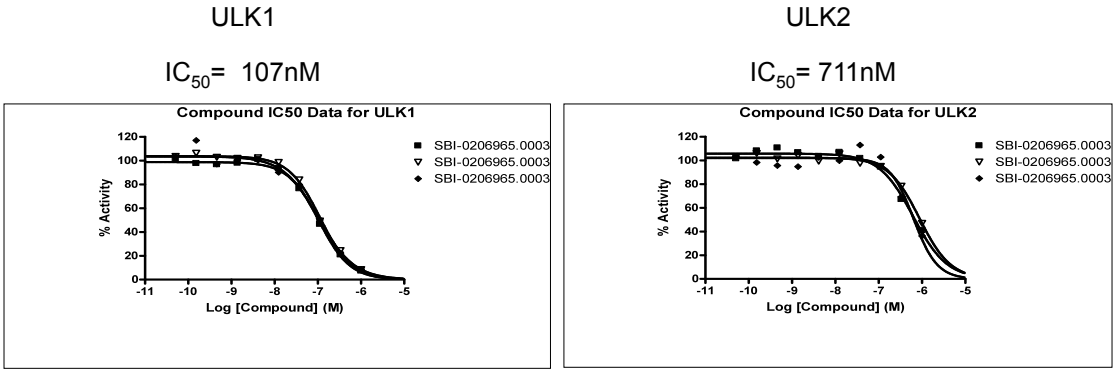

Figure 3.26: SBI-0206965 inhibits ULK1 and ULK2 in vitro
Wt ULK1(left) or ULK2 (right) were assayed using 10uM MBP in the presence of 30uM gamma 32 ATP with indicated concentrations of SBI-0206965. Compound was tested in triplicate in 10-dose IC_{50} mode with 3-fold serial dilution starting at 1 μM.

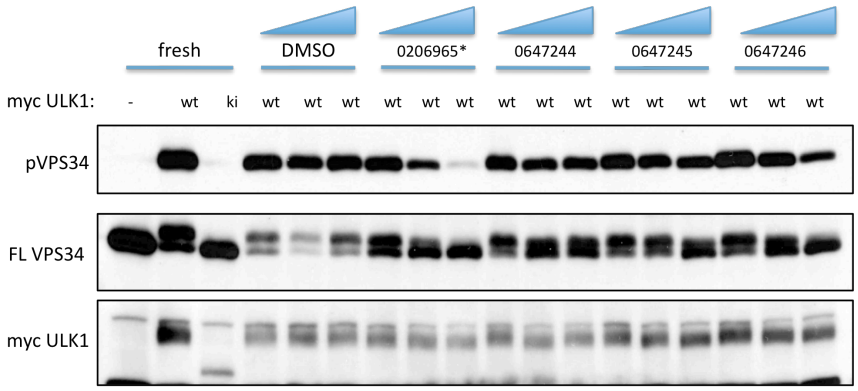

Figure 3.27: SBI-0206965 inhibits ULK1 in cells
HEK293T cells were co-transfected with Myc wt ULK1, or ki ULK1 and wt Flag VPS34. 94 compounds (only 4 are shown here) that were previously shown to affect ULK1 activity in vitro were tested at three different doses (1, 10, and 50uM) for 1 hour in cells. Cells were lysed, run out on SDS-PAGE and probed for indicated antibodies. Phospho-VPS34 indicates ULK1 kinase activity in cells.

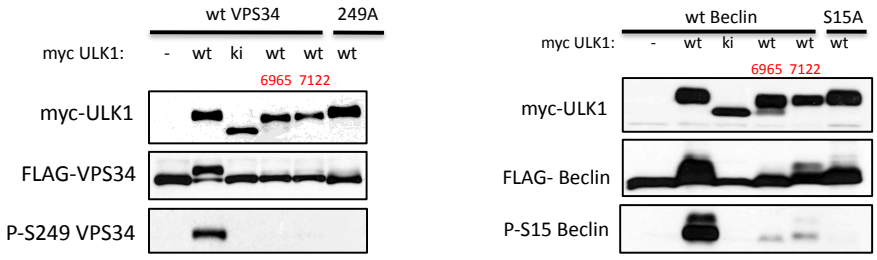

Figure 3.28: SBI-0206965 and SBI-0647122 inhibit ULK1 in cells
Of the 94 compounds (Figure 3.27) that were previously shown to affect ULK1 activity in vitro the two most potent were SBI-0206965 and SBI-0647122. HEK293T cells were co-transfected with Myc wt ULK1, or ki ULK1 and wt Flag VPS34 or Flag Beclin-1. Cells were treated with indicated compounds for 1 hour, lysed, and run out on SDS-PAGE and probed for indicated antibodies. DMSO is negative control.

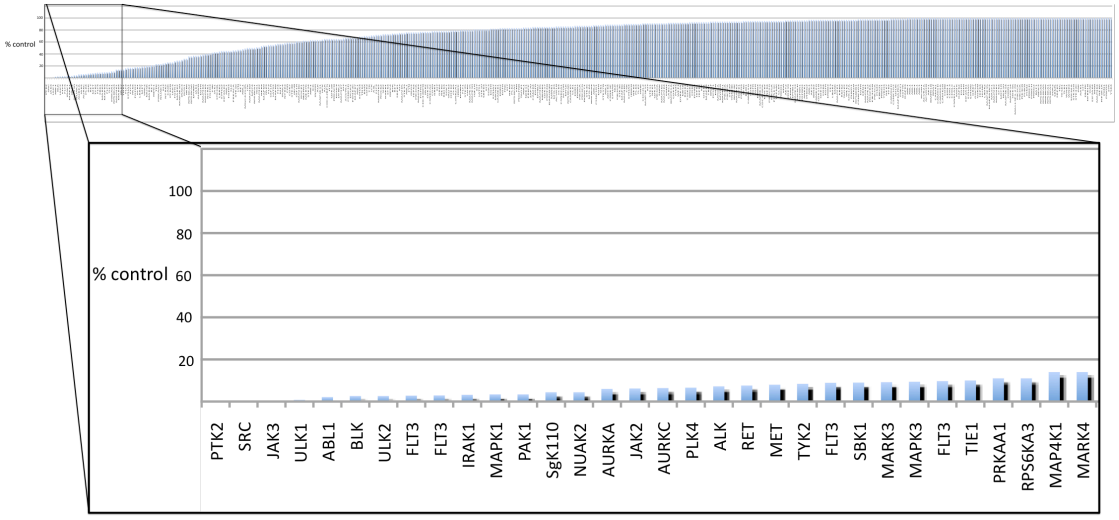

Figure 3.29: Selectivity profile of SBI-0206965
Kinase profiling of the SBI-0206965 inhibitor at 1 μM was carried out against the panel of 456 kinases using DiscoveRx KINOMEscan profiling service. Scores for primary screen hits are reported as a percent of the DMSO control (% Control).

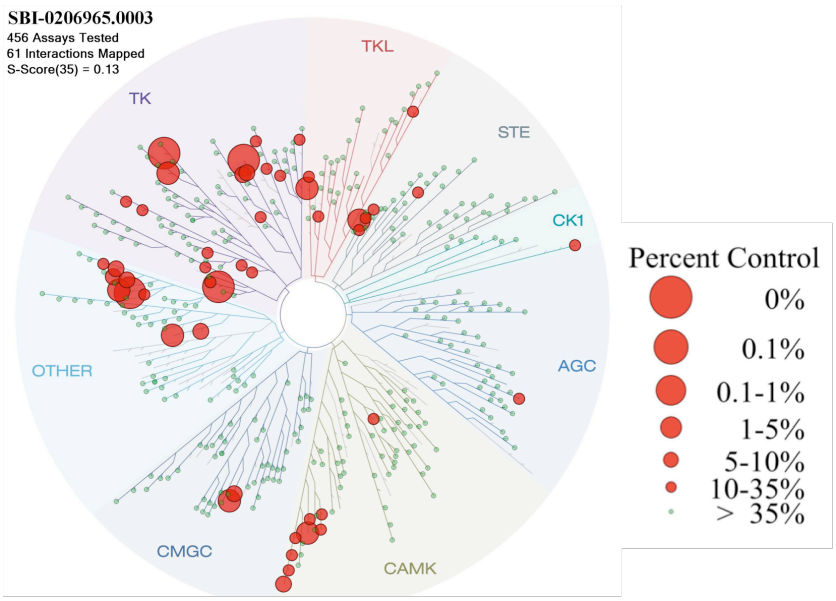

Figure 3.30: TREEspot interaction map of SBI-0206965 profile
Kinase profiling of the SBI-0206965 inhibitor at 1 μM was carried out against the panel of 456 kinases using DiscoveRx KINOMEscan profiling service. Scores for primary screen hits are reported as a percent of the DMSO control (% Control). Kinases found to bind are marked with red circles, where larger circles indicate higher-affinity binding.

Table 3.1: SBI-0206965 has negligible off-target activity against a diverse panel of kinases

Selectivity Score (S-score) of SBI-0206965. The quantitative measure of compound selectivity is calculated by dividing the number of kinases that compounds bind to by the total number of distinct kinases tested, excluding mutant variants.

Compound Name	Selectivity Score Type	Number of Hits	Number of Non-Mutant Kinases	Screening Concentration (nM)	Selectivity Score
SBI-0206965.0003	S(35)	49	397	1000	0.123
SBI-0206965.0003	S(10)	19	397	1000	0.048
SBI-0206965.0003	S(1)	4	397	1000	0.010

Table 3.2: Selectivity profiling of SBI-0206965
In vitro competition binding assay was used to evaluate the selectivity of SBI-0206965 using DiscoveRx KINOMEscan platform against a diverse set of 456 kinases. Kinases that are found to bind compound and inhibit less to less than 10% are in orange, and less than 1% are in red.

Compound Name	DiscoveRx Gene Symbol	Entrez Gene Symbol	Percent Control
SBI-0206965.0003	FAK	PTK2	0.2
SBI-0206965.0003	SRC	SRC	0.25
SBI-0206965.0003	JAK3(JH1domain-catalytic)	JAK3	0.4
SBI-0206965.0003	ULK1	ULK1	0.8
SBI-0206965.0003	ABL1(T315I)-phosphorylated	ABL1	2.1
SBI-0206965.0003	BLK	BLK	2.6
SBI-0206965.0003	ULK2	ULK2	2.6
SBI-0206965.0003	FLT3(D835Y)	FLT3	2.8
SBI-0206965.0003	FLT3(D835H)	FLT3	2.9
SBI-0206965.0003	IRAK1	IRAK1	3.2
SBI-0206965.0003	ERK2	MAPK1	3.4
SBI-0206965.0003	PAK1	PAK1	3.4
SBI-0206965.0003	SgK110	SgK110	4.4
SBI-0206965.0003	SNARK	NUAK2	4.4
SBI-0206965.0003	AURKA	AURKA	6
SBI-0206965.0003	JAK2(JH1domain-catalytic)	JAK2	6.2
SBI-0206965.0003	AURKC	AURKC	6.4
SBI-0206965.0003	PLK4	PLK4	6.6
SBI-0206965.0003	ALK(L1196M)	ALK	7.2
SBI-0206965.0003	RET(V804L)	RET	7.6
SBI-0206965.0003	MET(M1250T)	MET	8
SBI-0206965.0003	TYK2(JH1domain-catalytic)	TYK2	8.4
SBI-0206965.0003	FLT3(ITD)	FLT3	8.9
SBI-0206965.0003	SBK1	SBK1	9
SBI-0206965.0003	MARK3	MARK3	9.2

Table 3.3: In vitro IC_{50} data for off-target kinases
In vitro kinase assays were carried out in a dose response manner using Reaction Biology's kinase assay platform. The IC_{50} based on the dose response is listed in the table.

Kinase:	Relative IC50 (See Graph)	Fold vs ULK1
FAK	4.122E-08	0.4
JAK2	6.066E-08	0.6
Aurora A	6.447E-08	0.6
FLT3	7.932E-08	0.8
ULK1	1.08E-07	1.0
SNARK	1.368E-07	1.4
TYK2	2.273E-07	2.3

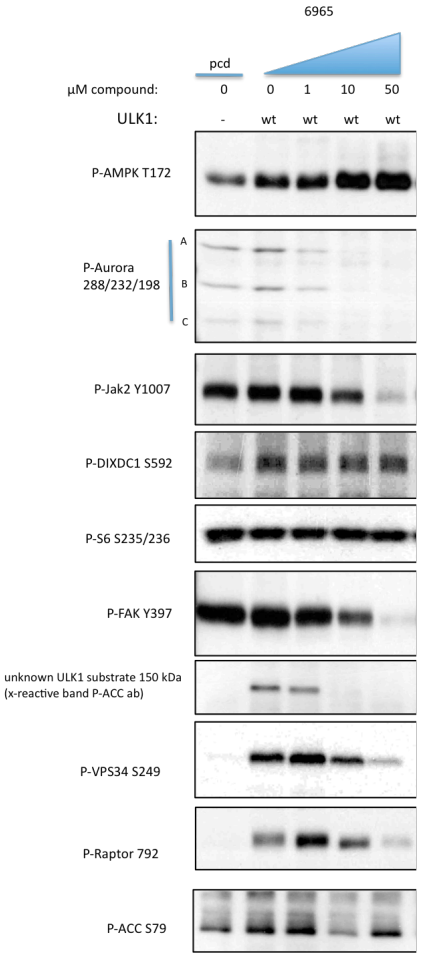

Figure 3.31: Effects of SBI-0206965 on off-target signalling in HEK293T cells
HEK293Ts were treated with indicated dose of SBI-0206965 for 1 hour. Cells were lysed, run on SDS-PAGE and probed with indicated antibodies.

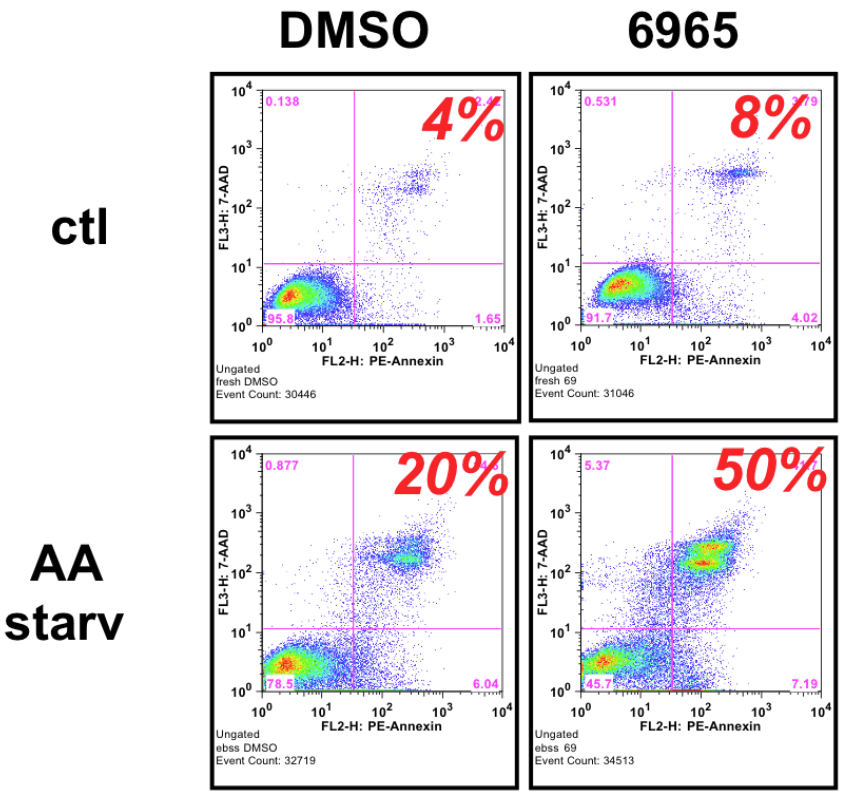

Figure 3.32: SBI-0206965 accelerates cell death during periods of starvation in MEFs

Wild type Mouse Embryonic Fibroblasts (MEFs) treated with either fresh media with DMSO, or starved (EBSS), or starved plus 10uM 6965 for 18 hours. Cells were collected and stained for 7-AAD and PE Annexin V and were quantified using FACS.

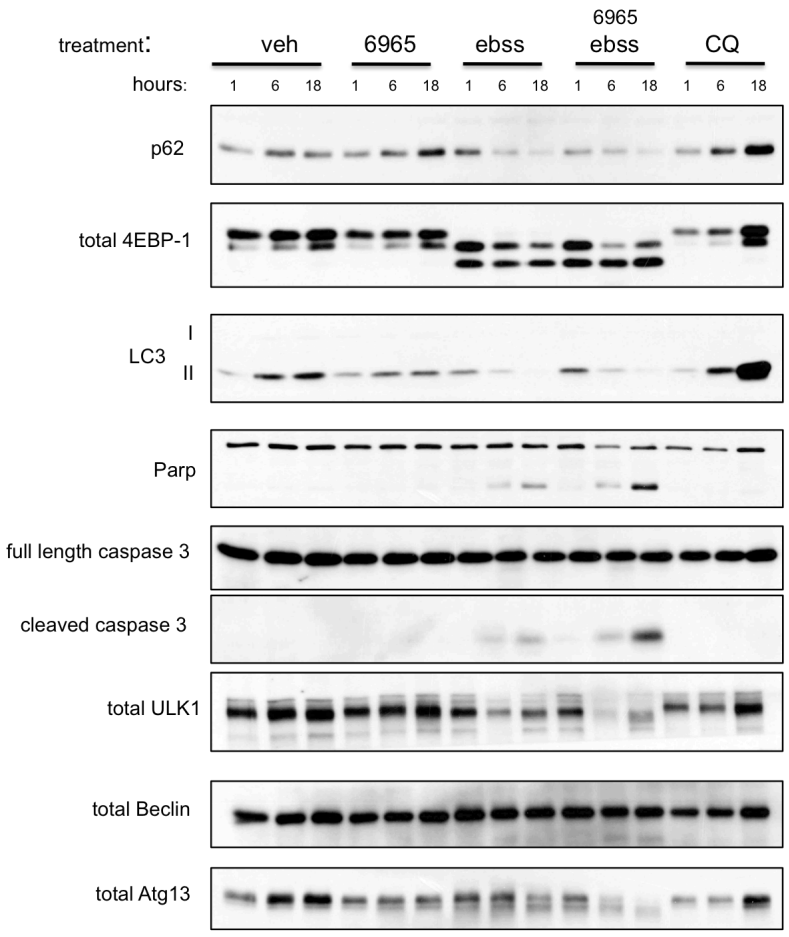

Figure 3.33: SBI-0206965 accelerates classic caspase activation during periods of starvation in MEFs

Timecourse of MEFs from Figure 32. Cells were treated for indicated timepoints, lysed in boiling SDS lysis buffer, and separated by SDS-PAGE and probed for indicated antibodies. Chloroquine (CQ) at 20uM serves as control for autophagy inhibition.

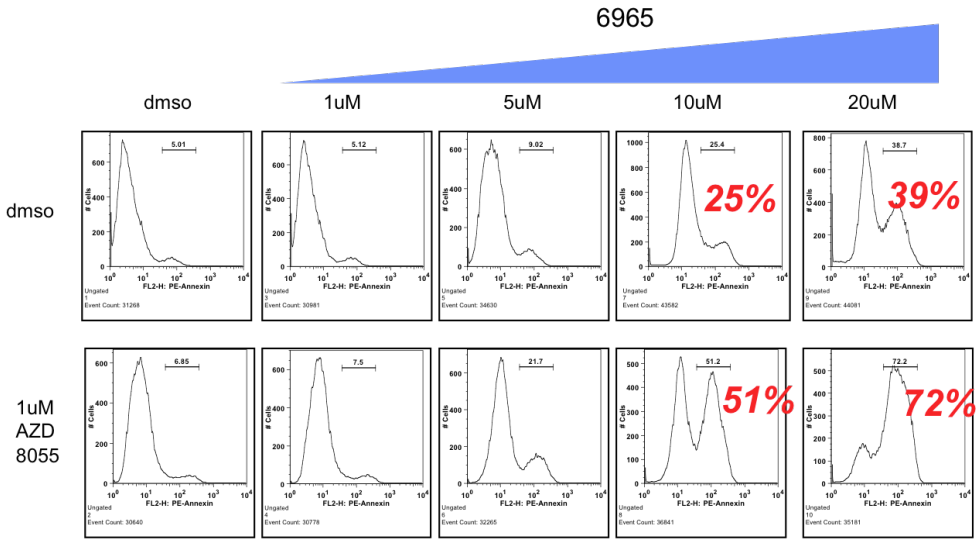

Figure 3.34: Combination of AZD8055 and SBI-0206965 results in synergistic death in A549 NSCLC tumor cells

A549 cells were treated with increasing amounts of SBI-0206965 and combination of AZD8055 as indicated for 72 hours. Cells were collected and stained with PE Annexin V for cells undergoing apoptosis and were quantified using FACS.

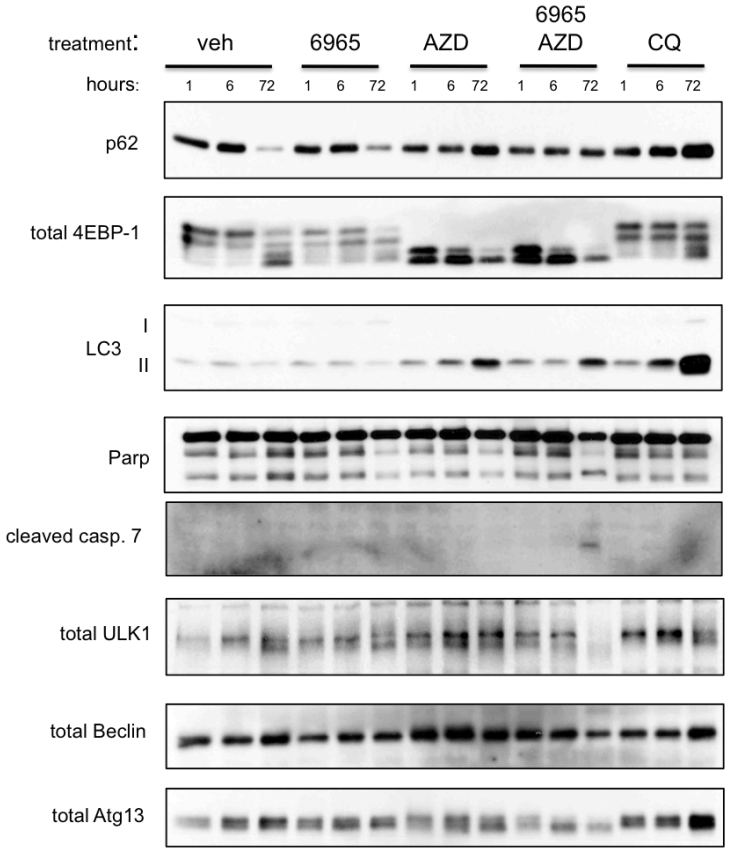

Figure 3.35: Combination of AZD8055 and SBI-0206965 results in synergistic death as read out by caspase activation in A549 NSCLC tumor cells
Timecourse of A549 cells from Figure 39. Cells were treated for indicated timepoints, lysed in boiling SDS lysis buffer, and separated by SDS-PAGE and probed for indicated antibodies. Chloroquine (CQ) at 20uM serves as control for autophagy inhibition.

REFERENCES

Aita, V.M., Liang, X.H., Murty, V.V., Pincus, D.L., Yu, W., Cayanis, E., Kalachikov, S., Gilliam, T.C., and Levine, B. (1999). Cloning and genomic organization of beclin 1, a candidate tumor suppressor gene on chromosome 17q21. Genomics *59*, 59–65.

Andreelli, F., Foretz, M., Knauf, C., Cani, P.D., Perrin, C., Iglesias, M.A., Pillot, B., Bado, A., Tronche, F., Mithieux, G., Vaulont, S., Burcelin, R., and Viollet, B. (2006). Liver adenosine monophosphate-activated kinase-alpha2 catalytic subunit is a key target for the control of hepatic glucose production by adiponectin and leptin but not insulin. Endocrinology *147*, 2432–2441.

Arsham, A.M., and Neufeld, T.P. (2009). A genetic screen in Drosophila reveals novel cytoprotective functions of the autophagy-lysosome pathway. PLoS ONE *4*, e6068.

Ashford, T.P., and Porter, K.R. (1962). Cytoplasmic components in hepatic cell lysosomes. J Cell Biol *12*, 198–202.

Behrends, C., Sowa, M.E., Gygi, S.P., and Harper, J.W. (2010). Network organization of the human autophagy system. Nature *466*, 68–76.

Carling, D., Zammit, V.A., and Hardie, D.G. (1987). A common bicyclic protein kinase cascade inactivates the regulatory enzymes of fatty acid and cholesterol biosynthesis. Febs Letters *223*, 217–222.

Chan, E.Y. (2009). mTORC1 phosphorylates the ULK1-mAtg13-FIP200 autophagy regulatory complex. Sci Signal *2*, pe51.

Chang, Y.-Y., and Neufeld, T.P. (2009). An Atg1/Atg13 complex with multiple roles in TOR-mediated autophagy regulation. Mol Biol Cell *20*, 2004–2014.

Chauhan, S., Goodwin, J.G., Chauhan, S., Manyam, G., Wang, J., Kamat, A.M., and Boyd, D.D. (2013). ZKSCAN3 Is a Master Transcriptional Repressor of Autophagy. Mol Cell.

Cool, B., Zinker, B., Chiou, W., Kifle, L., Cao, N., Perham, M., Dickinson, R., Adler, A., Gagne, G., Iyengar, R., Zhao, G., Marsh, K., Kym, P., Jung, P., Camp, H., and Frevert, E. (2006). Identification and characterization of a small molecule AMPK activator that treats key components of type 2 diabetes and the metabolic syndrome. Cell Metab *3*, 403–416.

Crute, B.E., Seefeld, K., Gamble, J., Kemp, B.E., and Witters, L.A. (1998). Functional domains of the alpha1 catalytic subunit of the AMP-activated protein kinase. J Biol Chem *273*, 35347–35354.

Cuervo, A.M., and Dice, J.F. (2000). Age-related decline in chaperone-mediated

autophagy. J Biol Chem *275*, 31505–31513.

Cuervo, A.M. (2008). Autophagy and aging: keeping that old broom working. Trends Genet *24*, 604–612.

Davies, S.P., Carling, D., Munday, M.R., and Hardie, D.G. (1992). Diurnal rhythm of phosphorylation of rat liver acetyl-CoA carboxylase by the AMP-activated protein kinase, demonstrated using freeze-clamping. Effects of high fat diets. Eur. J. Biochem. *203*, 615–623.

Deter, R.L., Baudhuin, P., and De Duve, C. (1967). Participation of lysosomes in cellular autophagy induced in rat liver by glucagon. J Cell Biol *35*, C11–C16.

Djimdé, A., Doumbo, O.K., Cortese, J.F., Kayentao, K., Doumbo, S., Diourté, Y., Coulibaly, D., Dicko, A., Su, X.Z., Nomura, T., Fidock, D., Wellems, T., and Plowe, C. (2001). A molecular marker for chloroquine-resistant falciparum malaria. N Engl J Med *344*, 257–263.

Donati, A., Cavallini, G., Paradiso, C., Vittorini, S., Pollera, M., Gori, Z., and Bergamini, E. (2001). Age-related changes in the autophagic proteolysis of rat isolated liver cells: effects of antiaging dietary restrictions. J Gerontol a Biol Sci Med Sci *56*, B375–B383.

Egan, D., Kim, J., Shaw, R.J., and Guan, K.-L. (2011a). The autophagy initiating kinase ULK1 is regulated via opposing phosphorylation by AMPK and mTOR. Autophagy *7*, 643–644.

Egan, D.F., Shackelford, D.B., Mihaylova, M.M., Gelino, S., Kohnz, R.A., Mair, W., Vasquez, D.S., Joshi, A., Gwinn, D.M., Taylor, R., Asara, J., Fitzpatrick, J., Dillin, A., Viollet, B., Kundu, M., Hansen, M., and Shaw, R. (2011b). Phosphorylation of ULK1 (hATG1) by AMP-activated protein kinase connects energy sensing to mitophagy. Science *331*, 456–461.

Evans, J.M.M., Donnelly, L.A., Emslie-Smith, A.M., Alessi, D.R., and Morris, A.D. (2005). Metformin and reduced risk of cancer in diabetic patients. Bmj *330*, 1304–1305.

Fabian, M.A., Biggs, W.H., Treiber, D.K., Atteridge, C.E., Azimioara, M.D., Benedetti, M.G., Carter, T.A., Ciceri, P., Edeen, P.T., Floyd, M., et al. (2005). A small molecule-kinase interaction map for clinical kinase inhibitors. Nat Biotechnol *23*, 329–336.

Fogarty, S., and Hardie, D.G. (2010). Development of protein kinase activators: AMPK as a target in metabolic disorders and cancer. Biochim Biophys Acta *1804*, 581–591.

Foretz, M., Hébrard, S., Leclerc, J., Zarrinpashneh, E., Soty, M., Mithieux, G., Sakamoto, K., Andreelli, F., and Viollet, B. (2010). Metformin inhibits hepatic gluconeogenesis in mice independently of the LKB1/AMPK pathway via a decrease in hepatic energy state. The Journal of Clinical Investigation *120*, 2355–2369.

Fullerton, M.D., Galic, S., Marcinko, K., Sikkema, S., Pulinilkunnil, T., Chen, Z.-P., O'Neill, H.M., Ford, R.J., Palanivel, R., O'Brien, M., Hardie, D.G., Macaulay, S.L., Schertzer, J., Dyck, J., Denderen, B., Kemp, B., and Steinberg, G. (2013). Single phosphorylation sites in Acc1 and Acc2 regulate lipid homeostasis and the insulin-sensitizing effects of metformin. Nat Med *19*, 1649–1654.

Geisler, S., Holmström, K.M., Skujat, D., Fiesel, F.C., Rothfuss, O.C., Kahle, P.J., and Springer, W. (2010). PINK1/Parkin-mediated mitophagy is dependent on VDAC1 and p62/SQSTM1. Nat Cell Biol *12*, 119–131.

Green, D.R., and Levine, B. (2014). To Be or Not to Be? How Selective Autophagy and Cell Death Govern Cell Fate. Cell *157*, 65–75.

Guo, J.Y., Chen, H.-Y., Mathew, R., Fan, J., Strohecker, A.M., Karsli-Uzunbas, G., Kamphorst, J.J., Chen, G., Lemons, J.M.S., Karantza, V., Coller, H., DiPaola, R., Gelinas, C., Rabinowitz, J., and White, E. (2011). Activated Ras requires autophagy to maintain oxidative metabolism and tumorigenesis. Genes & Development *25*, 460–470.

Guo, J.Y., Karsli-Uzunbas, G., Mathew, R., Aisner, S.C., Kamphorst, J.J., Strohecker, A.M., Chen, G., Price, S., Lu, W., Teng, X., Teng, X., Snyder, E., Santanam, U., DiPaola, R., Jacks, T., Rabinowitz, J., and White, E. (2013a). Autophagy suppresses progression of K-ras-induced lung tumors to oncocytomas and maintains lipid homeostasis. Genes & Development *27*, 1447–1461.

Guo, J.Y., Xia, B., and White, E. (2013b). Autophagy-mediated tumor promotion. Cell *155*, 1216–1219.

Gwinn, D.M., Shackelford, D.B., Egan, D.F., Mihaylova, M.M., Mery, A., Vasquez, D.S., Turk, B.E., and Shaw, R.J. (2008). AMPK phosphorylation of raptor mediates a metabolic checkpoint. Mol Cell *30*, 214–226.

Halseth, A.E., Ensor, N.J., White, T.A., Ross, S.A., and Gulve, E.A. (2002). Acute and chronic treatment of ob/ob and db/db mice with AICAR decreases blood glucose concentrations. Biochem Biophys Res Commun *294*, 798–805.

Hansen, M., Chandra, A., Mitic, L.L., Onken, B., Driscoll, M., and Kenyon, C. (2008). A role for autophagy in the extension of lifespan by dietary restriction in C. elegans. PLoS Genet *4*, e24.

Hara, T., Nakamura, K., Matsui, M., Yamamoto, A., Nakahara, Y., Suzuki-Migishima,

R., Yokoyama, M., Mishima, K., Saito, I., Okano, H., and Mizushima, N. (2006). Suppression of basal autophagy in neural cells causes neurodegenerative disease in mice. Nature *441*, 885–889.

Hara, T., Takamura, A., Kishi, C., Iemura, S.-I., Natsume, T., Guan, J.-L., and Mizushima, N. (2008). FIP200, a ULK-interacting protein, is required for autophagosome formation in mammalian cells. J Cell Biol *181*, 497–510.

Hardie, D.G. (2007). AMP-activated/SNF1 protein kinases: conserved guardians of cellular energy. Nat Rev Mol Cell Biol *8*, 774–785.

Hardie, D.G. (2011). AMP-activated protein kinase--an energy sensor that regulates all aspects of cell function. Genes & Development *25*, 1895–1908.

Hardie, D.G., and Alessi, D.R. (2013). LKB1 and AMPK and the cancer-metabolism link - ten years after. BMC Biol. *11*, 36.

Hardie, D.G., Ross, F.A., and Hawley, S.A. (2012). AMPK: a nutrient and energy sensor that maintains energy homeostasis. Nat Rev Mol Cell Biol *13*, 251–262.

Hardie, D.G. (2006). Neither LKB1 nor AMPK are the direct targets of metformin. Gastroenterology *131*, 973–authorreply974–5.

Hemminki, A., Markie, D., Tomlinson, I., Avizienyte, E., Roth, S., Loukola, A., Bignell, G., Warren, W., Aminoff, M., Höglund, P., and Aaltonen, L. (1998). A serine/threonine kinase gene defective in Peutz-Jeghers syndrome. Nature *391*, 184–187.

Hosokawa, N., Sasaki, T., Iemura, S.-I., Natsume, T., Hara, T., and Mizushima, N. (2009). Atg101, a novel mammalian autophagy protein interacting with Atg13. Autophagy *5*, 973–979.

Ingebritsen, T.S., Lee, H.S., Parker, R.A., and Gibson, D.M. (1978). Reversible modulation of the activities of both liver microsomal hydroxymethylglutaryl coenzyme A reductase and its inactivating enzyme. Evidence for regulation by phosphorylation-dephosphorylation. Biochem Biophys Res Commun *81*, 1268–1277.

Inoki, K., Zhu, T., and Guan, K.-L. (2003). TSC2 mediates cellular energy response to control cell growth and survival. Cell *115*, 577–590.

Irrcher, I., and Park, D.S. (2009). Parkinson's disease: to live or die by autophagy. Sci Signal *2*, pe21.

Itakura, E., and Mizushima, N. (2010). Characterization of autophagosome formation site by a hierarchical analysis of mammalian Atg proteins. Autophagy *6*.

Itakura, E., and Mizushima, N. (2011). p62 targeting to the autophagosome formation site requires self-oligomerization but not LC3 binding. J Cell Biol *192*, 17–27.

Itakura, E., and Mizushima, N. (2013). Syntaxin 17: The autophagosomal SNARE. Autophagy *9*.

Jaber, N., Dou, Z., Chen, J.-S., Catanzaro, J., Jiang, Y.-P., Ballou, L.M., Selinger, E., Ouyang, X., Lin, R.Z., Zhang, J., and Zong, W. (2012). Class III PI3K Vps34 plays an essential role in autophagy and in heart and liver function. Proceedings of the National Academy of Sciences *109*, 2003–2008.

Jung, C.H., Jun, C.B., Ro, S.-H., Kim, Y.-M., Otto, N.M., Cao, J., Kundu, M., and Kim, D.-H. (2009). ULK-Atg13-FIP200 complexes mediate mTOR signaling to the autophagy machinery. Mol Biol Cell *20*, 1992–2003.

Kamada, Y., Funakoshi, T., Shintani, T., Nagano, K., Ohsumi, M., and Ohsumi, Y. (2000). Tor-mediated induction of autophagy via an Apg1 protein kinase complex. J Cell Biol *150*, 1507–1513.

Kamath, R.S., Fraser, A.G., Dong, Y., Poulin, G., Durbin, R., Gotta, M., Kanapin, A., Le Bot, N., Moreno, S., Sohrmann, M., Welchman, D., Zipperlen, P., and Ahringer, J. (2003). Systematic functional analysis of the Caenorhabditis elegans genome using RNAi. Nature *421*, 231–237.

Kang, C., You, Y.-J., and Avery, L. (2007). Dual roles of autophagy in the survival of Caenorhabditis elegans during starvation. Genes & Development *21*, 2161–2171.

Kang, S.A., Pacold, M.E., Cervantes, C.L., Lim, D., Lou, H.J., Ottina, K., Gray, N.S., Turk, B.E., Yaffe, M.B., and Sabatini, D.M. (2013). mTORC1 phosphorylation sites encode their sensitivity to starvation and rapamycin. Science *341*, 1236566.

Karaman, M.W., Herrgard, S., Treiber, D.K., Gallant, P., Atteridge, C.E., Campbell, B.T., Chan, K.W., Ciceri, P., Davis, M.I., Edeen, P.T., and Zarrinkar, P. (2008). A quantitative analysis of kinase inhibitor selectivity. Nat Biotechnol *26*, 127–132.

Kenzelmann Broz, D., Spano Mello, S., Bieging, K.T., Jiang, D., Dusek, R.L., Brady, C.A., Sidow, A., and Attardi, L.D. (2013). Global genomic profiling reveals an extensive p53-regulated autophagy program contributing to key p53 responses. Genes & Development *27*, 1016–1031.

Kim, J., Kim, Y.C., Fang, C., Russell, R.C., Kim, J.H., Fan, W., Liu, R., Zhong, Q., and Guan, K.-L. (2013). Differential Regulation of Distinct Vps34 Complexes by AMPK in Nutrient Stress and Autophagy. Cell *152*, 290–303.

Kim, J., Kundu, M., Viollet, B., and Guan, K.-L. (2011). AMPK and mTOR regulate autophagy through direct phosphorylation of Ulk1. Nat Cell Biol.

Kimura, T., Takabatake, Y., Takahashi, A., and Isaka, Y. (2013). Chloroquine in cancer therapy: a double-edged sword of autophagy. Cancer Research *73*, 3–7.

Kinoshita, E., Kinoshita-Kikuta, E., Takiyama, K., and Koike, T. (2006). Phosphate-binding tag, a new tool to visualize phosphorylated proteins. Mol. Cell Proteomics *5*, 749–757.

Komatsu, M., Waguri, S., Chiba, T., Murata, S., Iwata, J.-I., Tanida, I., Ueno, T., Koike, M., Uchiyama, Y., Kominami, E., and Tanaka, K. (2006). Loss of autophagy in the central nervous system causes neurodegeneration in mice. Nature *441*, 880–884.

Kraft, C., Peter, M., and Hofmann, K. (2010). Selective autophagy: ubiquitin-mediated recognition and beyond. Nat Cell Biol *12*, 836–841.

Kuma, A., Hatano, M., Matsui, M., Yamamoto, A., Nakaya, H., Yoshimori, T., Ohsumi, Y., Tokuhisa, T., and Mizushima, N. (2004). The role of autophagy during the early neonatal starvation period. Nature *432*, 1032–1036.

Kundu, M., Lindsten, T., Yang, C.-Y., Wu, J., Zhao, F., Zhang, J., Selak, M.A., Ney, P.A., and Thompson, C.B. (2008). Ulk1 plays a critical role in the autophagic clearance of mitochondria and ribosomes during reticulocyte maturation. Blood *112*, 1493–1502.

Kurth-Kraczek, E.J., Hirshman, M.F., Goodyear, L.J., and Winder, W.W. (1999). 5' AMP-activated protein kinase activation causes GLUT4 translocation in skeletal muscle. Diabetes *48*, 1667–1671.

Laderoute, K.R., Amin, K., Calaoagan, J.M., Knapp, M., Le, T., Orduna, J., Foretz, M., and Viollet, B. (2006). 5'-AMP-activated protein kinase (AMPK) is induced by low-oxygen and glucose deprivation conditions found in solid-tumor microenvironments. Mol Cell Biol *26*, 5336–5347.

Laplante, M., and Sabatini, D.M. (2012). mTOR Signaling in Growth Control and Disease. Cell *149*, 274–293.

Levine, B., and Kroemer, G. (2008). Autophagy in the pathogenesis of disease. Cell *132*, 27–42.

Li, Y., Xu, S., Mihaylova, M.M., Zheng, B., Hou, X., Jiang, B., Park, O., Luo, Z., Lefai, E., Shyy, J.Y.J., Gao, B., Wierzbicki, M., Verbeuren, T., Shaw, R., Cohen, R., and Zang, M. (2011). AMPK phosphorylates and inhibits SREBP activity to attenuate hepatic steatosis and atherosclerosis in diet-induced insulin-resistant mice. Cell Metab *13*, 376–388.

Mammucari, C., Milan, G., Romanello, V., Masiero, E., Rudolf, R., Del Piccolo, P., Burden, S.J., Di Lisi, R., Sandri, C., Zhao, J., Goldberg, A., Schiaffino, S., and Sandri,

M. (2007). FoxO3 Controls Autophagy in Skeletal Muscle In Vivo. Cell Metab *6*, 458–471.

Martinez-Vicente, M., Talloczy, Z., Wong, E., Tang, G., Koga, H., Kaushik, S., de Vries, R., Arias, E., Harris, S., Sulzer, D., et al. (2010). Cargo recognition failure is responsible for inefficient autophagy in Huntington's disease. Nat Neurosci *13*, 567–576.

Mathew, R., and White, E. (2011). Autophagy in tumorigenesis and energy metabolism: friend by day, foe by night. Curr Opin Genet Dev *21*, 113–119.

Matsunaga, K., Morita, E., Saitoh, T., Akira, S., Ktistakis, N.T., Izumi, T., Noda, T., and Yoshimori, T. (2010). Autophagy requires endoplasmic reticulum targeting of the PI3-kinase complex via Atg14L. J Cell Biol *190*, 511–521.

Matsuura, A., Tsukada, M., Wada, Y., and Ohsumi, Y. (1997). Apg1p, a novel protein kinase required for the autophagic process in Saccharomyces cerevisiae. Gene *192*, 245–250.

Meléndez, A., Tallóczy, Z., Seaman, M., Eskelinen, E.-L., Hall, D.H., and Levine, B. (2003). Autophagy genes are essential for dauer development and life-span extension in C. elegans. Science *301*, 1387–1391.

Mercer, C.A., Kaliappan, A., and Dennis, P.B. (2009). A novel, human Atg13 binding protein, Atg101, interacts with ULK1 and is essential for macroautophagy. Autophagy *5*, 649–662.

Merrill, G.F., Kurth, E.J., Hardie, D.G., and Winder, W.W. (1997). AICA riboside increases AMP-activated protein kinase, fatty acid oxidation, and glucose uptake in rat muscle. Am. J. Physiol. *273*, E1107–E1112.

Mihaylova, M.M., and Shaw, R.J. (2011). The AMPK signalling pathway coordinates cell growth, autophagy and metabolism. Nat Cell Biol *13*, 1016–1023.

Mizushima, N. (2011). Autophagy in Protein and Organelle Turnover. Cold Spring Harbor Symposia on Quantitative Biology.

Mizushima, N. (2010). The role of the Atg1/ULK1 complex in autophagy regulation. Curr Opin Cell Biol *22*, 132–139.

Mizushima, N., Yoshimori, T., and Levine, B. (2010). Methods in Mammalian Autophagy Research. Cell *140*, 313–326.

Mok, J., Kim, P.M., Lam, H.Y.K., Piccirillo, S., Zhou, X., Jeschke, G.R., Sheridan, D.L., Parker, S.A., Desai, V., Jwa, M., and Turk, B. (2010). Deciphering protein kinase specificity through large-scale analysis of yeast phosphorylation site motifs. Sci

Signal *3*, ra12.

Nakada, D., Saunders, T.L., and Morrison, S.J. (2010). Lkb1 regulates cell cycle and energy metabolism in haematopoietic stem cells. Nature *468*, 653–658.

Obenauer, J.C., Cantley, L.C., and Yaffe, M.B. (2003). Scansite 2.0: Proteome-wide prediction of cell signaling interactions using short sequence motifs. Nucleic Acids Res. *31*, 3635–3641.

Papinski, D., Schuschnig, M., Reiter, W., Wilhelm, L., Barnes, C.A., Majolica, A., Hansmann, I., Pfaffenwimmer, T., Kijanska, M., Stoffel, I., and Kraft, C. (2014). Early Steps in Autophagy Depend on Direct Phosphorylation of Atg9 by the Atg1 Kinase. Mol Cell.

Qu, X., Yu, J., Bhagat, G., Furuya, N., Hibshoosh, H., Troxel, A., Rosen, J., Eskelinen, E.-L., Mizushima, N., Ohsumi, Y., and Levine, B. (2003). Promotion of tumorigenesis by heterozygous disruption of the beclin 1 autophagy gene. J. Clin. Invest. *112*, 1809–1820.

Rabinowitz, J.D., and White, E. (2010). Autophagy and metabolism. Science *330*, 1344–1348.

Rajesh, S., Bago, R., Odintsova, E., Muratov, G., Baldwin, G., Sridhar, P., Rajesh, S., Overduin, M., and Berditchevski, F. (2011). Binding to syntenin-1 protein defines a new mode of ubiquitin-based interactions regulated by phosphorylation. Journal of Biological Chemistry *286*, 39606–39614.

Ravikumar, B., Duden, R., and Rubinsztein, D.C. (2002). Aggregate-prone proteins with polyglutamine and polyalanine expansions are degraded by autophagy. Hum Mol Genet *11*, 1107–1117.

Ravikumar, B., Vacher, C., Berger, Z., Davies, J.E., Luo, S., Oroz, L.G., Scaravilli, F., Easton, D.F., Duden, R., O'kane, C.J., and Rubinsztein, D. (2004). Inhibition of mTOR induces autophagy and reduces toxicity of polyglutamine expansions in fly and mouse models of Huntington disease. Nat Genet *36*, 585–595.

Rodriguez-Enriquez, S., Kai, Y., Maldonado, E., Currin, R.T., and Lemasters, J.J. (2009). Roles of mitophagy and the mitochondrial permeability transition in remodeling of cultured rat hepatocytes. Autophagy *5*, 1099–1106.

Rosenfeldt, M.T., O'Prey, J., Morton, J.P., Nixon, C., MacKay, G., Mrowinska, A., Au, A., Rai, T.S., Zheng, L., Ridgway, R., Adams, P., Anderson, K., Gottlieb, E., Sansom, O., and Ryan, K. (2013). p53 status determines the role of autophagy in pancreatic tumour development. Nature.

Rual, J.-F., Ceron, J., Koreth, J., Hao, T., Nicot, A.-S., Hirozane-Kishikawa, T.,

Vandenhaute, J., Orkin, S.H., Hill, D.E., van den Heuvel, S., and Vidal, M. (2004). Toward improving Caenorhabditis elegans phenome mapping with an ORFeome-based RNAi library. Genome Research *14*, 2162–2168.

Russell, R.C., Tian, Y., Yuan, H., Park, H.W., Chang, Y.-Y., Kim, J., Kim, H., Neufeld, T.P., Dillin, A., and Guan, K.-L. (2013). ULK1 induces autophagy by phosphorylating Beclin-1 and activating VPS34 lipid kinase. Nat Cell Biol *15*, 741–750.

Sancak, Y., Peterson, T.R., Shaul, Y.D., Lindquist, R.A., Thoreen, C.C., and Bar-Peled, L. (2008). The Rag GTPases bind raptor and mediate amino acid signaling to mTORC1. Science *320*, 1496–1501.

Sanchez-Cespedes, M., Parrella, P., Esteller, M., Nomoto, S., Trink, B., Engles, J.M., Westra, W.H., Herman, J.G., and Sidransky, D. (2002). Inactivation of LKB1/STK11 is a common event in adenocarcinomas of the lung. Cancer Research *62*, 3659–3662.

Sardiello, M., Palmieri, M., di Ronza, A., Medina, D., Valenza, M., Gennarino, V., Di Malta, C., Donaudy, F., Embrione, V., Polishchuk, R., and Ballabio, A. (2009). A Gene Network Regulating Lysosomal Biogenesis and Function. Science 325, 473-477.

Scott, J.W., Norman, D.G., Hawley, S.A., Kontogiannis, L., and Hardie, D.G. (2002). Protein kinase substrate recognition studied using the recombinant catalytic domain of AMP-activated protein kinase and a model substrate. J Mol Biol *317*, 309–323.

Settembre, C., Di Malta, C., Polito, V.A., García-Arencibia, M., Vetrini, F., Erdin, S., Erdin, S.U., Huynh, T., Medina, D., Colella, P., and Ballabio, A. (2011). TFEB links autophagy to lysosomal biogenesis. Science *332*, 1429–1433.

Shackelford, D.B., and Shaw, R.J. (2009). The LKB1-AMPK pathway: metabolism and growth control in tumour suppression. Nat Rev Cancer *9*, 563–575.

Shackelford, D.B., Abt, E., Gerken, L., Vasquez, D.S., Seki, A., Leblanc, M., Wei, L., Fishbein, M.C., Czernin, J., Mischel, P.S., and Shaw, R. (2013). LKB1 Inactivation Dictates Therapeutic Response of Non-Small Cell Lung Cancer to the Metabolism Drug Phenformin. Cancer Cell.

Shackelford, D.B., Vasquez, D.S., Corbeil, J., Wu, S., Leblanc, M., Wu, C.-L., Vera, D.R., and Shaw, R.J. (2009). mTOR and HIF-1alpha-mediated tumor metabolism in an LKB1 mouse model of Peutz-Jeghers syndrome. Proc Natl Acad Sci USA *106*, 11137–11142.

Shang, L., Chen, S., Du, F., Li, S., Zhao, L., and Wang, X. (2011). Nutrient starvation elicits an acute autophagic response mediated by Ulk1 dephosphorylation and its subsequent dissociation from AMPK. Proc Natl Acad Sci USA.

Shaw, R.J., Lamia, K.A., Vasquez, D., Koo, S.-H., Bardeesy, N., DePinho, R.A., Montminy, M., and Cantley, L.C. (2005). The kinase LKB1 mediates glucose homeostasis in liver and therapeutic effects of metformin. Science *310*, 1642–1646.

Son, J., Lyssiotis, C.A., Ying, H., Wang, X., Hua, S., Ligorio, M., Perera, R.M., Ferrone, C.R., Mullarky, E., Shyh-Chang, N., and Kimmelman, A. (2013). Glutamine supports pancreatic cancer growth through a KRAS-regulated metabolic pathway. Nature 7443, 101-105.

Suter, M., Riek, U., Tuerk, R., Schlattner, U., Wallimann, T., and Neumann, D. (2006). Dissecting the role of 5'-AMP for allosteric stimulation, activation, and deactivation of AMP-activated protein kinase. J Biol Chem *281*, 32207–32216.

Tsukada, M., and Ohsumi, Y. (1993). Isolation and characterization of autophagy-defective mutants of Saccharomyces cerevisiae. Febs Letters *333*, 169–174.

Ubersax, J.A., and Ferrell, J.E. (2007). Mechanisms of specificity in protein phosphorylation. Nat Rev Mol Cell Biol *8*, 530–541.

Weekes, J., Ball, K.L., Caudwell, F.B., and Hardie, D.G. (1993). Specificity determinants for the AMP-activated protein kinase and its plant homologue analysed using synthetic peptides. Febs Letters *334*, 335–339.

White, E. (2012). Deconvoluting the context-dependent role for autophagy in cancer. Nat Rev Cancer.

Wingo, S.N., Gallardo, T.D., Akbay, E.A., Liang, M.-C., Contreras, C.M., Boren, T., Shimamura, T., Miller, D.S., Sharpless, N.E., Bardeesy, N., and Castrillon, D. (2009). Somatic LKB1 mutations promote cervical cancer progression. PLoS ONE *4*, e5137.

Wolfe, D.M., Lee, J.-H., Kumar, A., Lee, S., Orenstein, S.J., and Nixon, R.A. (2013). Autophagy failure in Alzheimer's disease and the role of defective lysosomal acidification. Eur. J. Neurosci. *37*, 1949–1961.

Wolff, S., Weissman, J.S., and Dillin, A. (2014). Differential Scales of Protein Quality Control. Cell *157*, 52–64.

Yang, Z., and Klionsky, D.J. (2009). Mammalian autophagy: core molecular machinery and signaling regulation. Curr Opin Cell Biol.

Yeh, L.A., Lee, K.H., and Kim, K.H. (1980). Regulation of rat liver acetyl-CoA carboxylase. Regulation of phosphorylation and inactivation of acetyl-CoA carboxylase by the adenylate energy charge. J Biol Chem *255*, 2308–2314.